

Proposal on spin physics using the RHIC polarized collider: Update

G. Bunce

September 1993

Collider Accelerator Department
Brookhaven National Laboratory

U.S. Department of Energy

USDOE Office of Science (SC)

Notice: This technical note has been authored by employees of Brookhaven Science Associates, LLC under Contract No. DE-AC02-76CH00016 with the U.S. Department of Energy. The publisher by accepting the technical note for publication acknowledges that the United States Government retains a non-exclusive, paid-up, irrevocable, world-wide license to publish or reproduce the published form of this technical note, or allow others to do so, for United States Government purposes.

DISCLAIMER

This report was prepared as an account of work sponsored by an agency of the United States Government. Neither the United States Government nor any agency thereof, nor any of their employees, nor any of their contractors, subcontractors, or their employees, makes any warranty, express or implied, or assumes any legal liability or responsibility for the accuracy, completeness, or any third party's use or the results of such use of any information, apparatus, product, or process disclosed, or represents that its use would not infringe privately owned rights. Reference herein to any specific commercial product, process, or service by trade name, trademark, manufacturer, or otherwise, does not necessarily constitute or imply its endorsement, recommendation, or favoring by the United States Government or any agency thereof or its contractors or subcontractors. The views and opinions of authors expressed herein do not necessarily state or reflect those of the United States Government or any agency thereof.

Accelerator Division
AGS Department
BROOKHAVEN NATIONAL LABORATORY
Associated Universities, Inc.
Upton, NY 11973

AGS/AD/Tech. Note No. 408

Proposal on Spin Physics Using the RHIC

Polarized Collider

UPDATE

September 2, 1993

Abstract

We propose to study the spin dependence of various reactions using longitudinally and transversely-polarized beams at RHIC.

We present the design and construction of polarized beams, along with proposed measurements using PHENIX and STAR detectors.

This update to the August 1992 proposal covers work done over the past year. Part A is submitted by the RHIC Spin Collaboration, Part B by the PHENIX/Spin Collaboration and Part C by the STAR/Spin Collaboration.

Introduction to the Update of the RHIC Spin Proposal

The RHIC Spin, PHENIX/Spin, and STAR/Spin Collaborations propose to collide polarized protons at RHIC. Two RHIC experiments, STAR and PHENIX, will measure produced W^\pm , Z^0 , Drell-Yan pairs, and direct photons, jets, and J/ψ with very high transverse momentum (>50 GeV/c for jets), well into the domain where perturbative QCD should apply. Physics goals include the measurement of gluon and sea quark polarization in longitudinally polarized protons, parity violation of W and Z production, and a search for parity violation in other processes. With transversely polarized protons, quark polarization will be measured that is sensitive to the difference between relativistic and nonrelativistic quark models of protons.

The key breakthrough that made it possible to accelerate polarized protons to high energy, maintaining polarization, was the invention of the Siberian Snake by Novosibirsk. Snakes are strings of dipole magnets that rotate the proton's spin 180 degrees, which have the effect of removing spin resonances from the acceleration process. Four snakes are required for polarized beams at RHIC. In addition, eight spin rotators are required for the physics program with the two detectors. The AGS also requires a Partial Snake solenoid.

The STAR/Spin experiment proposes to measure W, Z, jets, direct photons, and Drell-Yan pairs (electrons). STAR requires the addition of an electromagnetic calorimeter to the approved RHIC apparatus. STAR features a large acceptance and jet reconstruction. The PHENIX/Spin experiment emphasizes direct photons, W, and J/ψ with excellent photon and electron detection, jets with leading π^0 s, and Drell-Yan pairs (di-muons). PHENIX does not require additions for the spin program.

RHIC spin submitted its proposal in August 1992, in three parts. Part A is authored by the RHIC Spin Collaboration, including accelerator experts, particle theorists, and experimenters, and covers the overall proposed physics program and the machine requirements for accelerating and colliding polarized protons. RSC has developed the physics program for the proposal, and will be responsible for the required accelerator changes and commissioning for polarized protons. Part B is submitted by the PHENIX/Spin Collaboration and Part C is submitted by the STAR/Spin Collaboration. Parts B and C propose specific complementary spin experiments for the two detectors and together emphasize the unique program that will become available at RHIC from colliding beams of polarized protons.

This UPDATE contains additional material for all three parts of the initial proposal. It represents work done over the past year.

In Part A we include the Conceptual Design Report for accelerating polarized protons at RHIC, and the report of a committee of accelerator experts which was convened in June 1993 by the RHIC management to review our plans. The review committee was chaired by Lee Teng (ANL), with members Alex Chao (SSCL), Steve Peggs (BNL), Bob Pollock (IUCF), and Bill Weng (BNL). The review report concludes in its executive summary,

"The proposal has the flavor of the application of an ingenious technological invention (Siberian snakes) to make possible exciting physics research (polarization

physics), reminiscent of the application of stochastic cooling to obtain \bar{p} -p beams for W and Z in the CERN SPS. We are indeed enthusiastic about this total program."

"...we believe that the feasibility of producing, storing and colliding 250 GeV polarized proton beams in RHIC is established with reasonable confidence."

They recommend that the collaboration submit a full Design Report for detailed review in a year.

The updates for Parts B and C include further simulation studies including backgrounds. Part C (STAR/Spin) also includes work on the proposed electromagnetic calorimeter.

The estimated costs are

Part A.	Hardware for accelerating polarized protons. This includes snakes, polarimeters, and spin rotators (to give longitudinal polarization for PHENIX and STAR). The estimate is based on a RHIC magnet design and was done by the RHIC magnet group. It includes contingency.	\$10M
Part B.	PHENIX/Spin. No additions are required for the proposed spin program.	0
Part C.	STAR/Spin. An electromagnetic calorimeter barrel with shower maximum detector. The estimate was done by LBL and ANL. Contingency is included.	\$11M

TOTAL		\$21M

We request approval at this time for this unique program.

PART A

UPDATE FOR PROPOSAL OF THE RHIC SPIN COLLABORATION

September 2, 1993

Contents:

1. RSC author list.
2. Conceptual design report for the acceleration of polarized protons in RHIC.
3. Report of the RHIC Polarized Proton Review.

RHIC SPIN COLLABORATION

September 2, 1993

M. Beddo, D. Grosnick, D. Lopiano, D. Hill, H. Spinka, D. Underwood,
A. Yokosawa, *Argonne*;

G. Bunce, E. Courant, R. Fernow, Y.Y. Lee, D. Lowenstein, A. Luccio,
Y. Makdisi,
L. Ratner, T. Roser, M. Tannenbaum, *Brookhaven*;

J.B. Carroll, T. Hallman, G.J. Igo, *UCLA*;

N. Törnqvist, *Helsinki*;

N. Akchurin, Y. Onel, *Iowa*;

S.Y. Lee, *Indiana*;

S. Hiramatsu, T. Mori, H. Sato, *KEK*;

L. Madansky, R. Welsh, *Johns Hopkins*;

H. Enyo, K. Imai, A. Masaike, *Kyoto*;

J. Soffer, *Marseille*;

R. Jaffe, *MIT*;

A. Bravar, M. Conte, A. Penzo, M. Pusterla, P. Schiavon, *Italy*;

J. Collins, S. Heppelmann, G. Ladinsky, E. Minor, R. Robinett, *Penn State*;

A.S. Akimenko, Yu.I. Arestov, N.I. Belikov, B.V. Chujko, A.M. Davidenko,
A.A. Derevschikov, S.V. Erin, O.A. Grachov, A.S. Konstantinov,
I.V. Kotov,

Yu.A. Matulenko, A.P. Meschanin, A.I. Mysnick, S.B. Nurusev,
A.I. Pavlinov,

A.Yu. Polyarush, A.I. Ronzhin, V.L. Rykov, V.A. Sergeev, K.E. Shestermanov,
L.F. Soloviev, O.D. Tsay, A.G. Ufimtsev, A.N. Vasiliev, *IHEP*;

A.Y. Efremov, *JINR*;

M. Werlen, *Lausanne*.

Spin Spokesmen:

RSC coordinators: A. Yokosawa, G. Bunce

Accelerator physics and hardware: T. Roser

Conceptual Design for the Acceleration of Polarized Protons in RHIC ¹

K.Brown (BNL)	G.Bunce (BNL)	E.Courant (BNL)
R.Fernow (BNL)	S.Y.Lee (Indiana)	A.Luccio (BNL)
Y.Makdisi (BNL)	S.Mane (BNL)	L.Ratner (BNL)
T.Roser (Coordinator, BNL)	H.Spinka (ANL)	
S.Tepikian (BNL)	A.G.Ufimtsev (IHEP)	
D.Underwood (ANL)		

May 24, 1993

Revised: September 3, 1993

¹Work was performed under the auspices of the U.S. Department of Energy and was supported by grants from the U.S. National Science Foundation

CONTENTS

1	Introduction	3
2	Polarized Ion Source, AGS and Transfer of the Polarized Beam to RHIC	4
3	Siberian Snakes and Spin Rotators in RHIC	6
3.1	General Lay-out	6
3.2	Siberian Snake and Spin Rotator Design	7
3.3	Effect on Lattice	9
3.4	Compensation for Detector Solenoids	11
3.5	Cost Estimate and Schedule	11
4	Acceleration of Polarized Protons in RHIC	13
4.1	Depolarizing Resonance Strengths	13
4.2	Effect of Siberian Snakes	14
4.3	Sextupole Depolarizing Resonances	15
4.4	Spin Tune Spread and Modulation	16
4.5	Betatron Tune Spreads and Modulations	17
5	Storage of Polarized Protons in RHIC	18
6	Measuring the Beam Polarization in RHIC	20
6.1	Polarimeter Lay-out	20
6.2	Heating of the Carbon Fiber	22
7	Luminosity of Polarized Proton Collisions	24
8	Spin Reversal of the Stored Beams	25
9	Operational Modes of RHIC for Polarized Proton Running	27

10 Conclusions	28
11 Figure Captions	29

1. INTRODUCTION

The Relativistic Heavy Ion Collider (RHIC) at Brookhaven allows for the unique possibility of colliding 250 GeV polarized proton beams at luminosities of up to $2 \times 10^{32}\text{ cm}^{-2}\text{s}^{-1}$. This report describes the technical considerations of accelerating polarized proton beams in RHIC to a top energy of 250 GeV and of performing collisions of longitudinally and transversely polarized protons in the two interaction regions occupied by the PHENIX and STAR detectors.

Fig. 1 shows all the major components that are required for the acceleration of polarized beams to RHIC top energy. The feasibility of accelerating polarized protons in RHIC was the basis of the proposal the RHIC Spin Collaboration (RSC) submitted to the Brookhaven PAC in October 1992[1].

2. POLARIZED ION SOURCE, AGS AND TRANSFER OF THE POLARIZED BEAM TO RHIC

To achieve high luminosity, high energy polarized proton collisions in RHIC the intensity of the present AGS polarized proton source[2] is sufficient. The source produces about $35 \mu A$ of H^- with 75 – 80% polarization in $350 \mu s$ pulses at a repetition rate of $5 Hz$. The polarized H^- ions are accelerated to $200 MeV$ with an RFQ and the $200 MHz$ LINAC with an efficiency of about 50%. Twenty pulses of H^- ions are strip-injected, accumulated, and captured into a single bunch in the AGS Booster with an estimated efficiency of about 50%. The bunch in the Booster will then contain $N_B = 4 \times 10^{11}$ polarized protons with a normalized emittance of about $\epsilon_N = 10\pi mm mrad$. The single bunch of polarized protons is accelerated in the Booster to $1.5 GeV$ kinetic energy and then transferred to the AGS, where it is accelerated to $25 GeV$.

During acceleration, the polarization may be lost when the spin precession frequency passes through a depolarizing resonance. These resonances occur when the number of spin precession rotations per revolution $G\gamma$ ($G = 1.793$ is the anomalous magnetic moment of the proton, $\gamma = \frac{E}{m}$) is equal to an integer (imperfection resonances) or equal to $kP \pm \nu_y$ (intrinsic resonances). Here $P = 12$ is the superperiodicity of the AGS, $\nu_y = 8.8$ is the vertical betatron tune and k is an integer. The depolarization is caused by the small horizontal magnetic fields present in all ring accelerators which, at the resonance condition, act coherently to move the spin away from the stable vertical direction. Imperfection resonances are due to the horizontal fields caused by the vertical closed orbit errors and intrinsic resonances are caused by the horizontal focusing fields which are sampled due to the vertical betatron motion. The two resonances in the Booster ($G\gamma = 3$ and $G\gamma = 4$) are too weak to cause any significant depolarization. Traditionally, the depolarizing resonances in the AGS were corrected by the tedious harmonic correction method for the imperfection resonances and the tune jump method for

the intrinsic resonances[3].

In the approved experiment E-880 at the AGS to be started in 1993, the feasibility of polarized proton acceleration by using a 5% partial Siberian Snake[4] will be tested. Previous experience with polarized proton acceleration in the AGS indicates that a 5% Snake is sufficient to avoid depolarization due to the imperfection resonances without using the harmonic correction method. The remaining six important intrinsic resonances can be corrected by the proven tune jump method. At 25 *GeV*, the polarized protons are transferred to RHIC. At this energy the transfer line between the AGS and RHIC is spin transparent[5].

We estimate that the overall efficiency of the acceleration and beam transfer is better than 50%, giving 2×10^{11} protons per bunch. With proper care in the tune jump procedure the normalized emittance of the bunch is expected to be less than 20π *mm mrad*. We repeat the process until all 57 bunches of each ring are filled. Since each bunch is accelerated independently, we have the option of preparing the polarization direction of each bunch independently. Filling both RHIC rings with 57 bunches each and acceleration to full energy will only take about 10 minutes which is short compared to the expected lifetime of the stored polarized proton beams in RHIC of many hours.

3. SIBERIAN SNAKES AND SPIN ROTATORS IN RHIC

3.1. General Lay-out

By inserting two full Siberian Snakes on opposite sides of each of the two RHIC rings, depolarization from imperfection and intrinsic depolarizing resonances can be avoided up to the top energy of 250 *GeV*. In addition to the Siberian Snakes, spin rotators are required at the intersection points used by PHENIX and STAR to allow for measurements of spin effects with longitudinally polarized protons. The spin rotators rotate the polarization from the vertical direction into the horizontal plane on one side of the interaction region and restore it to the vertical direction on the other side.

The Siberian Snakes introduce a 180° spin rotation without generating a net orbit distortion. The spin rotators placed around the experiments rotate the spin by 90° to provide longitudinal polarization at the interaction region again without generating net orbit distortions. In both cases the spin rotation is accomplished with a sequence of large bore, constant field, superconducting dipole magnets. The large bore is necessary to accommodate the orbit excursions inside the Snake and the spin rotators.

Each Snake rotates the spin by 180° around a horizontal axis and the two axes of the two Snakes of each ring have to be perpendicular on each other. We are planning to use pairs of Siberian Snakes with one Snake rotating the spin around an axis that points 45° to the outside and the other Snake rotating around an axis that points 45° to the inside of the ring. In this case all Snakes can be constructed in same way. Also, the two Snakes of each ring have to be installed on opposite sides of the ring. In fact, the beam direction in one Snake has to be exactly opposite to the beam direction in the other Snake to within 0.3 *mrad*.

The following is a summary of the proposal for the locations and construction of the Siberian Snakes and the spin rotators (see Fig. 1):

- Two pairs of full Siberian Snakes, one pair in each ring, are installed at the 4 o'clock and 10 o'clock regions as shown in Fig. 2. These Snakes rotate the spin around axes that point 45° to the inside or outside of the ring. We are planning to install the Siberian Snakes in the 13 m long, cold straight sections between Q7 and Q8.
- The two pairs of spin rotators, for PHENIX at the 8 o'clock region and STAR at the 6 o'clock region, are installed in the 40 m long straight sections between Q3 and Q4 on either side of the interaction region. The beam direction in the straight sections is different from the direction in the collision area by 3.67 mrad which introduces a spin rotation that is larger by a factor of $G\gamma$. This means that the spin rotators have to prepare a horizontal polarization direction such that after this spin rotation the desired longitudinal polarization direction is obtained at the interaction point. Fig. 3 shows the size of the maximum orbit excursion inside the spin rotators as a function of beam energy. To limit the orbit excursions in the spin rotators to the same value as in the Snakes, which is about 70 mm , we are planning to inject with the spin rotators turned off and only turn them on at an energy of 75 GeV or higher if needed by the experiments. The turn-on can be done adiabatically without loss of polarization.

3.2. Siberian Snake and Spin Rotator Design

For both the Siberian Snake and the spin rotators we used the 200 mm bore, superconducting RHIC DX dipole magnets as a basis for the design. The Snake consists of seven magnets with dimensions listed in Table 3.1. The parameters are a result of an optimization using a three dimensional orbit and spin tracking program that includes the effects of fringe fields. The maximum beam excursion at the injection energy is 60 mm . The result of the orbit and spin tracking is shown in Fig. 4. As can be seen from Fig. 4 the orbit excursion is mainly in the vertical plane. By installing the Snake magnets with a centerline that is offset by 30 mm from the undisturbed orbit, 70 mm of the aperture on either side is available for the beam size. This is more than ten times the expected 95 % beam width at injection for the 95 % beam emittance of $20 \pi \text{ mm mrad}$. The horizontal and vertical dipole magnets are powered by separate power supplies. This allows for an adjustment of the spin tune to $1/2$ and also for small changes of the direction of the rotation axis to compensate for the effect of the detector solenoids as will

Number of Dipoles				7
Number of independent power supplies				2 (A,B)
Total length [m]				7
Magnet bore [mm]				200
Dipoles				Field [Tesla]
	center[m]	length[m]	orientation	
1	0.956	0.184	H (A)	3.144
2	1.596	0.528	V (B)	-4.084
3	2.404	0.528	H (A)	-3.842
4	3.500	1.266	V (B)	4.055
5	4.596	0.528	H (A)	3.842
6	5.404	0.528	V (B)	-4.084
7	6.044	0.184	H (A)	-3.144
Max. orbit excursion @ $\gamma = 250$ [mm]				1.9 (hor), 5.8 (ver)
Max. orbit excursion @ injection [mm]				19.0 (hor), 58.4 (ver)
Total field integral [Tm]				11.9 (hor), 8.0 (ver)
Orbit lengthening [mm]				0.038

Table 3.1: Parameters of the Siberian Snake magnets

be discussed below. This is shown in Fig. 5

For the spin rotators we have two solutions: (1) with 3 vertical and 3 horizontal dipole magnets with a 200 mm bore, and (2) with 6 horizontal and 6 vertical dipole magnets with a 100 mm bore. In both solutions it is possible to rotate the polarization into any direction of the horizontal plane according to the requirements outlined in the previous section. For the first solution an analytic condition to meet these requirements was worked out[8]. To ensure that the spin lies in the horizontal plane the spin rotation angles ψ_H and ψ_V in the horizontal and vertical dipoles, respectively, have to obey the equation

$$\sin \psi_H \sin \psi_V = \pm \frac{1}{2}.$$

The relative sign of ψ_H and ψ_V for different directions in the horizontal plane are shown in Fig. 6. Two independent power supplies are therefore adequate to configure the spin rotator to produce any horizontal polarization direction. Table 3.2 shows the parameters for this rotator solution and Fig. 7 shows the result of tracking calculations for the spin rotator that produces longitudinal polarization (top) and radial polarization (bottom). The maximum orbit excursion at injection

Number of Dipoles				6	
Number of independent power supplies				2 (A,B)	
Total length [m]				11	
Magnet bore [mm]				200	
Dipoles				Field [Tesla]	
	center[m]	length[m]	orientation	radial pol.	longitudinal pol.
1	1.000	0.260	V (A)	1.843	1.843
2	3.000	0.660	H (B)	-1.176	-3.605
3	4.400	0.900	V (A)	-2.000	-2.000
4	6.200	1.700	H (B)	1.240	3.800
5	7.800	0.260	V (A)	1.843	1.843
6	9.400	0.660	H (B)	-1.176	-3.605
Max. orbit excursion @ $\gamma = 250$ [mm]				4.8 (hor), 5.6 (ver)	14.4 (hor), 5.6 (ver)
Max. orbit excursion @ injection [mm]				48.0 (hor), 56.0 (ver)	144.0 (hor), 56.0 (ver)
Total field integral [Tm]				5.6 (hor), 5.5 (ver)	5.6 (hor), 16.7 (ver)
Orbit lengthening [mm]				0.024	0.112

Table 3.2: Parameters of the Spin Rotator magnets for solution (1)

energy is 144 *mm*, thus requiring the rotators to be turned on only at higher energies.

For the second solution it was shown by spin tracking that with 3 independent power supplies any horizontal polarization direction can be produced. Table 3.3 and Fig. 8 show the magnet parameters and tracking results for the spin rotator solution 2. The maximum orbit excursion is much smaller in this case, only 31 *mm* at injection energy. The design of the second solution was motivated by the idea of using a helical wiggler as spin rotator [9]. The much smaller orbit excursions and consequently reduced requirements for the magnet bore makes the second solution much preferable and we are investigating the possibility to use the same concept not just for the rotators but also for the Siberian Snakes.

3.3. Effect on Lattice

Calculations of the changes to the RHIC lattice parameters were performed using MAD. It is worth noting that the survey algorithm in MAD does not work properly since the Snakes introduce torsion into coordinate system. The following changes in the lattice parameters are caused by the introduction of two Snakes, each

Number of Dipoles				12	
Number of independent power supplies				4 (A,B,C,D)	
Total length [m]				9	
Magnet bore [mm]				100	
Dipoles				Field [Tesla]	
	center[m]	length[m]	orientation	radial pol.	longitudinal pol.
1	0.715	0.358	H (D)	-2.767	-3.864
2	1.430	0.250	V (C)	-1.868	-2.620
3	2.145	0.447	H (A)	4.074	4.074
4	2.860	0.447	V (C)	2.992	4.196
5	3.575	0.447	H (B)	-0.944	3.944
6	4.290	0.447	V (C)	-2.922	-4.196
7	5.005	0.447	H (B)	0.944	-3.944
8	5.720	0.447	V (C)	2.922	4.196
9	6.435	0.447	H (A)	-4.074	-4.074
10	7.150	0.447	V (C)	-2.922	-4.196
11	7.865	0.358	H (D)	2.767	3.864
12	8.580	0.250	V (C)	1.868	2.620
Max. orbit excursion @ $\gamma = 250$ [mm]				2.0 (hor), 0.7 (ver)	3.1 (hor), 1.5 (ver)
Max. orbit excursion @ injection [mm]				20.0 (hor), 7.2 (ver)	31.2 (hor), 15.2 (ver)
Total field integral [Tm]				7.9 (hor), 8.0 (ver)	11.0 (hor), 12.3 (ver)
Orbit lengthening [mm]				0.012	0.031

Table 3.3: Parameters of the Spin Rotator magnets for solution (2)

located between Q7 and Q8 as described above:

Comment	v_x	v_y	D_x^{\max}	D_y^{\max}	β_x^*	β_y^*
No Snakes	28.827	28.823	1.674 <i>m</i>	0	2.0 <i>m</i>	2.0 <i>m</i>
With Snakes, Injection energy	28.837	28.836	1.738 <i>m</i>	0.110 <i>m</i>	2.0 <i>m</i>	2.1 <i>m</i>
With Snakes, Top energy	28.827	28.823	1.678 <i>m</i>	0.009 <i>m</i>	2.0 <i>m</i>	2.0 <i>m</i>

Clearly the changes of the lattice parameters are very small and can easily be corrected for.

3.4. Compensation for Detector Solenoids

The STAR and PHENIX detectors use solenoid magnets as spectrometers. With transverse polarization at the collision point the solenoid contributes to the imperfection resonance strength,

$$\epsilon_{imp,sol} = \frac{1 + G}{2\pi} \frac{\int B_{\parallel} d\ell}{B\rho}$$

For a 5 Tesla-meters integrated solenoid field strength, the resulting spin resonance strength is about 0.02 at the injection energy and 0.003 at 250 GeV/c.

With longitudinal polarization at the collision point the longitudinal field rotates the polarization around its axis and thus changes the spin tune. The spin tune is changed by 0.03 to 0.003 at 25 GeV and 250 GeV, respectively, by a 5 Tm solenoid. This can be compensated by adjusting the direction of the axes around which the Snakes rotate the spin. By adjusting up to $\pm 2.5^\circ$ the spin tune can be adjusted for energies down to 50 GeV.

3.5. Cost Estimate and Schedule

Erich Willen from the RHIC magnet group compiled a cost estimate for the four Siberian Snakes and the eight solution (1) spin rotators. His estimate is based on using the 20 *mm* bore RHIC DX dipole magnets and scaling them to the required length shown in Tables 3.1 and 3.2. The cost estimate is shown in Table 3.4 and a construction schedule is shown in Table 3.5. The total cost including contingency is 10 M\$. The much smaller bore for the solution (2) spin rotators would reduce the cost significantly.

	Number	Each K\$	Total K\$
Tooling additions and modifications			500
Siberian Snakes	4	388	1551
Spin Rotators	8	353	2821
EDIA: 10 MY @ 100 K\$			1000
Testing	12	50	600
Power Supplies and Controls	24	50	1200
Cryogenic leads	48	5	240
Subtotal			7911
Contingency @ 25%			1978
Total			9889

Table 3.4: Summary of the cost estimate for Siberian Snakes and spin rotators

	Start [month]	End [month]
Engineering planning and design	1	3
Detailed engineering and design	3	6
Tooling production and assembly	5	12
Parts fabrication and acquisition	7	12
Construction and assembly	13	18
Testing	14	20

Table 3.5: Schedule for construction of Siberian Snakes and spin rotators

4. ACCELERATION OF POLARIZED PROTONS IN RHIC

4.1. Depolarizing Resonance Strengths

Without Siberian Snakes there are numerous depolarizing resonances in RHIC, both intrinsic and imperfection resonances. The strengths of the intrinsic resonances can be calculated quite accurately from the appropriate integral over the horizontal focusing fields. Fig. 9 shows the result for the RHIC92 lattice with $\beta^* = 10\text{ m}$ at all intersections. A calculation with $\beta^* = 1\text{ m}$ gave only a slightly different result. The calculation was performed for a particle with a normalized Courant-Snyder invariant of $\varepsilon_0 = 10\pi\text{ mm mrad}$. For a different value of the invariant the strength scales according to

$$\epsilon = \epsilon_0 \sqrt{\frac{\varepsilon}{\varepsilon_0}}$$

where ϵ_0 is the resonance strength for the invariant ε_0 .

Important intrinsic spin resonances are located at

$$G\gamma = kP \pm \nu_y \approx mPM \pm \nu_B, \quad (4.1)$$

where k and m are integers, P is the superperiodicity of the accelerator, M is the number of FODO cells per superperiod, and $2\pi\nu_B = 2\pi(\nu_y - 6)$ is the accumulated phase advance of all FODO cells, which contain bending dipoles. The locations of the 3 strongest intrinsic resonances are

$$\begin{array}{lll} G\gamma = 3 \times 81 + (\nu_y - 6), & 5 \times 81 - (\nu_y - 6), & 5 \times 81 + (\nu_y - 6) \\ E = & 139\text{ GeV}, & 200\text{ GeV}, & 224\text{ GeV} \end{array}$$

where 81 is the product of superperiodicity, 3, and the “effective” FODO cells per superperiod, 27, which includes dispersion suppressors. The strengths of all 3 strong resonances are less than 0.5.

Important imperfection resonances are located at an integer closest to strong intrinsic resonances. This is clearly shown in the top part of Fig. 10 which shows the calculated imperfection resonance strengths for an uncorrected closed orbit obtained from a random sample of magnet misalignments with a rms spread of $\pm 0.5\text{ mm}$, dipole roll angles with a spread of $\pm 1\text{ mrad}$, dipole field errors of $\pm 5 \times 10^{-4}$, and position monitor errors of $\pm 0.5\text{ mm}$. After the closed orbit correction scheme MICADO was applied the strengths are greatly reduced as shown in the lower part for Fig. 10. The strengths of the imperfection resonances generally increase linearly with the beam energy and are bounded by

$$\epsilon_{imp} = 0.25 \frac{\gamma}{250} \sigma_y$$

where σ_y is the rms value of the residual closed orbit excursions. The strength is smaller than 0.04 for all energies.

4.2. Effect of Siberian Snakes

With the installation of Siberian Snakes, which are local 180° spin rotators, the spin tune becomes $1/2$, independent of the beam energy. Clearly the depolarizing resonance conditions cannot be met anymore as long as the fractional betatron tune $\Delta\nu_y \neq 1/2$ and therefore, in principle, no depolarization would occur. This is in fact true as long as the depolarizing resonances are not too strong. However, in the presence of strong resonances depolarization can occur from resonance conditions extended over more than just one turn. This leads to additional possible depolarizing resonance conditions:

$$\Delta\nu_y = \frac{\nu_{sp} \pm k}{n}$$

They are called Snake resonances[6] and n , the number of turns, is called the Snake resonance order. For two Snakes, as proposed here for RHIC, significant depolarization from Snake resonances only occurs for an intrinsic resonance strength of about 0.5 and even order Snake resonances require in addition an imperfection resonance strength of about 0.05. Fig. 11 shows the result of tracking through a region with an intrinsic resonance of strength 0.5 and an imperfection resonance of strength 0.05. There are clearly regions of the betatron tune that do not experience any depolarization. Since the betatron tunes of RHIC were chosen to be located between $4/5$ and $5/6$, the betatron tune could be fit between the Snake

resonances $13/16 = 0.8125$ and $5/6 = 0.8333$. With the betatron tune including its spread located between 0.815 and 0.830, a 0.015 range, no depolarization will occur over the whole RHIC energy range up to the top energy.

If the betatron tune spread is too large to fit into this range, some depolarization will be caused by the Snake resonance $\Delta\nu_y = 13/16$. Tracking calculations performed with an acceleration rate of $\dot{\gamma} = 3.9$ /sec showed that a gaussian beam with $\varepsilon_{N,95\%} = 20 \pi \text{ mm mrad}$ and with 10 % of the beam overlapping the 13/16 Snake resonance less than 5 % of the polarization is lost for each passage through one of the strong intrinsic resonances. The final polarization after passing all 3 strong resonances would then be at least 86 % of the injected polarization. It is important to note that, unlike for electron beams, the betatron tune distribution within the proton beam is basically static and does not get mixed. This means that depolarization experienced by a part of the beam is confined to this part only and will not affect the whole beam. In other words, there is no diffusion of polarization.

4.3. Sextupole Depolarizing Resonances

Spin resonances arising from sextupoles are located at

$$\nu_{sp} = kP \pm \nu_x \pm \nu_y = mPM \pm (\nu_x - 6) \pm (\nu_y - 6)$$

with resonance strength given by,

$$\epsilon_K \approx \frac{1 + G\gamma}{8\pi} \sqrt{\frac{\varepsilon_x \varepsilon_y}{\pi^2}} \sqrt{\beta_x \beta_y} PM(|S_F| + |S_D|),$$

where S_F, S_D are respectively strengths of sextupoles located at the focusing and defocusing quadrupole locations. Because the emittance decreases with energy, the sextupole spin resonance strength is energy independent in hadron storage rings. For RHIC, the resonance strength is about 0.0003 at a normalized emittance of $20 \pi \text{ mm mrad}$. Such a sextupole driven resonance has been observed in the IUCF Cooler Ring. However, because of their small spin resonance strength, depolarizing resonances due to sextupoles are not important as long as the betatron tunes are chosen to avoid the resonance condition, which for a spin tune of $1/2$ is

$$\frac{1}{2} = kP \pm \nu_x \pm \nu_y$$

The current working point for RHIC certainly avoids this condition.

4.4. Spin Tune Spread and Modulation

With snakes, the spin tune is independent of energy. Therefore the synchrotron motion does not give rise to spin tune spread. This has been verified indirectly in the snake experiment at the IUCF Cooler Ring, where one finds that there is no depolarization at the synchrotron side band for a 100% snake. However the spin tune modulation may still arise from imperfect spin rotation in the snake, and imperfect orbital angle between snakes. The errors in orbital angle may arise from survey error, closed orbit error, and/or betatron motion.

For an imperfection resonance strength $\epsilon = 0.05$ with two snakes, the perturbed spin tune shift is given by, $\Delta\nu_{sp} = \frac{\pi|\epsilon|^2}{4} = 0.002$. The error in the spin rotation angle of two snakes contributes also to the imperfection resonance strength. Assuming that the relative error of the integrated field strength of each snake dipole is 10^{-3} , the error in the spin rotation angle of a snake should be about $\sqrt{8} \times 180 \times 10^{-3} = 0.5^\circ$, where we have assumed that a snake is constructed from 8 dipoles. The effect of 2 snakes in the accelerator will give a resonance strength of the order $\epsilon_{imp}^{eq} \approx 0.004$, which is smaller than the imperfection resonances due to closed orbit errors.

The error $\Delta\theta$ in the orbital angle between the two snakes can give rise to a spin tune shift of $\Delta\nu_{sp} = \frac{1}{\pi}G\gamma\Delta\theta$. Since the error in the orbital angle gives rise to spin tune shift and not a spin tune spread, one can compensate the effect by adjusting the spin rotation axes of the snakes. A survey error of about $\Delta\theta \approx 0.1 \text{ mrad}$ leads to a spin tune shift of 0.01 at the highest energy. For such a survey error, active compensation by adjusting the snake spin rotation axes is needed but is well within the tuning range of the Snake design.

The closed orbit can also cause orbital angle error between snakes. Let us assume that the maximum closed orbit is about $\hat{a} \approx 6\sigma \approx 1.0 \text{ mm}$. The angular deviation is of the order of $\Delta x'_{co} \approx \frac{\hat{a}}{\sqrt{\beta\hat{\beta}}}$, where \hat{a} is the maximum orbit error and $\sqrt{\beta\hat{\beta}} \approx \frac{R}{\nu}$ is the average betatron amplitude function. The expected error is about $\Delta x'_{co} \approx 2 \times 10^{-5}$ for RHIC, which gives rise to a spin tune shift of 0.002.

Similarly the betatron oscillation can cause orbital angle modulations. The spin tune modulation is given by

$$\Delta\nu_{s,\beta} \approx \frac{1}{\pi}G\gamma\sqrt{\frac{\epsilon}{\beta}} = \frac{1}{\pi}G\sqrt{\frac{\gamma\epsilon_N}{\beta}}$$

The resulting spin tune spread is about 0.007 for a beam with $20\pi \text{ mm-mrad}$ normalized emittance at 250 GeV.

Combining all the possible sources, we expect that the total spin tune *spread* to be about 0.009 (imperfection resonance and betatron motion) and a correctable spin tune *shift* of 0.012 (Snake survey error and closed orbit error).

4.5. Betatron Tune Spreads and Modulations

In avoiding snake resonances up to the 13th order, the available tune space is about 0.015. With a spin tune spread of 0.009, the betatron tune needs to be controlled to better than 0.006. The tight requirements for the spin and betatron tune spread are only relevant while accelerating through the 3 strong intrinsic resonances when the beam-beam tune shift is negligible.

At the injection energy, the space charge tune spread can be as large as 0.02 for RHIC. However, the corresponding spin resonance strength at low energy is also about a factor of 3 smaller and therefore the available tune space is much larger.

5. STORAGE OF POLARIZED PROTONS IN RHIC

In storage mode even a very small depolarizing resonance strength can in principle lead to significant depolarization. This was observed at the ZGS where the effect of high order depolarizing resonances were studied on a 1 second flat top as shown in Fig. 12[11]. In an accelerator without Snakes like the ZGS the spin tune is energy dependent ($\nu_{sp} = G\gamma$) and therefore if the resonance condition is within the energy spread of the beam each proton will cross the resonance condition repeatedly and eventually the whole beam can be depolarized. With Snakes, however, the spin tune is energy independent and therefore all Snake resonance conditions are energy independent. As pointed out earlier and shown in Fig. 11 the beam can overlap higher order Snake resonances due to the betatron tune spread. Results of spin tracking calculations for a proton with $\Delta\nu_y = \frac{13}{16}$ and a Snake resonance strength of 0.15 showed that the spin vector is precessing about the vertical axis. At a resonance strength of 0.15, the vertical projection is about 90%. This precession is in fact a spin closed orbit in a broader sense of 16 turns. Spin tracking calculations were calculated over 8×10^9 turns without significant deviations from this spin closed orbit. Only a small fraction of particles are located within the width of the resonance and therefore effective depolarization in the storage mode is small.

When the spin vector is acted on with an adiabatic modulation within the tolerable limit, the spin vector will follow the spin closed orbit adiabatically. Non-adiabatic processes, arising from rf noise at the spin precession frequency, can indeed cause beam depolarization. Let us consider that a single dipole with strength θ_k is modulated at $\nu_{sp}f_0$, which is about 39 kHz for RHIC. The corresponding induced spin precession kick is $G\gamma\theta_k$. The number of turns that occur before the spin is perturbed to 80% of the original polarization is given by,

$$N_p = \frac{\arccos[0.8]}{G\gamma\theta_k}$$

Let us now consider the same angular kick to the orbital motion. If there is an rf source at $\nu_{sp}f_0$, one expects a similar angular kick at the frequency qf_0 , where q is the fractional part of the betatron tune. The orbital survival turn number is given by

$$N_o = \frac{A}{\langle\beta\rangle\theta_k}$$

where $\langle\beta\rangle$ is the average betatron amplitude, and A is the dynamic aperture. Using $A = 0.01$ m, $\langle\beta\rangle = 20$ m for RHIC, we find that the orbital lifetime is only half as long as the polarization lifetime.

Indeed, any rf source at high frequencies around the synchrotron and betatron tunes, are dangerous to the orbital stability of particles in accelerators. Similarly, any rf source at the spin tune can cause beam depolarization. These high frequency rf sources should be addressed carefully in hardware design.

6. MEASURING THE BEAM POLARIZATION IN RHIC

6.1. Polarimeter Lay-out

We propose to construct two polarimeters that are capable of measuring the polarization of the circulating beam in each ring independently at various stages in the acceleration cycles.

These polarimeters utilize the asymmetries (A_n) in inclusive pion production at high X that were measured at the Argonne ZGS [12] and at Fermilab[13]. The asymmetries increase linearly with X and appear to be independent of the incident polarized beam momentum. Moreover, the ZGS data which were taken with both liquid hydrogen and deuterium targets show no dependence on target nuclei.

Since these polarimeters will use a fixed target, the ZGS and Fermilab measurements cover the full energy range of the RHIC beams. We would like to measure the pion asymmetry at the desired kinematic region at the AGS to obtain directly the analyzing power at the RHIC injection energy, and to verify the apparent energy independence of the analyzing power. The polarimeters are designed to probe the kinematic region of 0.5 in X and $0.8 \text{ GeV}/c$ in transverse momentum of the scattered pions. This was optimized from the Fermilab data based on the fact that the asymmetry rises linearly with X while the cross section is falling as $(1 - X)^2$, and that the error in the asymmetry measurement is the inverse of the square root of the total number of events.

We propose to use π^- asymmetry, since π^- are a relatively large fraction of negatives, and particle identification is therefore not necessary. At the chosen parameters, the measured π^- asymmetry is 18% and the invariant cross section is about $100 \frac{\mu b}{\text{GeV}^2}$ [14].

The polarimeters are designed to fit in the 40 meter long straight sections between Q3 and Q4. The apparatus consists of a $5 \mu m$ carbon fiber target, followed by a 2 meter long dipole magnet with a $1 \text{ GeV}/c$ transverse momentum kick,

and then a hadron calorimeter. The scattering angle and selected spectrometer momentum depend on the beam energy: at RHIC injection of $25\text{ GeV}/c$, the scattering angle would be 64 mrad and the π^- momentum $12.5\text{ GeV}/c$; at $250\text{ GeV}/c$ RHIC beam momentum, the scattering angle is 6.4 mrad and the π^- momentum is $125\text{ GeV}/c$. For the smallest angle, 6.4 mrad , the spectrometer magnet will be 30 meters from the target, giving a 20 cm. displacement from the beam center. The magnet aperture will be 3 cm.(H) x 6 cm.(V), and the small angle position constrains the magnet septum width. The detector system will extend 10 meters downstream from the magnet. The magnet kick and the positioning of the downstream detection elements will minimize the contamination from straight through neutrals. Upstream of this magnet we envisage using collimation to cut down on background. The detection apparatus will consist of several trigger counters followed by a hadron calorimeter with energy resolution $\frac{\Delta E}{E} = 40\%/\sqrt{E}$, with E in GeV. This provides an 11 % measurement at $12.5\text{ GeV}/c$. The whole assembly will rotate in order to accommodate the changes in the scattered angle as the circulating beam energy increases. In addition, we require that the magnet and detector move upstream for the lower energy, wide-angle measurements. An increased acceptance is necessary at lower energy due to lower rates: the emittance blow-up from multiple-scattering in the fiber target over the measuring time must be kept to within acceptable limits. The table below uses a 9.5 meter position for the magnet for the 25 GeV measurements. We also envision that the assembly will translate together with the fiber target when the target is moved into the beam, maintaining a fixed geometry independent of the transverse position of the target.

We use a $5\text{ }\mu\text{m}$ carbon fiber target, a π^- momentum bite of 0.1. $X = .5$, and $p_T = 0.8\text{ GeV}/c$ in the following table. $10^4\text{ }\pi^-$ are collected to obtain a 5 % error in polarization. The emittance increase from multiple scattering is proportional to the lattice β function at the fiber target, so we must place the target near Q4 in the RHIC lattice and scatter toward the intersection region, giving $\beta = 25\text{ m}$ at the fiber target. (The polarimeter measurements are for short periods, and the experiment at that intersection region would be gated off for these periods.) We obtain the following table:

	25 GeV	250 GeV
$\Delta\Omega$	$20 \mu sr$	$2 \mu sr$
$\Delta\epsilon_N$	$4 \pi mm mrad$	$0.04 \pi mm mrad$
interacting beam fraction:	2×10^{-3}	2×10^{-4}
measuring time:	$3 s$	$0.1 s$

These calculations are for 57 bunches and 10^{11} protons/bunch. The emittance growth at 25 GeV is about 20 % for the measurement. Thus, the measurements at 25 GeV would be considered destructive. Measurements at 250 GeV can be parasitic. Beam loss from nuclear interactions is quite small – about 0.2 % for the 25 GeV measurements. As can be seen from the table, measurement time is quite short. The target thickness, acceptance, and number of bunches used (for example, for commissioning) will be optimized, since these choices depend on the number of stored protons, rates in the detector, and the desired polarization error.

6.2. Heating of the Carbon Fiber

To minimize the contribution of multiple scattering to the emittance growth, the polarimeter fiber is located close to Q4. The betatron functions in x and y are small and similar at this location [RHIC Conceptual Design Rep., p.74]

$$\beta_{x,y} \simeq 25 m$$

We then obtain the rms beam size for the worst case, 250 GeV,

$$\sigma = \sqrt{\frac{\beta\epsilon_N}{\pi\gamma}} = 2.43 mm$$

Since $\sigma \gg d_{fiber}$ the irradiation of the fiber is essentially uniform (i.e. there isn't any "hot spot" at the beam core).

Since we will fill only 52 bunches, the bunch interaction frequency is $f_B = 52 \times 78.2 kHz = 4.07 MHz$. Incident power

$$P_i = N \left(\frac{2Rd}{\pi R^2} \right) f_B \frac{dE}{dx} \rho d = 150 mW$$

and radiated power

$$P_r = \sigma_B \epsilon R d T^4 = 2.16 \times 10^{-15} T^4$$

The equilibrium temperature is then

$$T_{eq} = \left(\frac{2N f_B \frac{dE}{dx} \rho d}{\pi \sigma_B \epsilon R^2} \right)^{\frac{1}{4}} = 2880 \text{ K}$$

This is about 700 degrees below the sublimation temperature of Carbon.

7. LUMINOSITY OF POLARIZED PROTON COLLISIONS

The luminosity at the RHIC beam energy $E[GeV]$ is given by[15]

$$\mathcal{L} = 5.7 \times 10^{31} \frac{\left(\frac{N_B}{10^{11}}\right)^2 \left(\frac{B}{57}\right) \left(\frac{E}{250}\right)}{\left(\frac{\epsilon_N}{20\pi}\right)^2} \text{ cm}^{-2} \text{ s}^{-1}$$

where B is the number of bunches in each ring, N_B is the number of particles per bunch, and ϵ_N is the normalized emittance. Thus the polarized proton luminosity will be $2 \times 10^{32} \text{ cm}^{-2} \text{ s}^{-1}$, which corresponds to two interactions per crossing for the $B = 57$ bunches per ring. Note the importance of smaller emittance in obtaining higher luminosity. The luminosity will gain a factor of four when the emittance is smaller by a factor of two. This is due to the fact that the betatron amplitude function β^* at the interaction point can be squeezed by a factor of two at the smaller emittance while maintaining the same dynamic aperture at the high betatron amplitude quadrupole triplets. This is also the reason behind the linear dependence of the luminosity on energy, since the unnormalized emittance depends on $E^{-\frac{1}{2}}$.

We show in Fig. 13 the luminosity vs. energy as described above ("enhanced luminosity"), emphasizing the linear dependency of the luminosity with energy. The RHIC design luminosity for proton-proton is also shown which, for the emittance used above, would represent 5×10^{10} protons per bunch.

8. SPIN REVERSAL OF THE STORED BEAMS

Since the proposed asymmetry measurements are high precision measurements, frequent polarization sign reversal is imperative to avoid systematic errors. Possible sources for systematic errors are luminosity variations, crossing angle variations, and detector efficiency variations. As mentioned earlier different bunches will have different polarization sign and therefore different bunch crossings will measure interactions with different combinations of incoming beam polarization signs. Although this will greatly reduce systematic errors it is still true that one pair of bunches would always cross with the same combination of polarization signs during the whole lifetime of the stored beams which is at least several hours. To eliminate the possibility of systematic errors from this situation we propose to install a spin flipper in each ring which is capable of reversing the polarization sign of all bunches. The spin flipper consists of three horizontal DC dipole magnets interleaved with three laminated vertical dipole magnets[8]. Exciting the vertical magnets with about 40 kHz AC current would drive an artificial spin resonance which can be used to adiabatically reverse the polarization direction. Fig. 14 shows the result of a test of this concept performed at the Indiana University Cyclotron Facility (IUCF)[10]. We estimate that complete spin reversal would take less than 1 second.

The same device will be used to accurately measure the spin tune by measuring the spin reversal efficiency as a function of the frequency of the spin flipper excitation. This is instrumental to adjust the spin tune to 0.500.

Since the orbit might not be completely corrected by the spin flipper magnets, emittance blow-up could result the residual beam deflection. The total deflection in the vertical magnets is about $100\text{ }\mu\text{rad}$ at 25 GeV and correspondingly less at higher energies. The residual deflection can then be less than $\Delta y' = 1\text{ }\mu\text{rad}$. The betatron amplitude after n turns is then

$$\begin{aligned} y &= \beta \Delta y' \sum_{m=1}^n \cos(2\pi\nu_{sp}m) \sin(2\pi\nu_y(n-m)) \\ &= \frac{1}{2}\beta \Delta y' \left[\cos(2\pi\nu_y n) - \sin(2\pi\nu_y) \frac{\cos(2\pi\nu_{sp}n) - \cos(2\pi\nu_y n)}{\cos(2\pi\nu_{sp}) - \cos(2\pi\nu_y)} \right] \end{aligned}$$

with a maximum value of 0.024 mm for $\nu_{sp} = 0.5$ and $\nu_y = 0.8$. This results in a contribution of $7 \times 10^{-4} \pi \text{ mm mrad}$ to the normalized emittance of the beam. The above formula is only valid if the coherence of the kicked beam is maintained. In reality the motion will decohere but not faster than within about 100 turns, corresponding to a tune spread of less than 0.01. As a result the emittance will increase linearly during the time the spin flipper is on. However, the emittance increase is less than

$$\frac{1\text{ s} \times f_{rev}}{100} \times 7 \times 10^{-4} \pi \text{ mm mrad} = 0.6 \pi \text{ mm mrad}$$

which is negligible compared to the $20 \pi \text{ mm mrad}$ beam emittance.

9. OPERATIONAL MODES OF RHIC FOR POLARIZED PROTON RUNNING

For normal operation no special operational modes of RHIC are required for the acceleration and storage of polarized protons. Since depolarizing resonances are driven predominantly by vertical orbit excursions, particular care has to be given to the corrected vertical closed orbit and the vertical beam emittance. This means that beam blow-up from beam-beam interactions and stop-bands should be minimized. To avoid depolarization from snake resonances the fractional vertical betatron tune including tune spread has to be kept well within $\frac{13}{16} = 0.8125$ and $\frac{5}{6} = 0.8333$, especially at the energies of the 3 strongest intrinsic resonances: $G\gamma = 3 \times 81 + (\nu_y - 6)[E = 139 GeV]$, $5 \times 81 - (\nu_y - 6)[E = 200 GeV]$, $5 \times 81 + (\nu_y - 6)[E = 224 GeV]$. Also the acceleration rate would have to be at least $\dot{\gamma} = 4.2 s^{-1}$, which corresponds to $\frac{dB}{dt} = 0.05 T/s$.

During commissioning, acceleration cycles that allow for polarization measurements at various energies are required, in particular at the injection energy, at energies below and above the 3 strongest intrinsic resonances, and at some intermediate energies: $25 GeV$, $50 GeV$, $100 GeV$.

10. CONCLUSIONS

Polarized Proton acceleration and storage in RHIC have been carefully examined. We found that

1. The current polarized ion source at the AGS is capable of providing a sufficient number of polarized protons for RHIC
2. The partial Snake experiment at the AGS, E880, will provide the bunch beam intensity of $N \geq 2 \times 10^{11}$ and $\varepsilon \leq 20\pi mm mrad$ at 25 GeV.
3. Two Snakes per ring in RHIC will allow for the acceleration of polarized beams.

Relevant issues such as spin tune and betatron tune spread, the Snake and spin rotator design and their effect on the lattice functions, polarimeters in RHIC, and the polarization lifetime have been carefully addressed. It is indeed technically feasible to achieve polarized proton beam collisions in RHIC at a luminosity of $2 \times 10^{32} cm^{-2} s^{-1}$.

11. FIGURE CAPTIONS

1. Layout of the AGS-RHIC accelerator complex showing all the major component that are necessary for the acceleration of polarized proton beams to the RHIC top energy.
2. View of RHIC overemphasizing the interaction regions to show the location of the Siberian Snakes and the spin rotators placed around the collider experiments STAR and PHENIX. Also shown are the polarization directions around the rings and around the detectors for collisions with longitudinal polarization.
3. Maximum beam orbit excursions inside the spin rotators for longitudinal polarization at the collision point shown as a function of beam energy.
4. Orbit and spin tracking through the seven magnet Siberian Snake at $\gamma = 200$. The spin tracking shows the reversal of the vertical polarization.
5. Change of the direction of the Snake rotation axes as function of the excitation of the horizontal and vertical dipole strings.
6. Top view of the horizontal polarization immediately after the spin rotator which rotates the vertical polarization into the horizontal plane. The sign of the horizontal (ψ_H) and vertical (ψ_V) bending magnets is shown in order to obtain polarization in the indicated quarter of the plane.
7. Orbit tracking through the spin rotator solution 1. The top figure shows the tracking for the excitation that produces longitudinal polarization, the bottom figure is for radial polarization. The orbit excursions are calculated for $\gamma = 200$.
8. Orbit tracking through the spin rotator solution 1. The top figure shows the tracking for the excitation that produces longitudinal polarization, the

bottom figure is for radial polarization. The orbit excursions are calculated for $\gamma = 200$.

9. Strengths of the intrinsic depolarizing resonances in RHIC calculated for the RHIC92 lattice and for both $\beta^* = 10\text{ m}$ and $\beta^* = 1\text{ m}$ at all six intersection points. There is no noticeable difference of the calculated strengths for the two values of β^* .
10. Strengths of the imperfection depolarizing resonances in RHIC calculated after simulating the MICADO orbit correction scheme.
11. Vertical component of the polarization after acceleration through a strong intrinsic resonance and a moderate imperfection resonance shown as a function of the fractional vertical betatron tune.
12. Depolarization on the 1 second flat top at the ZGS.
13. Expected luminosity (enhanced luminosity) as a function of energy for a normalized 95 % emittance of $20\pi\text{ mm rad}$ and $\beta^* = 2\text{ m}$. The RHIC design luminosity for proton collision is also shown.
14. Adiabatic spin reversal of a stored beam of polarized protons at the IUCF Cooler ring. The RF voltage is proportional to the strength of the artificial spin resonance driving the spin reversal.

BIBLIOGRAPHY

- [1] Proposal on Spin Physics Using the RHIC Polarized Collider (R5), submitted to the BNL PAC October 1992
- [2] J.G. Alessi et al., AIP Conf. Proc. No. 187, p. 1221 (1988)
- [3] F.Z.Khiari et al., Phys. Rev. D39, 45 (1989)
- [4] T.Roser, AIP Conf. Proc. No. 187, p.1442 (1988)
- [5] S.Y.Lee and E.D.Courant, BNL Technical Note AD/RHIC-63
- [6] S.Y.Lee and S.Tepikian, Phys. Rev. Lett. 56, 1635 (1986)
- [7] S.Y.Lee, Nucl. Inst. Methods, A306, 1 (1991)
- [8] T.Roser, Spin Rotators and Split Siberian Snakes, submitted to NIM A.
- [9] A. Luccio and M. Conte, Wiggler as Spin Rotators for RHIC, contribution to 1993 Particle Accelerator Conf., Washington, D.C.; E.A. Perevedentsev, V.I. Ptitsin and Yu.M. Shatunov, Spin Behavior in Helical Undulators, to be published.
- [10] V.A.Anferov et al., IUCF Newsletter No. 50, p. 11 (1992)
- [11] L.Ratner, private communication.
- [12] Dragoset et al., Phys. Rev. D 18, 3939 (1976)
- [13] D.L.Adams et al., Phys. Lett. B264, 462 (1991)
- [14] L.G. Ratner et al., Proc. of the Rochester Meeting APS/DPF, Rochester, p. 99 (1971)
- [15] S.Y.Lee, in Proc. of the Polarized Collider Workshop, Penn State University, 1990, AIP Conf. Proc. No. 223, p. 30 (1991)

POLARIZED PROTON COLLISIONS AT BROOKHAVEN

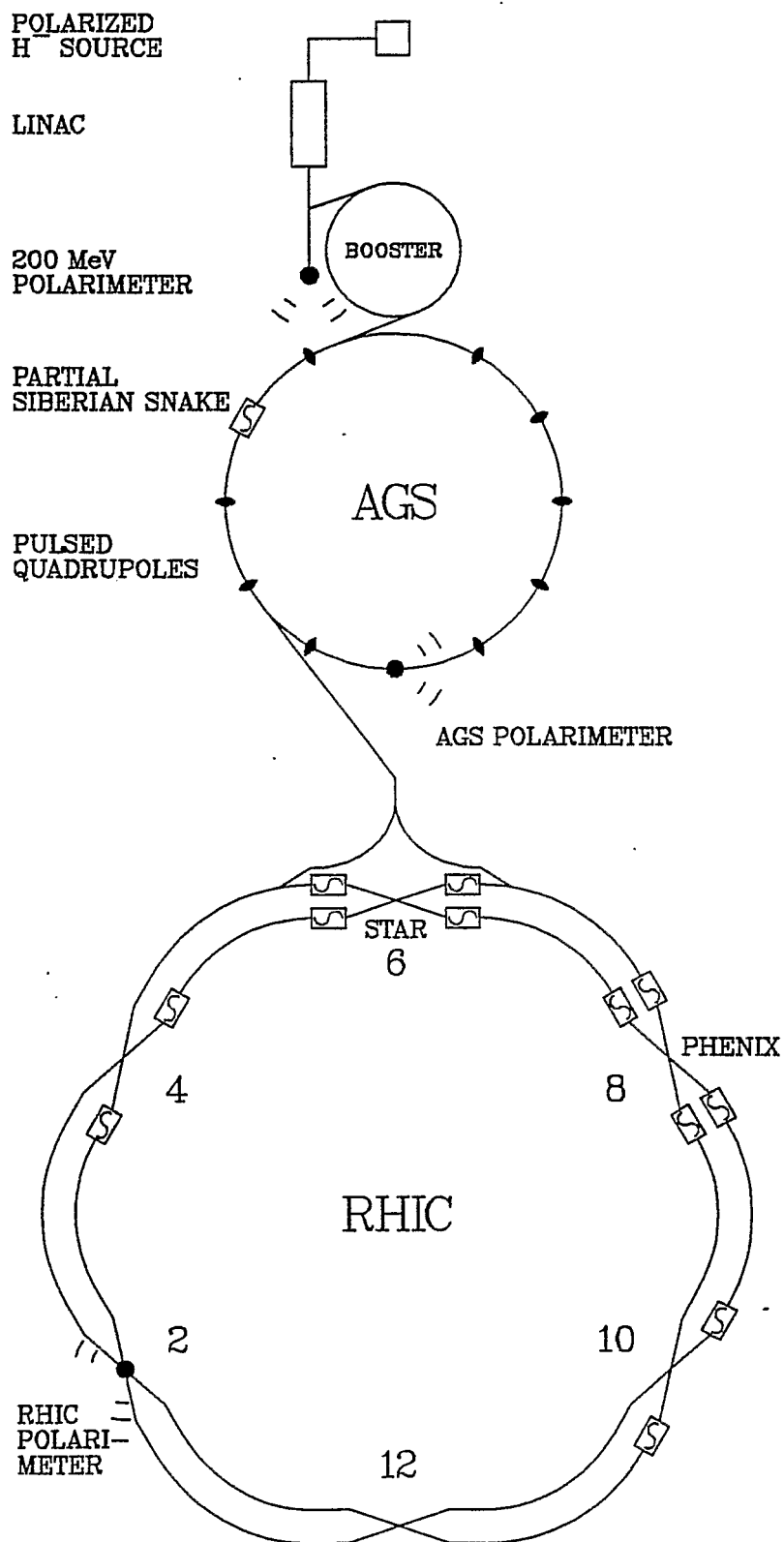


Figure 1

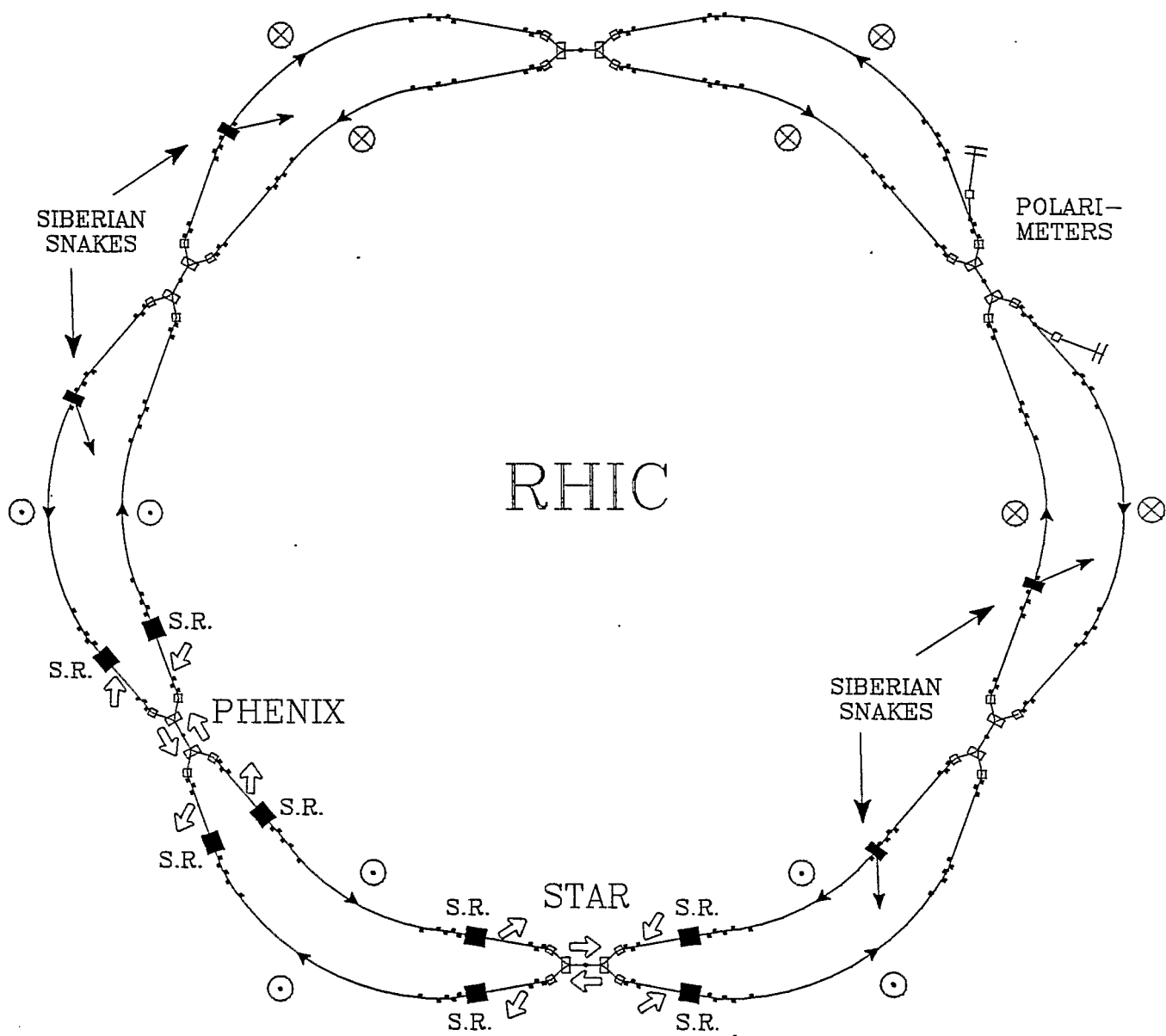


Figure 2

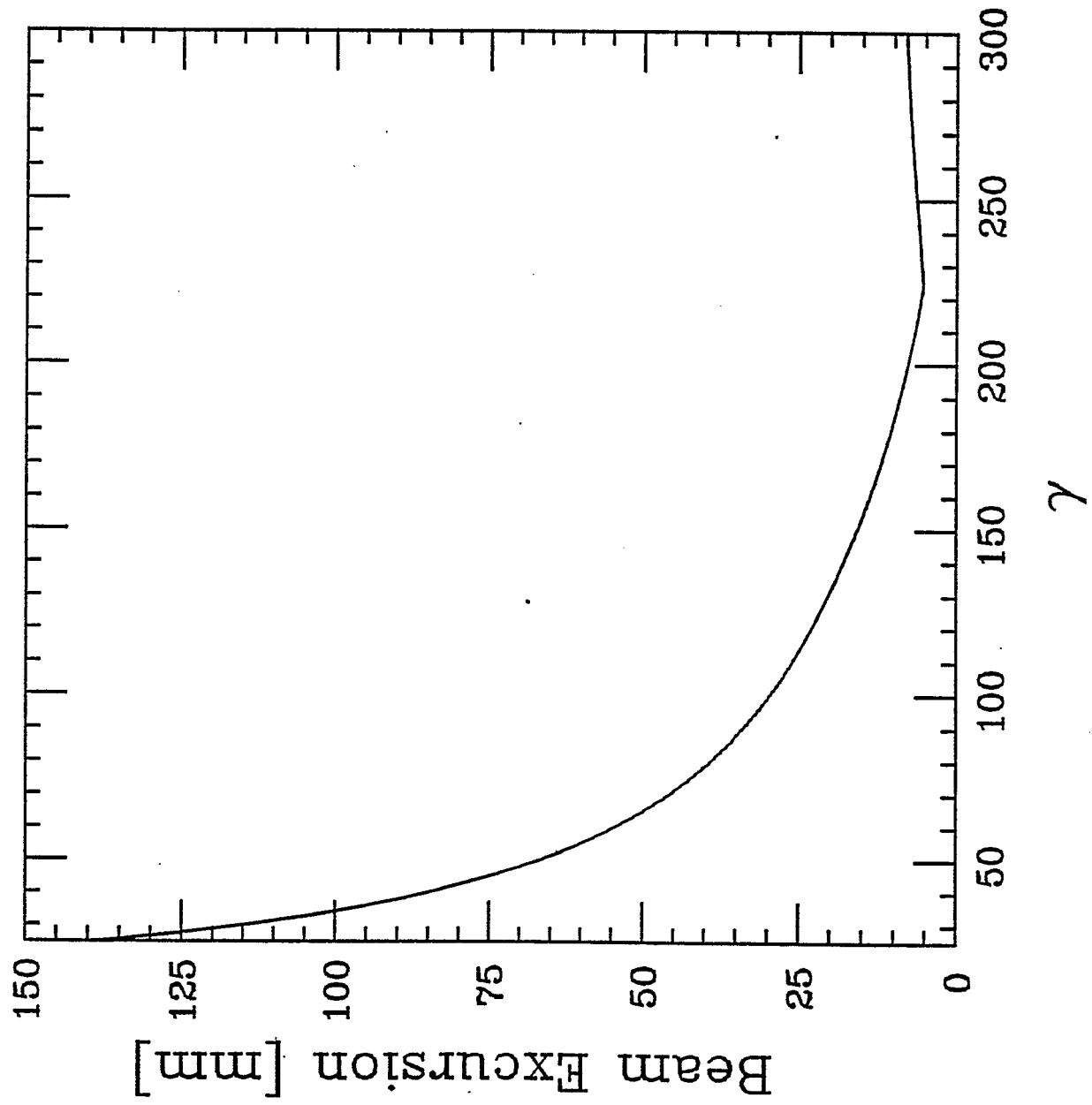


Figure 3

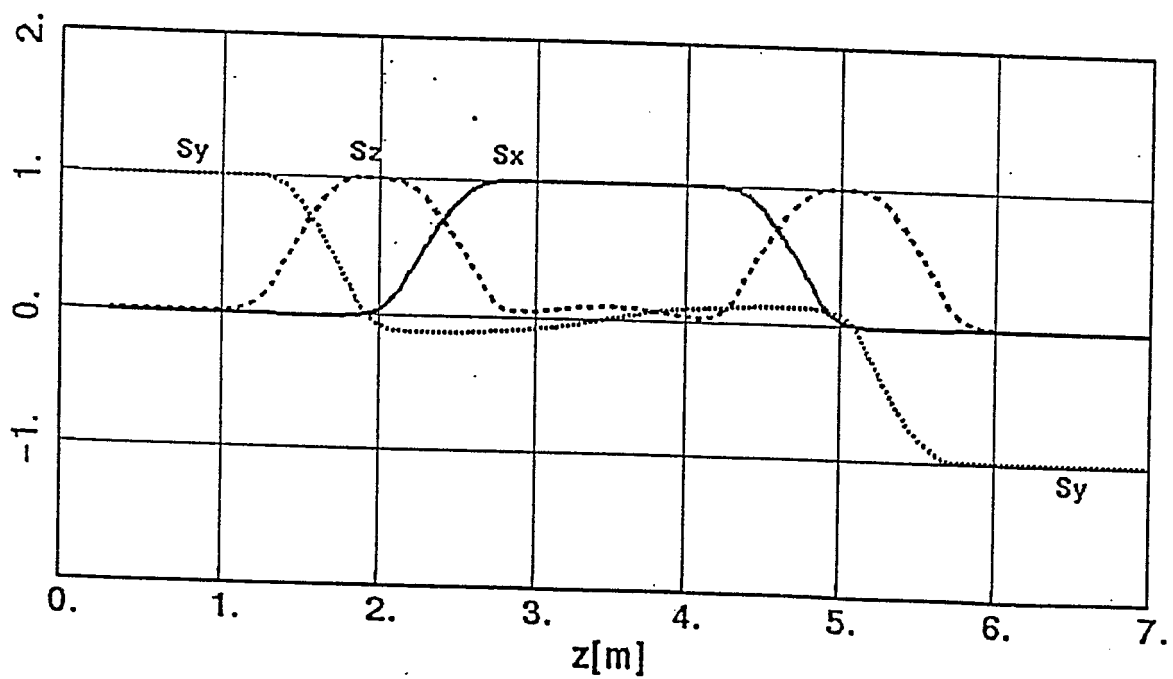
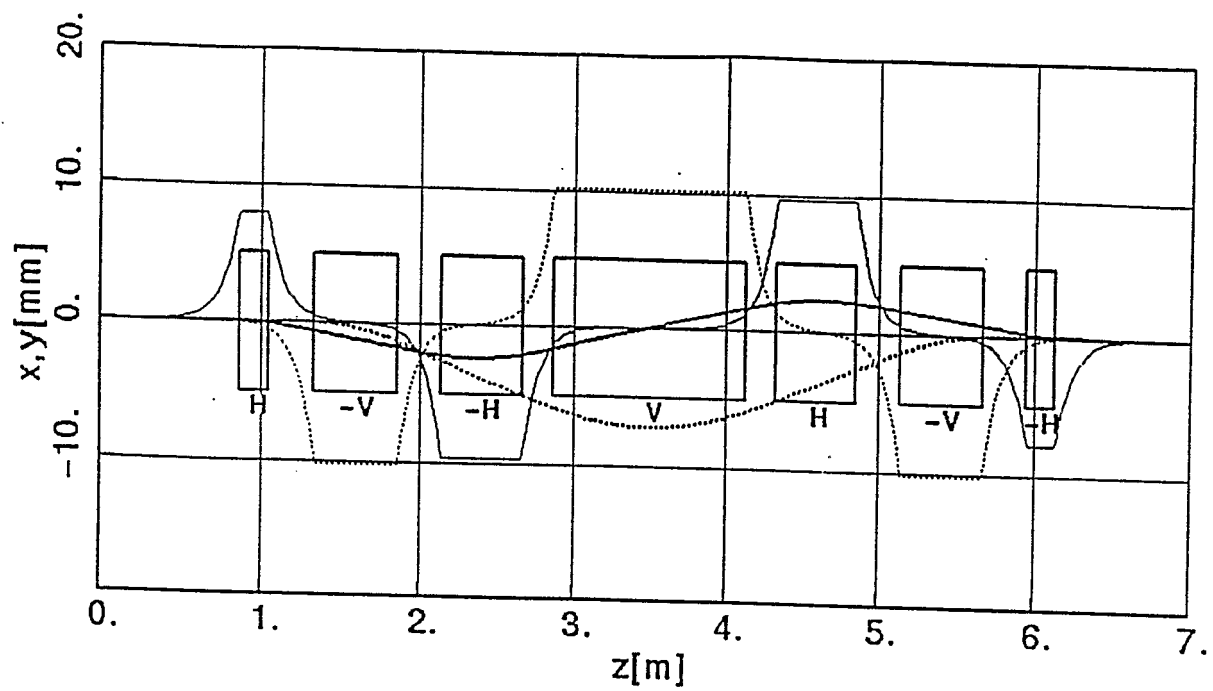


Figure 4

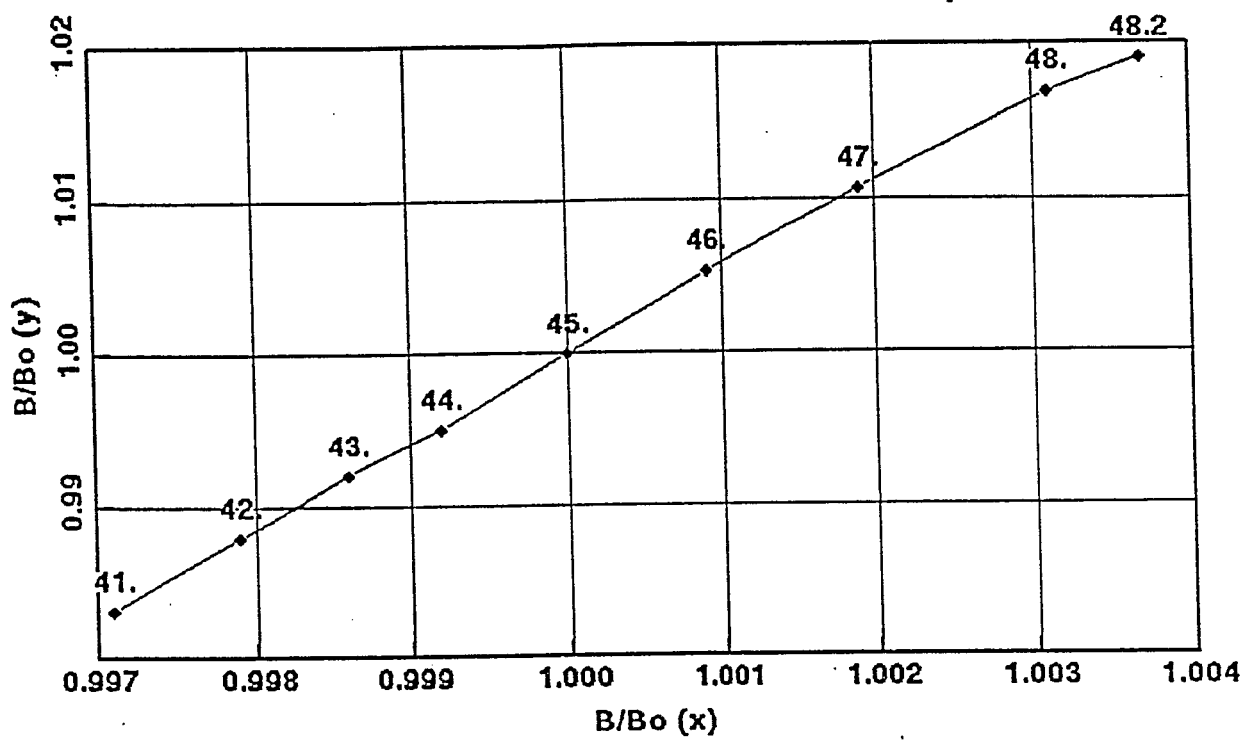


Figure 5

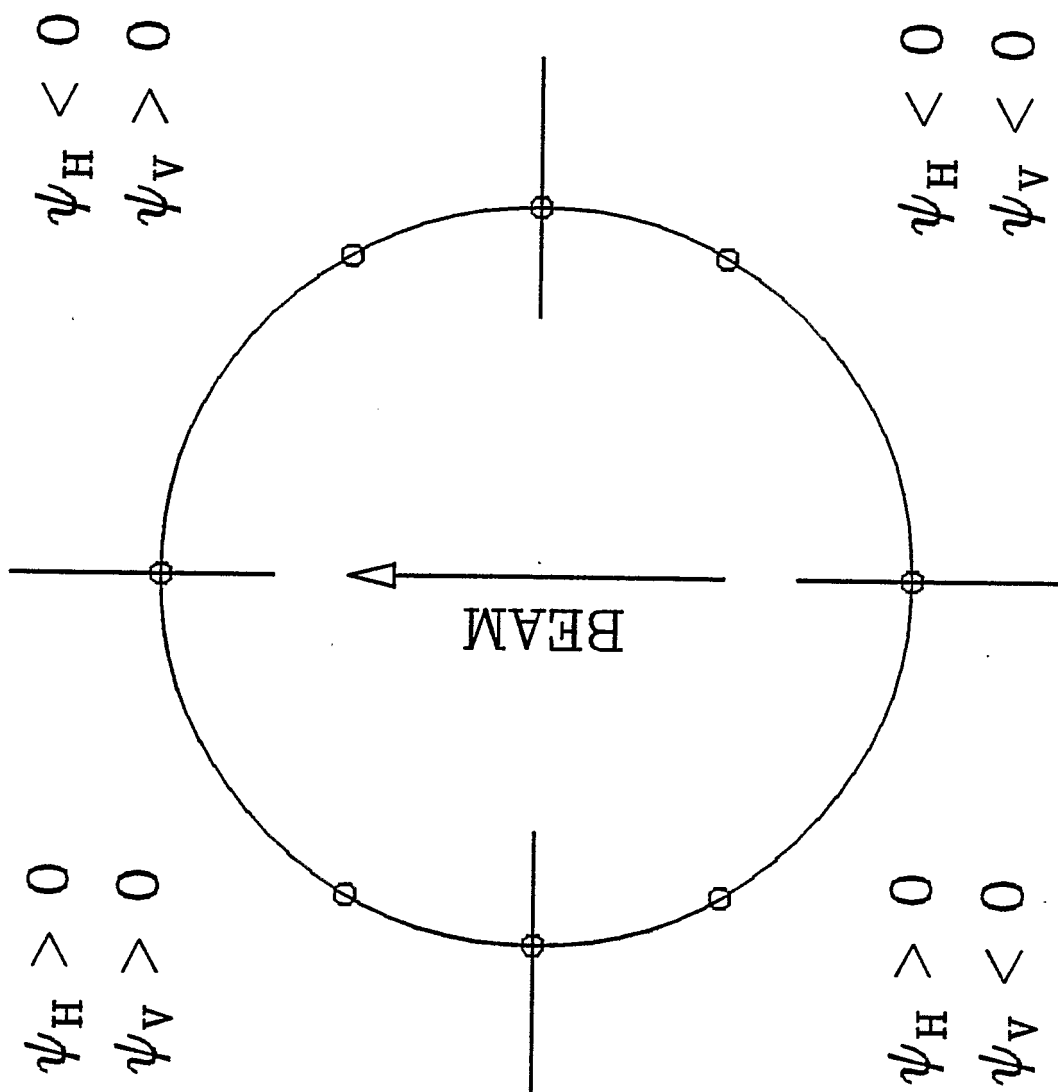


Figure 6

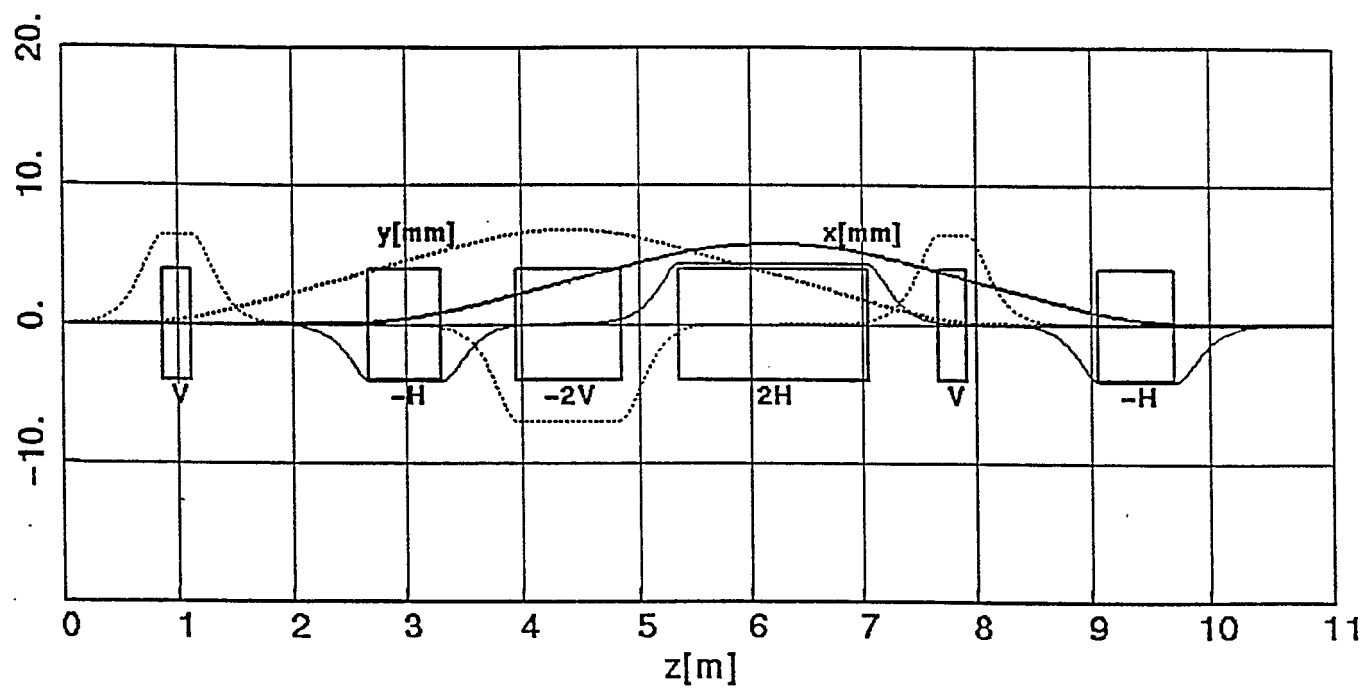
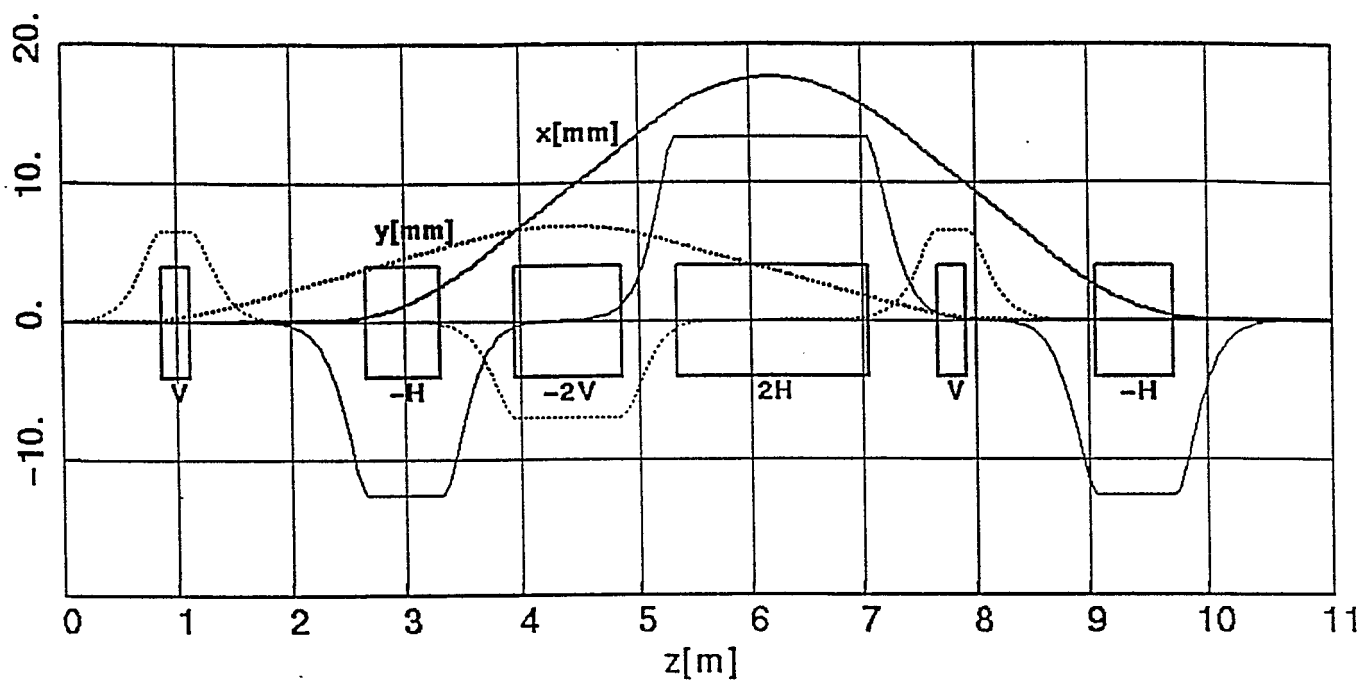


Figure 7

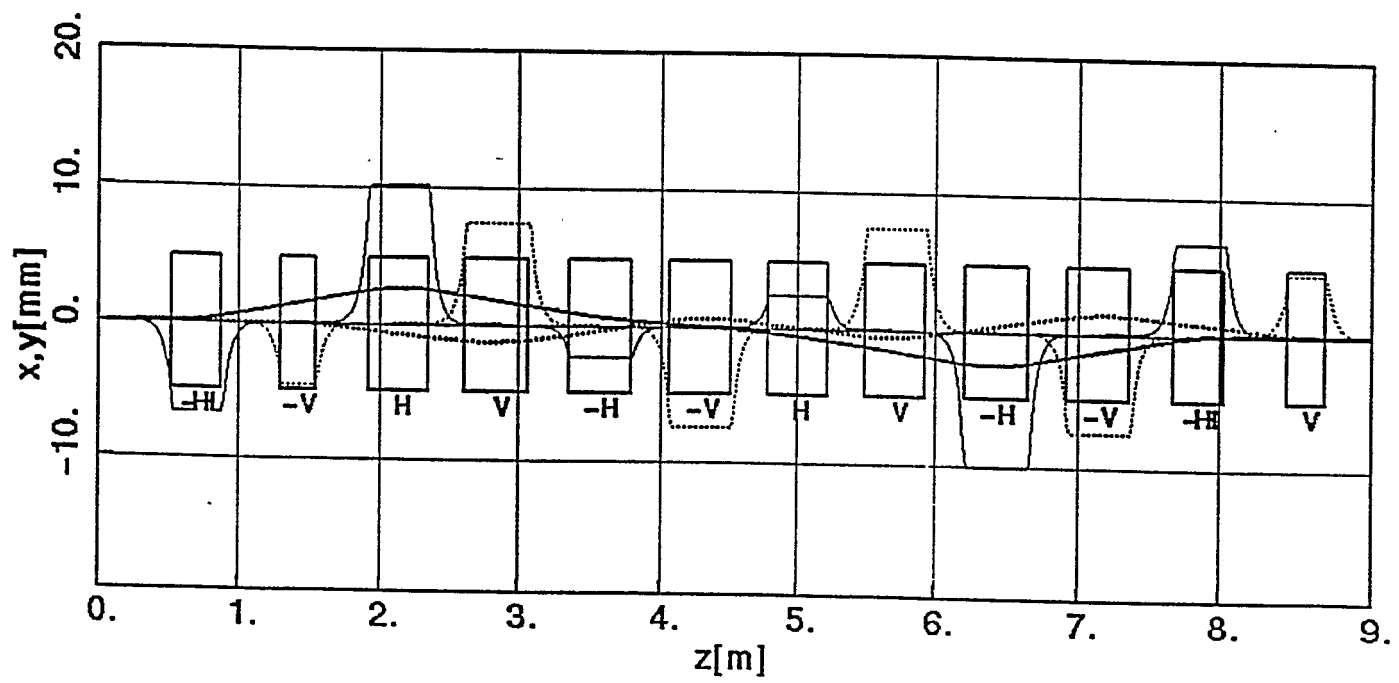
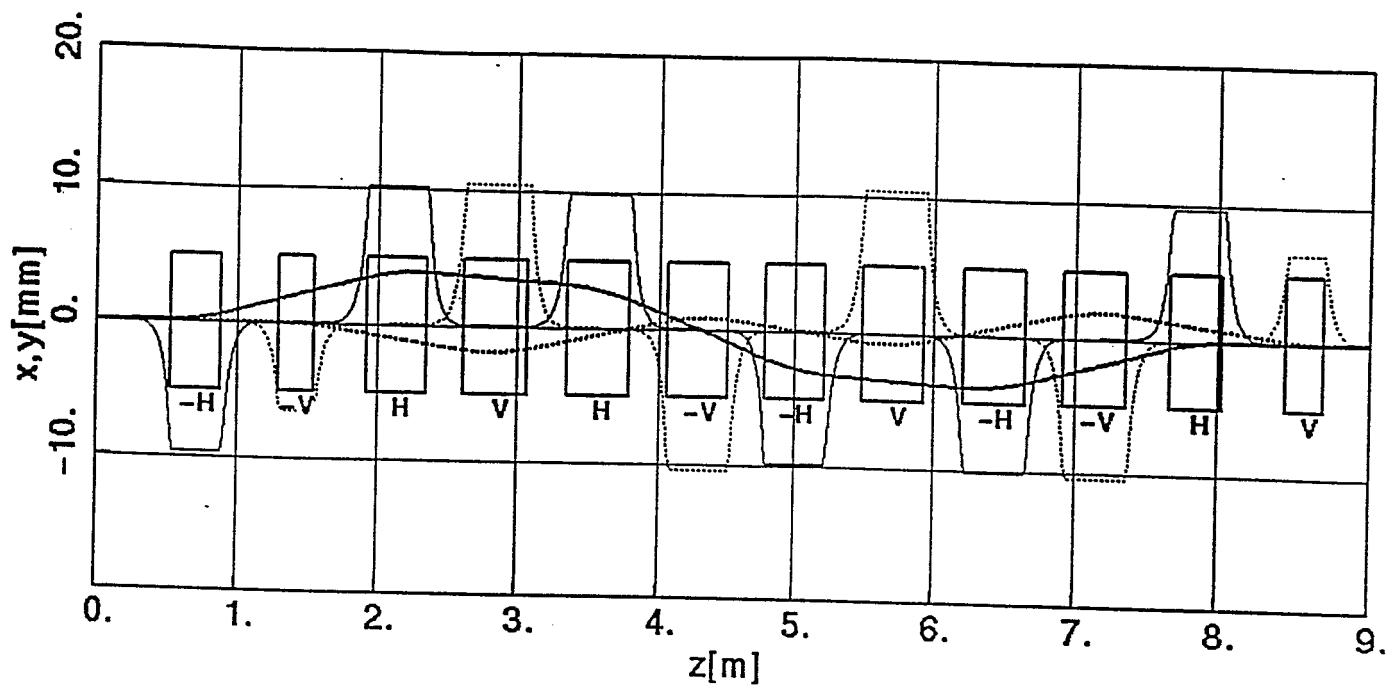


Figure 8

Intrinsic resonance strength

RHIC; invar. emittance $10 \mu\text{rad-m}$

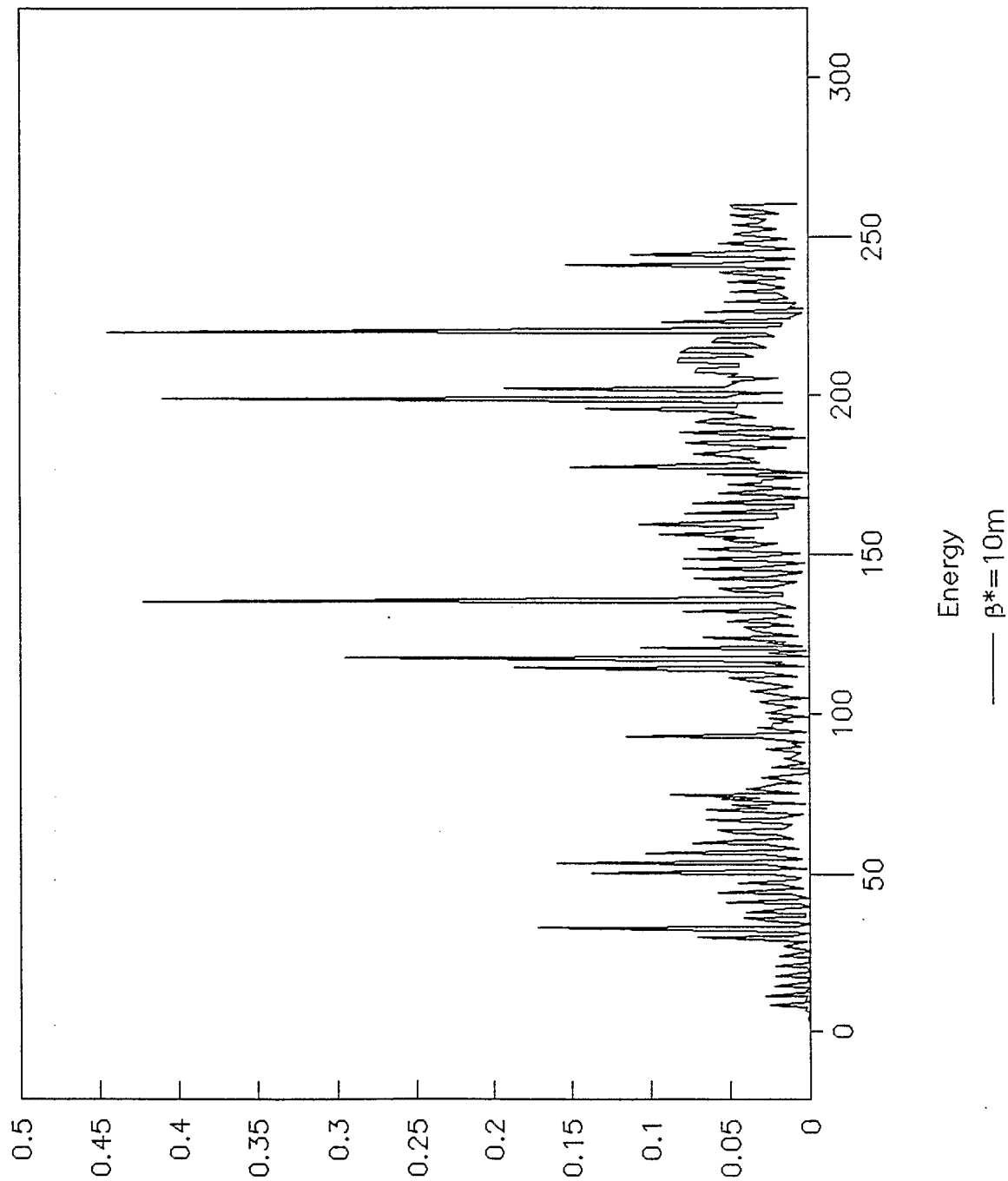
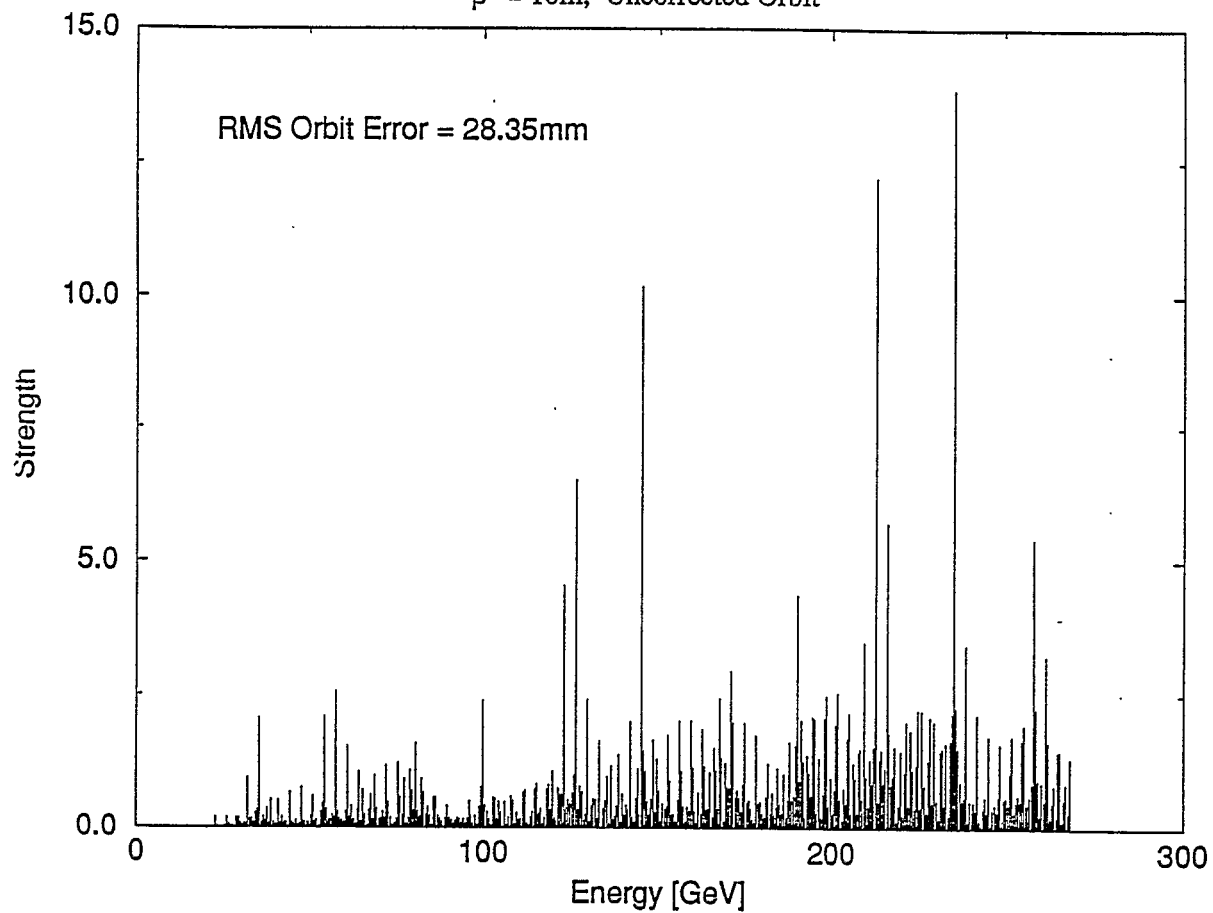


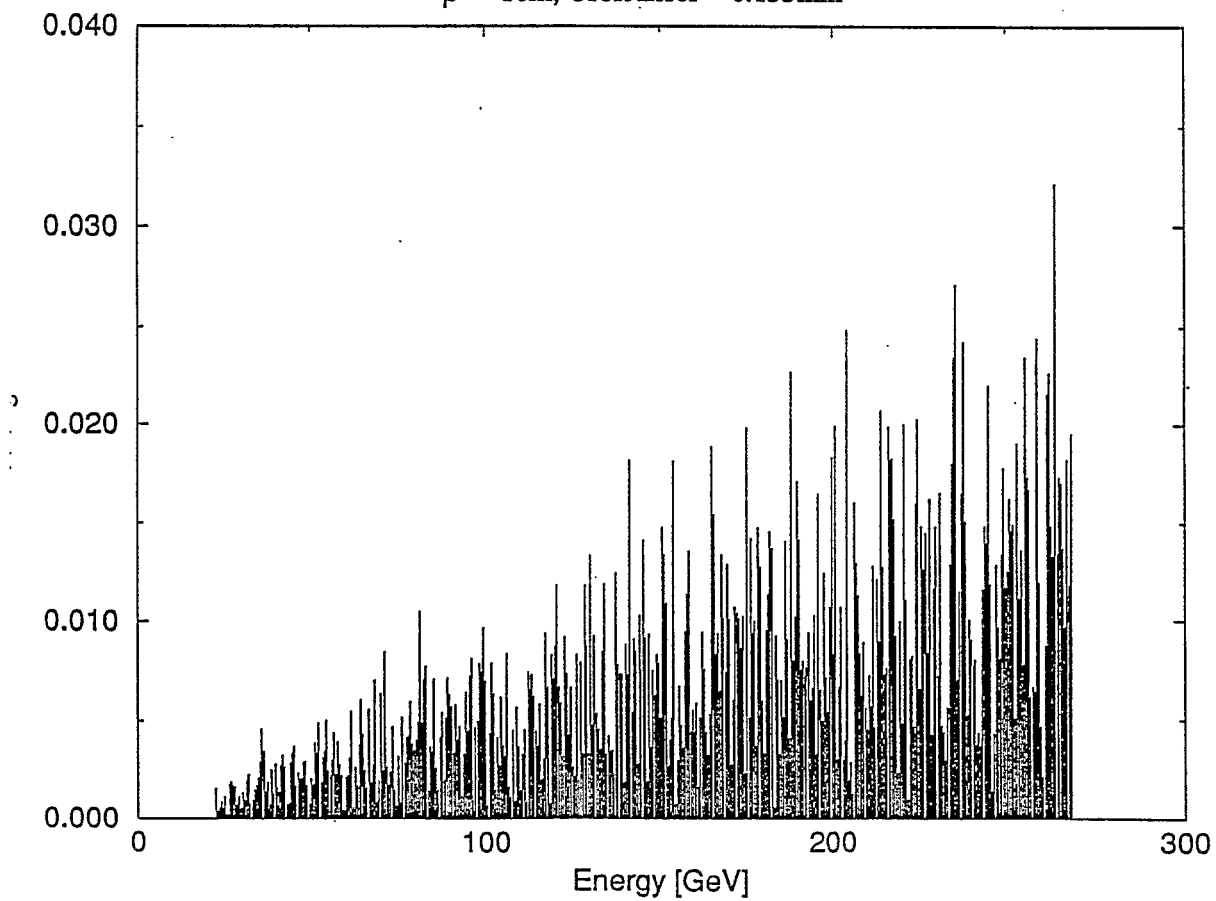
Figure 9

Imperfection Depolarizing Resonances

$\beta^* = 10\text{m}$, Uncorrected Orbit



$\beta^* = 10\text{m}$, Orbit Error = 0.155mm



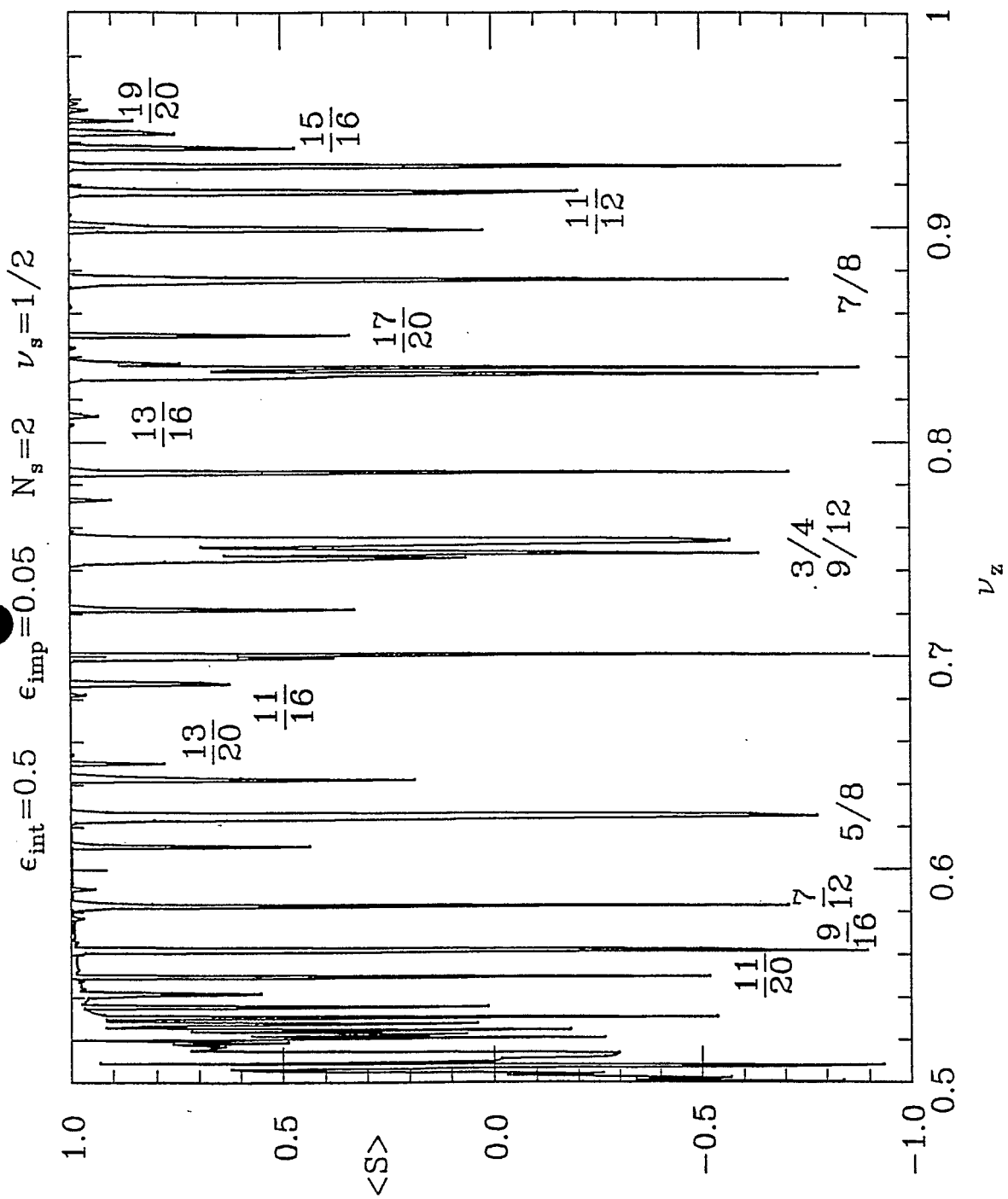
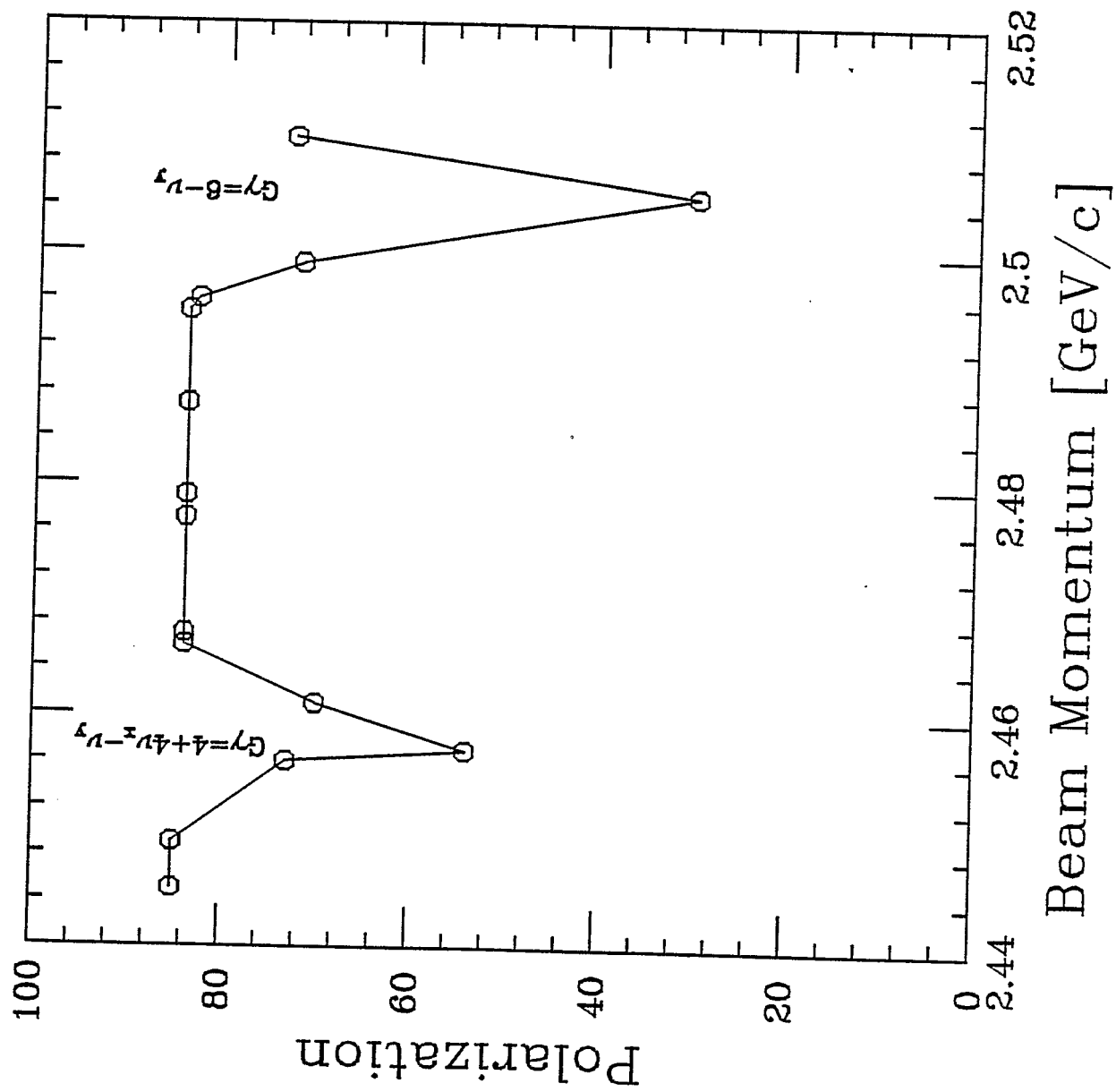


Figure 11



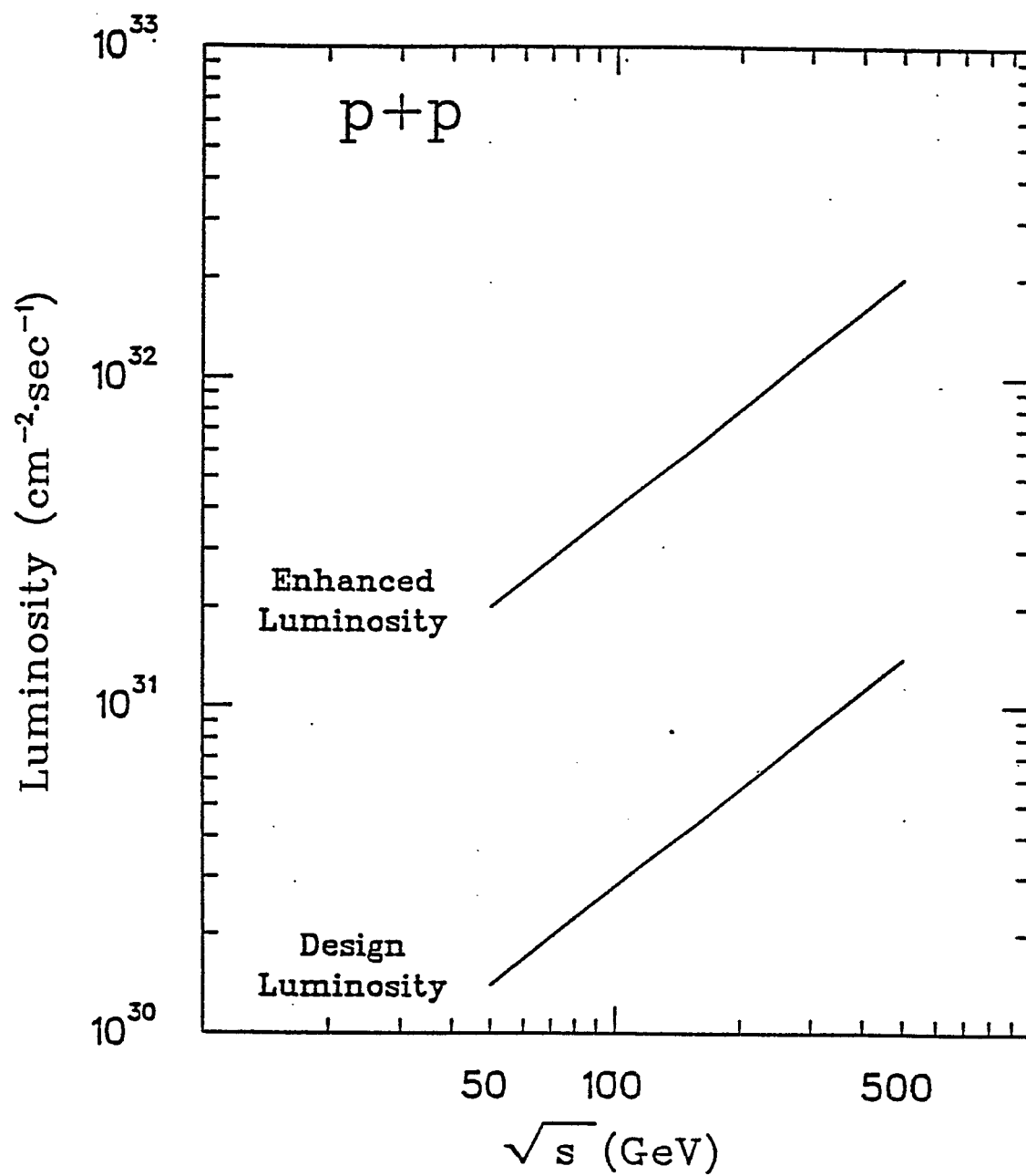


Figure 13

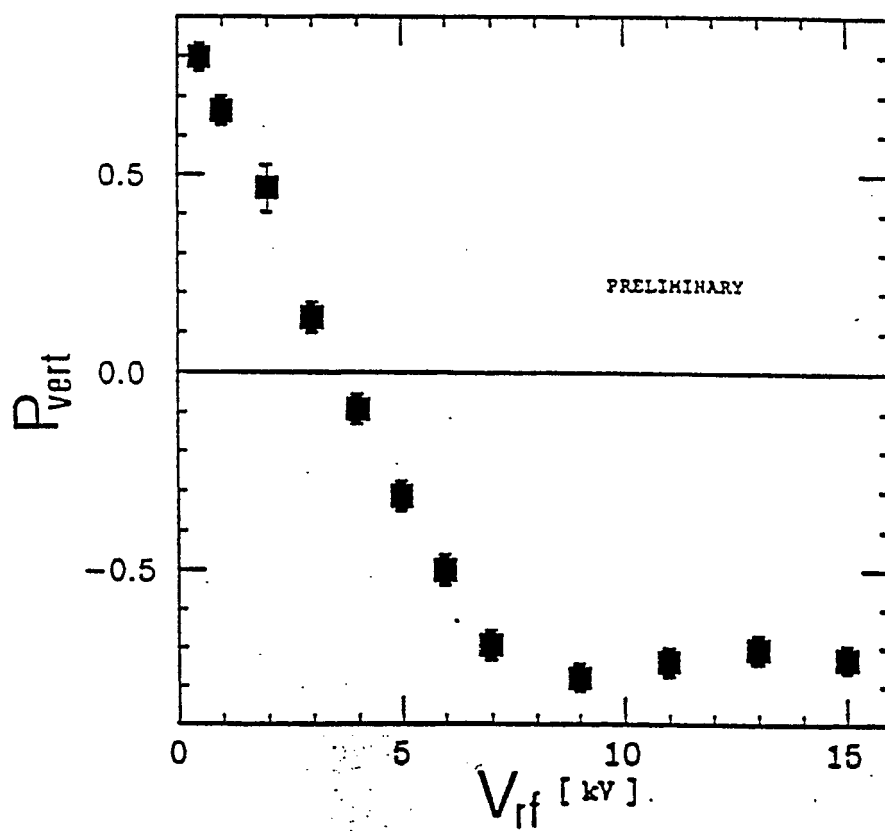


Figure 14

REPORT OF THE RHIC POLARIZED PROTON REVIEW

The Committee to review the accelerator aspects of the "Proposal on Spin Physics Using the RHIC" submitted by the RHIC Spin Collaboration was assembled by Mike Harrison and consists of the following five members:

Alex Chao	SSCL
Steve Peggs	BNL
Bob Pollock	IUCF
Lee Teng	ANL (Chair)
Bill Weng	BNL

The Committee met for 1-1/2 days on June 21 and 22, 1993 in the RHIC Central Office Bldg. BNL. Mike Harrison first gave a brief introductory talk about the RHIC project. The polarized proton beam proposal was then described by members of the Collaboration in a number of presentations. Vigorous and detailed questionings and discussions were carried on between members of the committee and members of the Collaboration. This is a report of the committee's findings and recommendations. The report contains first a brief executive summary, then more detailed discussions of modifications of individual subsystems and features of the proposal.

Executive Summary

1. Although it is not our primary function to evaluate spin physics, we did hear a presentation of the physics opportunities of polarized proton colliding-beams in RHIC. The polarization physics obtainable appears to be both important and exciting. It may very well become a unique segment of the RHIC experimental program.
2. The "proposal" submitted does not contain enough detail to be considered a fully developed Proposal. It should be more appropriately considered as a feasibility study report. As such, we believe that the feasibility of producing, storing and colliding 250 GeV polarized proton beams in RHIC is established with reasonable confidence.
3. The stated performance of $\sim 2 \times 10^{32} \text{ cm}^{-2} \text{ sec}^{-1}$ luminosity with $\sim 70\%$ polarization is optimistic but should be attainable with substantial commissioning and tuning efforts. No known accelerator physics limit is violated. It is however advisable to have some less demanding experimental program to fall back on during the initial operations.
4. The next step is to produce the full Proposal which should contain optimum design choices, preliminary engineering designs, detailed study of error effects and tolerances, detailed simulation to give the design performance, and convincing cost estimate and schedule. For this phase of work continued close interaction of the Collaboration with the RHIC Accelerator Physics group is necessary.
5. The proposal has the flavor of the application of an ingenious technological invention (Siberian snakes) to make possible exciting physics research (polarization physics), reminiscent of the application of stochastic cooling to obtain $\bar{p}p$ beams for W and Z in the CERN SPS. We are indeed very enthusiastic about this total program.
6. We recommend that after the Collaboration has produced a full Proposal, say, in about a year, another detailed review should be made at that time. It is then possible to evaluate the likelihood of attaining the desired performance (luminosity, polarization, etc.) with the specified design at the proposed cost and schedule.

Detailed Report

A. Injector System

This includes the polarized H^- source, the Linacs, the Booster, and the AGS. The polarized H^- beam from the source accelerated in the linacs to 200 MeV is strip-injected, accumulated, and accelerated in the Booster. The 1.5 GeV high intensity polarized proton beam from the Booster is then transferred to the AGS and accelerated to 25 GeV for injection into the RHIC. Throughout the acceleration, the polarization of the beam is to be preserved. The proposed scheme is qualitatively effective. To reliably assess the quantitative performance we need details which are not fully available at the present. We will only list here items for which we have concerns.

1. The ability of running the polarized H^- source at 5 Hz for 20 pulses is questionable. This is an extrapolation of existing experience.
2. Accumulation for 4 sec (20 pulses) in the booster to get 2×10^{11} protons with emittance 10π mm-mrad when the beam lifetime in the booster is no more than 10 sec should be investigated.
3. The main problem is the preservation of polarization through acceleration in the AGS. The proposed scheme of using a solenoid partial snake to eliminate imperfection resonances and using pulsed quadrupoles to jump the betatron tune across intrinsic resonances should be effective as expected. Experiments at IUCF have clearly demonstrated the effectiveness of the solenoid partial snake. The pulsed quadrupoles will, however, cause emittance blowup, especially in the presence of horizontal/vertical coupling generated by the solenoid snake. The allowed factor-2 blowup may not be sufficient. This needs further investigation. The efficiency of polarization preservation also needs detailed study. The assumed 90% preservation (from 80% polarization to 70%) seems high. The approved AGS experiment E-880 will go a long way in assuring the performance and efficiencies of the scheme. If E-880 is to have an impact on this proposal, its schedule should be advanced.

B. RHIC Ring

Similarly here the effectiveness of the use of Siberian snakes and rotators to preserve and precess the beam polarization has been proven by the IUCF experiments and the successful operation of the Fermilab polarized proton beam line. The only question is whether the design is optimal and how much effort and time is required to attain the stated performance. Here also we list those features of the design for which we have concerns.

1. The 10 cm ID of the DX magnet seems inadequate to contain the ~ 7 cm orbit excursion in a snake. It is likely that larger aperture dipoles need to be designed and built for the snakes.

2. The theory of snake resonances has been published and is known. What is needed is a definitive design of the snake configuration and magnets, and a detailed application of the "snake theory" to calculating the percentage survival of polarization from injection to storage and colliding beams. This simulation should take into account all known errors--including multipole fringe fields, dispersive effects, and effects of the detector solenoids, the rotators and the flippers, and the beam-beam effects.
3. The use of only one pair of snakes per ring leaves rather narrow tune spacings between spikes at snake resonances for the betatron tune to navigate through. The possibility of using more than one pair of snakes per ring should perhaps be re-examined. Also since it appears that snake resonances impose a maximum emittance beyond which particles are fully depolarized, the question of emittance growth should be further critically examined.

C. Luminosity and Polarization

The proposed luminosity of $2 \times 10^{32} \text{ cm}^{-2} \text{ sec}^{-1}$ seems optimistic, at least for the initial operation. This luminosity is based on the following assumed beam parameters:

Intensity = 2×10^{11} p/bunch and 57 bunch/ring
 Normalized emittance = 20π mm-mrad
 $\beta^* = 1 \text{ m}$

The intensity and emittance are both consistent with the goals of AGS and its Booster and with the nominal RHIC operation for unpolarized proton beam. It is likely that this beam can be injected and accelerated in RHIC without unsurmountable collective instabilities, but more detailed studies are needed to establish this. The 20π mm-mrad emittance should be achievable, but all possible sources of blowup as mentioned above must be carefully controlled. RHIC is officially committed to a β^* of 2.0 m, and 1 m does look reasonable. The beam-beam tune shift is 0.007 per crossing which is a reasonable value. There does not seem to be any violation of known accelerator physics limits. However, significant commissioning efforts will be needed to materialize these parameter goals. This suggests that it is advisable for the Collaboration to develop a fallback plan when the luminosity falls short of the proposed goal.

The same can be remarked for the polarization. First the estimate of the depolarization should be firmed up by a detailed simulation as described above. Then, fallback plans should be made when the polarization falls short of this maximum value as simulated.

D. Beam Polarization Measurement in RHIC

The scheme proposed is a measurement of the inclusive pion production. The asymmetry at moderate P_t is fairly large ($A \approx 0.2$) when measured at constant $X \approx 0.5$ and is only slightly dependent on beam energy. This asymmetry affords a good means

to measure polarization over a wide energy range. With a 5 μm diameter carbon fiber as target the production cross-section yields acceptably rapid measurements of good precision over the full RHIC energy range. The heating of the fiber and the beam emittance blowup from scattering appear to be tolerable, but more detailed studies are needed. This very promising concept should be developed into a full optimized design.

It would be a great advantage if the concept of this polarimeter could be verified at 25 GeV in an appendage to E-880.

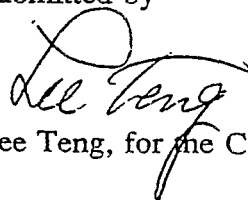
E. Cost and Schedule

The present proposal is not sufficiently complete or detailed to allow a reliable cost estimate. The preliminary gross cost presented is around M\$25 which is composed of ~M\$10 for additions and modifications to the injector system and the RHIC, and ~M\$14 for addition of the barrel EM calorimeter to the STAR detector. However crude this estimate may be, it does point out that at the cost of some 5% of the RHIC project, the unique capability of doing polarization physics could be added with the prospect for a very interesting enrichment of the RHIC scientific program.

The schedule recognizes a number of severe constraints. The lattice design of the RHIC rings is already frozen, and the design of the major detectors for RHIC must soon be fixed. There is, therefore, a strong argument for making a decision on this proposal within the next few months, as soon as a consistent design for the major subsystems is available. Slippage of the AGS schedule for budgetary reasons will mean that results from E-880 will not likely be available for this decision making process, however desirable it may be.

While there is a risk associated with extrapolation of spin-resonance-crossing technology into the higher energy regime of RHIC operation, it is unlikely that this situation will be materially altered by another year or two of theoretical study or AGS tests. If the physics goals are compelling, the risk is acceptable.

Submitted by



Lee Teng, for the Committee

PART B

Update of Proposal R5 for Experiments on Spin Physics at RHIC with the PHENIX Detector by The PHENIX/SPIN Collaboration September 3, 1993

- **Brookhaven National Laboratory, Upton, NY 11973**
S. H. Aronson, M. Fatyga, S. Gavin, W. Guryan*, J. Harder, S. Kahn, E. Kistenev, P. Kroon, Y. Makdisi, M. J. Murtagh, E. O'Brien, L. Paffrath, S. Rankowitz, S. Rescia, T. K. Shea, M. Tanaka, M. J. Tannenbaum, C. L. Woody
- **University of California - Riverside, Riverside, CA 92521**
P. Beery, Sun-Yiu Fung*, Ju-Hwan Kang, R. Seto
- **China Institute of Atomic Energy, Beijing, P. R. China**
Xixiang Bai, Kexing Jing, Xiaoping Liu, Zuhua Liu, Yajun Mao, Benhao Sa, Zuxun Sun*, Yude Wan, Zhongqi Wang, Jincheng Xu, Xiaozhe Zhang, Yuming Zheng, Shuhua Zhou
- **Columbia University, Nevis Labs., Irvington, NY 10533**
C. Y. Chi, B. Cole, G. David, J. Dodd, Qiming Li, S. Nagamiya, T. Nayak, W. Sippach, O. Vossnack, Fuqiang Wang, Yufeng Wang, Yuedong Wu, Xihong Yang, W. A. Zajc*
- **Hiroshima University, Saijo, Hiroshima, Japan**
H. Iwata, A. Sakaguchi, T. Sugitate, Y. Sumi*
- **Institute of High Energy Physics, Academia Sinica, Beijing, P. R. China**
Zheng-dong Cheng, Shao-min Chen, Qi-ming Li, Jun-guang Lu, Ji-mao Ma, De-wu Wang, Ming-han Ye, Wei-qin Zhao, Zhi-peng Zheng, Yu-can Zhu*
- **Institute of High Energy Physics, Protovino, Russia**
V. V. Ammosov, A. Denisov, A. Durum, V. Gapienko, Yu. Galitsky, Yu. Gutnikov, A. Ivanilov, V. I. Kochetkov, B. Korablev, A. Kozelov, V. V. Makeev, E. Melnikov, Yu. Mikhailov, V. Onuchin, Yu. Pischalnikov, Yu. Protopopov, V. I. Rykalin, K. Shestermanov, A. Starkov, D. Strustymov, A. Surkov, V. Zaetz, A. Zaichenkov
- **Institute for Nuclear Study, (U. Tokyo), Tanashi, Tokyo, Japan**
Y. Akiba, H. Hamagaki*, S. Homma, H. Sako, M. Sekimoto
- **KEK, Institute for High Energy Physics, Tsukuba, Japan**
J. Chiba*, Y. Mori, M. Nomachi, O. Sasaki, H. Sakamoto, T. Shintomi, K. H. Tanaka
- **Kyoto University, Kyoto, Japan**
H. Enyo*, K. Imai, H. Kaneko, A. Masaike

- **Los Alamos National Laboratory, *Los Alamos, NM 87545***
J. G. Boissevain, T. A. Carey, A. Gavron, H. van Hecke, B. Jacak*, J. Kapustinsky, M. Leitch,
J. Lillberg, P. L. McGaughey, J. Moss, J. Simon-Gillo, W. E. Sondheim, J. P. Sullivan,
L. Waters
- **Lund University, *Lund, Sweden***
S. Garpman, H.-A. Gustafsson, A. Oskarsson*, I. Otterlund, K. Soderstrom,
E. Stenlund
- **Massachusetts Institute of Technology, *Cambridge, MA 02139***
M. Chen, K. Sumorok
- **McGill University, *Montreal, Quebec, Canada***
J. Barrette, S. K. Mark*, L. Nikkinen, L. Normand, M. Rosati
- **National Institute of Radiation Science, *Chiba-ken, Japan***
E. Takada*
- **State University of New York - Stony Brook, *Stony Brook NY 11794***
P. Braun-Munzinger, T. Hemmick, B. Hong, Y. Kwon, W. J. Llope, S. Panitkin, M. Rao,
J. Stachel*, N. Xu, Y. Zhang, C. Zou
- **Oak Ridge National Laboratory, *Oak Ridge, TN 37831***
G. Alley, T. Awes, C. Britton, Hee Kim, F. Obenshain*, F. Plasil, S. Saini, M. Simpson,
P. Stankus, A. Wintenberg, G. R. Young
- **St. Petersburg Nuclear Physics Institute, *Gatchina, Leningrad, Russia***
N. K. Abrosimov, N. N. Chernov, V. G. Ivochkin, L. M. Kochenda, G. A. Rjabov, V. Schegelski,
D. M. Seliverstov, N. Smirnov, E. M. Spiridenkov, A. Vorobyov*
- **University of Tokyo, *Tokyo, Japan***
R. Hayano*, T. Ishikawa, H. Sakurai, K. Shigaki, H. Tamura
- **University of Tsukuba, *Tsukuba, Japan***
I. Arai, Y. Igarashi, T. Ikeda, M. Ise, S. Kato, H. Kitayama, A. Kumagai,
K. Kurita, Y. Miake*, Y. Nagasaka, H. Tobinai, K. Tomizawa, S. Ueno, K. Waki, K. Yagi,
Y. Yamashita
- **Vanderbilt University, *Nashville, TN 37235***
E. Cornell, C. Maguire*, A. K. Ramayya
- **Individual Participation,**
W. L. Kehoe (M.I.T.)

* Contact person for each institution.

Representative:	H. En'yo
Local coordinators:	Y. Makdisi
	M.J. Tannenbaum

1 Status of the PHENIX Detector

A Conceptual Design Report for the PHENIX experiment at RHIC[1] has been presented, and successfully reviewed by the PAC/TAC. PHENIX is a very high granularity, high resolution, electron, photon and charged hadron spectrometer, in the central region $|\eta| \leq 0.35$, with full azimuth di-muon measurement in one endcap, $1.1 \leq y \leq 2.5$. The electron/photon central spectrometer emphasizes electron identification at the trigger level, with RICH, TRD and EM calorimetry. The EM calorimeter also serves as an excellent gamma and π^0 trigger because of its 5 by 5 cm^2 segmentation at 5.1 m. The central spectrometer consists of two arms, each subtending 90° in azimuth (Φ) and ± 0.35 units in pseudorapidity (η). The total coverage is 1/2 of the azimuth—however, the two arms are not back-to-back: the gap between the edges of the two 90° arms is 45° on one side and hence 135° on the other. The EM calorimeter, $\sigma_E/E = 7\%/\sqrt{E(\text{GeV})}$, has a small, high resolution, $\sigma_E/E = 2\%/\sqrt{E(\text{GeV})}$, subsection in one 90° arm, which covers $|\eta| \leq 0.05$. The charged particle momentum resolution is 2% at 5 GeV/c, and charged hadron identification is provided by TOF($\sigma=100\text{ps}$) for 1/3 of the azimuth of one arm. In addition, a silicon detector array is installed over a wide rapidity region.

Of particular importance to polarized proton physics is the 5 by 5 cm^2 segmentation of the EM calorimeter in the Baseline detector configuration of PHENIX—this is the “0.01” radian configuration of R5[2] capable of reconstructing π^0 out to $p_T = 25$ GeV/c. The muon arm is not in the Baseline Detector—however efforts are underway to secure additional funds to complete the muon arm fabrication and installation with the rest of the baseline detector. The TRD and also the small, High Resolution Photon Detector are among the several possible upgrades to the Baseline Detector and efforts are being made to secure the additional funding for these detectors.

2 Polarized Protons at RHIC

The operation of RHIC with high luminosity polarized protons will provide a unique opportunity for study of the spin structure of QCD and the first possibility of systematic exploration of parity violation at high energy. The PHENIX Baseline detector[1], without addition, can provide excellent measurements of both these phenomena, and more. If the additional funding efforts for the muon arm are successful, a program of Drell-Yan di-muon longitudinal and transverse spin physics would also be done.

For the detailed discussion of rates and sensitivities which follows, the “enhanced” luminosity will be taken as $\mathcal{L} = 2 \times 10^{32} \text{ cm}^{-2} \text{ sec}^{-1}$ at $\sqrt{s} = 500$ GeV and $\mathcal{L} = 8 \times 10^{31} \text{ cm}^{-2} \text{ sec}^{-1}$ at $\sqrt{s} = 200$ GeV. We use 100 days of polarized proton runs with a duty factor of $\sim 50\%$ (4×10^6 sec), which leads to the integrated luminosity of $\int \mathcal{L} dt = 8 \times 10^{38} \text{ cm}^{-2}$ and $\int \mathcal{L} dt = 3.2 \times 10^{38} \text{ cm}^{-2}$ at 500 GeV and 200 GeV respectively. The polarization of both beams is taken as 70%.

The statistical error on the two spin asymmetry is estimated as

$$\delta A = \frac{1}{P_1 P_2} \frac{1}{\sqrt{N}} \quad (1)$$

where P_1 and P_2 are the beam polarizations and N is the number of events. Thus, 1600 events are required for $\delta A = \pm 0.05$. On the other hand the one spin asymmetry has an error of

$$\delta A = \frac{1}{P_1} \frac{1}{\sqrt{N}} \quad (2)$$

Besides the beam energy, the spin configuration (L-type or N-type) is another issue for the running condition. For the time being we leave this question open, and the yield estimates in the following sections are done assuming the above integrated beam time with an appropriate spin setting. Detailed rate calculations are given in R5[2] which will be quoted in the following sections.

3 PHENIX/SPIN Physics Goals and Capabilities

The strengths of the PHENIX detector, notably the ability to run at the highest luminosities with very selective triggers, will allow measurements of a wide variety of spin phenomena. The philosophy is to use the existing PHENIX detector, which is designed for Relativistic Heavy Ion Physics, to make a survey of spin effects in many specific channels over a large range of kinematic variables (m , p_T). Conventional longitudinal spin effects, single and double transverse spin asymmetries and a general parity violation search will be made in all channels. Although spin physics is notable for its surprises, there are several channels for which precise and clear-cut predictions exist so that rates and sensitivities can be given:

- $W^\pm \rightarrow e^\pm + \nu$, with the electron detected in the central detector. The parity violating spin asymmetry in the production channel will be measured for the first time with real W 's, via the parity violating longitudinal spin asymmetry:

$$A_{LL}^{PV} = \frac{1}{P_{beam}^2} \frac{N(++) - N(--)}{N(++) + N(--)} \quad (3)$$

There will be 12,000 (4000) W^+ (W^-) detected, for an uncertainty δA_{LL}^{PV} of 0.02 (0.03) compared to the predicted magnitude of $A_{LL}^{PV} \sim 0.30$ for the W^+ . The predictions for the W^- depend dramatically on the sea-quark spin structure functions (see following section) and could represent the birth of *Structure Function Physics using Parity Violation as a tool*.

- Direct Photon production with $p_T \leq 25$ GeV/c. This is a measurement of the spin dependent gluon structure function $\Delta G/G$ with longitudinally polarized protons, via the conventional longitudinal spin asymmetry:

$$A_{LL} = \frac{1}{P_{beam}^2} \frac{N(++) + N(--)-N(+-)-N(-+)}{N(++) + N(--)+N(+-)+N(-+)} \quad (4)$$

The sensitivity is $\delta A_{LL} = 0.008$ for $p_T \sim 25$ GeV/c (Bjorken $x_{bj} \sim 0.1$), where the prediction of A_{LL} is 0.01 (0.10) for the standard (large) $\Delta G/G$.

- Jets via leading π^0 , with identified π^0 up to 25 GeV/c and unresolved clusters above 25 GeV/c. Here both longitudinal and single and double transverse spin asymmetries will be examined. The large cross section of π^0 production implies a statistical error δA_{LL} approaching 0.001, which allows exploration of small and perhaps unexpected effects, and possibly a check of the parity violation in hadron interactions due to strong-weak interference.
- Drell-Yan in the muon-pair channel, with $5 \leq m \leq 12$ GeV/c². Transverse and longitudinal spin asymmetries will be measured and the correlation between the spin axis and the angular distribution of muon-pair will be studied. The statistical error δA_{LL} is between 1% and 2% over this mass range. Measurements can be made at masses down to 2 GeV/c², but there may be significant background from charm production at low masses.
- J/Ψ and χ_2 production. Here the open geometry of PHENIX is exploited: gamma rays of a few hundred MeV are detected in the High Resolution Photon Detector in coincidence with $J/\Psi \rightarrow l^+ l^-$. The spin dependent gluon structure function can be measured, and the production mechanism of charmed particles will be studied with additional spin information. The event rates are large, 200K $J/\psi \rightarrow e^+ e^-$ and over 1M $J/\psi \rightarrow \mu^+ \mu^-$.

4 $W^\pm \rightarrow e^\pm + X$

The production of the intermediate vector boson W^\pm of the weak interactions, and its leptonic decay, $W^\pm \rightarrow e^\pm + \nu$, are the classical examples of processes with huge parity violation in hadronic collisions. Yet there is a complete absence of searches for, or measurements of, parity violation at high energy hadron colliders[3]. To quote Maurice Goldhaber (who was quoting astronomers), “The absence of evidence is not the evidence of absence.” It is important to measure this production asymmetry. Any discrepancy from the predictions will lead to new physics. In addition, a systematic search for parity violation in all channels is proposed. However, it is difficult to estimate rates for this search, since it is totally exploratory, i.e. it is beyond the standard model.

In the context of the standard model, the leading parity violating process in hadron collisions is W^\pm production. In PHENIX, detection of the W^\pm is in the leptonic decay channel, $W^\pm \rightarrow e^\pm + X$, where the X means that the measurement is via the inclusive e^\pm channel with no “missing energy” detection. This channel is both clean and spectacular. It is a textbook example[4] of a process with virtually no background. A prediction of the cleanliness of this channel dating from Snowmass[5, 6] is shown in Fig. 1a, with a recent simulation[7] of the Jacobean peak in the PHENIX detector shown in Fig. 1b. In order to obtain a clean sample of e^\pm from W^\pm decays, one needs the following[4]:

- 10^{-3} charged hadron rejection for $p_T \geq 10$ GeV/c,
- Precision EM Calorimetry out to 50 GeV,
- Momentum Resolution sufficient to resolve the charge of e^\pm out to 50 GeV/c,

- A good trigger, as W^\pm is only $\sim 10^{-8}$ of the total cross section.

This will be no problem for PHENIX. The EM calorimeter will provide a factor of more than 300 rejection for charged pions above 10 GeV and an isolation cut (e.g. see section B.3.3 in Ref. [2]) should provide an additional factor of ≥ 7 rejection against hadrons (and Dalitz pairs) from jets. Furthermore, even though PHENIX has a relatively small aperture, $|\eta| \leq 0.35$, $\Delta\phi = \pi$, the acceptance for the $W^\pm \rightarrow e^\pm + X$ channel is 13%, so that ~ 120 $W^+ \rightarrow e^+ + X$ and 40 $W^- \rightarrow e^- + X$ per day will be collected. The momentum resolution of 20% at 50 GeV/c gives excellent charge separation.

4.1 “Yesterday’s sensation is today’s calibration...”

A recent article by Bourrely and Soffer[8] has presented the formalism for proton structure function measurements using the parity violating asymmetry of W^\pm and Z^0 production. This really brings to mind Val Telegdi’s statement, partially quoted above. In the standard model, the differential cross section for the reaction

$$pp \rightarrow W^\pm + \text{anything} \quad (5)$$

is given in leading order[8] by the quark-antiquark fusion reactions $u\bar{d} \rightarrow W^+$ and $\bar{u}d \rightarrow W^-$,

$$\frac{d\sigma^{W^+}}{dy} = G_F \pi \sqrt{2} \tau \frac{1}{3} [u(x_1, M_W^2) \bar{d}(x_2, M_W^2) + (u \rightarrow \bar{d})] \quad (6)$$

where G_F is the Fermi constant and $u(x)$ and $\bar{d}(x)$ are the structure functions of u and \bar{d} quarks in the proton at momentum fraction x . The kinematics are given simply by the production of a constituent state with $\hat{s} = M_W^2 = x_1 x_2 s$ at rapidity $y = \frac{1}{2} \ln \frac{x_1}{x_2}$, where $\tau \equiv M_W^2/s$ and $x_1 = \sqrt{\tau} e^y$, $x_2 = \sqrt{\tau} e^{-y}$.

The computed W^+ production cross section[8] is given in Fig. 2a and shows a surprisingly large factor of 2 variation due to the still large uncertainty of the anti-quark structure functions. For W^- production the uncertainty in cross section is nearly a factor of 4. The PHENIX detector measures near $y_W = 0$, so that $x_1 = x_2 = M_W/\sqrt{s} \equiv x_0 = 0.16$ at 500 GeV. The individual W^+ and W^- cross sections and their ratio will be measured to high precision allowing a much improved determination of $\bar{d}(x_0)$ and $\bar{u}(x_0)$. Feynman and Field[9] originally assumed that $\bar{u} \leq \bar{d}$ in the proton due to suppression by Fermi statistics, and the subject has again become interesting due to recent precision measurements[10, 11, 12, 13].

The parity violating asymmetry for W production is given by[8]

$$A_L(y) = \frac{\Delta u(x_1, M_W^2) \bar{d}(x_2, M_W^2) - (u \rightarrow \bar{d})}{u(x_1, M_W^2) \bar{d}(x_2, M_W^2) + (u \rightarrow \bar{d})} \quad , \quad (7)$$

and with the reasonable assumption that $\Delta u \Delta \bar{d} \ll u \bar{d}$, the two-spin and single-spin PVA ’s are simply related by[8]

$$A_{LL}^{PV}(y) = A_L(y) + A_L(-y) \quad . \quad (8)$$

The single-spin asymmetry A_L^W is shown in Fig. 2b[8], and is huge as previously advertised. This figure illustrates the amusing feature of the single-spin asymmetry—the variables x_1

and x_2 can be distinguished in the otherwise symmetric p-p collision, since the spin breaks the symmetry. Also, single-spin asymmetries could be used in p+A collisions to measure the evolution of the spin-dependent sea quark structure functions in nuclei—a combination of the two most famous “*EMC effects*.”

The sensitivity to the spin structure function is much larger for the W^- than the W^+ , which is easy to understand by a simple argument[8]: near $y=0$, the *PVA*’s are given to a good approximation by

$$A_L^{W^+} = \frac{1}{2} \left(\frac{\Delta u}{u} - \frac{\Delta \bar{d}}{\bar{d}} \right) \quad \text{and} \quad A_L^{W^-} = \frac{1}{2} \left(\frac{\Delta d}{\bar{d}} - \frac{\Delta \bar{u}}{\bar{u}} \right), \quad (9)$$

and $\Delta u/u$ is large. PHENIX will measure $A_{LL}^{PV}(y=0) = 2A_L(y=0)$, with expected sensitivity of $\delta A_{LL}^{PV} \simeq 0.02$ (0.03) for W^+ (W^-). The W^+ channel will be used to verify the predicted Parity Violation of the Standard Model, since the structure function uncertainty is small, while the measurement in the W^- channel is in effect a measurement of $\Delta \bar{u}/\bar{u}$. This could be the birth of *Structure Function Physics using parity violation as a tool*.

5 Direct Photon Production

This should be a clean measurement of the spin dependent gluon structure function since the dominant subprocess in pp collisions is

$$g + q \rightarrow \gamma + q, \quad (10)$$

with $q\bar{q}$ contributing on the order of 10%. The major sources of background for direct photon detection are bremsstrahlung from a jet, and π^0 and η decays which produce a *fake* direct γ signal. These backgrounds are effectively eliminated, as discussed in R5[2] by π^0 reconstruction and gamma isolation cuts. By applying both of these rejection methods, the purity of direct photon candidates will be excellent. The high segmentation of the PHENIX EM calorimeter, which is driven by the issues of occupancy and energy resolution in the high multiplicity, low p_T environment of Heavy Ion Collisions, allows the two gammas from π^0 decay to be resolved for $p_T(\pi^0) \leq 25 \text{ GeV}/c$ [1]. For the worst case, where $\gamma_{\text{real}}/\pi \sim 0.1$, $\gamma_{\text{fake}}/\gamma_{\text{real}}$ will be ~ 1 after the elimination of photons from reconstructed π^0 ’s. The isolation cut will then bring $\gamma_{\text{fake}}/\gamma_{\text{real}}$ down to ~ 0.15 . For the bremsstrahlung gammas (20% to 30% of the signal), $\gamma_{\text{brems}}/\gamma_{\text{real}}$ will be ~ 0.05 after the isolation cut.

5.1 Yield estimate of direct photons in PHENIX

To estimate the yield of direct photons we used the Lund Monte Carlo program PYTHIA which uses the EHLQ set #1 structure functions. We have considered runs at $\sqrt{s} = 200 \text{ GeV}$ consistent with the proton-proton runs for the heavy ion physics program, and at $\sqrt{s} = 500 \text{ GeV}$ to explore a higher Q^2 region at the highest luminosity. A full discussion was given in R5[2]. The PYTHIA predictions for the direct photon yield for the integrated luminosities listed above are repeated here in Table 1. The quoted errors are statistical only. Asymmetry errors of less than 4% and 1% are achieved at the highest p_T bins for 200 and 500 GeV respectively.

	$\sqrt{s} = 200 \text{ GeV}$		$\sqrt{s} = 500 \text{ GeV}$	
Total	Yield	ΔA_{LL}	Yield	ΔA_{LL}
	136000	0.0054	1260000	0.0018
$10 < p_{t\gamma} < 15 \text{ GeV/c}$	118000	0.0058	860000	0.002
$15 < p_{t\gamma} < 20 \text{ GeV/c}$	13800	0.017	270000	0.004
$20 < p_{t\gamma} < 25 \text{ GeV/c}$	2900	0.037	63000	0.008

Table 1: Expected number of direct photon events above 10 GeV/c and statistical errors in the asymmetry measurement. The rates increase exponentially below 10 GeV/c.

PYTHIA also provides the relative contributions to direct photon production from the various partonic processes; 88% from the $qg \rightarrow q\gamma$ process and 12% from the $q\bar{q} \rightarrow g\gamma$ process. This small contribution from the annihilation channel can be neglected in the analysis of ΔG (the gluon helicity distribution) in the measurement of the longitudinal spin asymmetry A_{LL} .¹

6 π^0 production—Jets via leading particles

The inclusive π^0 polarization asymmetry can be measured with reconstructed $\pi^0 \rightarrow \gamma + \gamma$ in the range $10 \leq p_T \leq 25 \text{ GeV/c}$. In this p_T range most π^0 s are produced from QCD jets. Compared to other jet fragments, π^0 triggering should be quite simple in the PHENIX apparatus.

At the parton level, high p_T π^0 s originate from several subprocesses. Major channels are:

- $qq \rightarrow qq$ ($\sim 20\%$),
- $qg \rightarrow qg$ ($\sim 50\%$) and
- $gg \rightarrow gg$ ($\sim 30\%$).

Due to this mixture, the theoretical prediction for the production asymmetry becomes difficult. However, the higher yield of π^0 ($\gamma/\pi^0 \simeq 1/4 - 1/10$ at the upper p_T range) results in an asymmetry error, $\delta A \leq \pm 1\%$, thus π^0 measurements could be used to explore other spin phenomena:

- Parton helicity distributions: Theoretical predictions for $A_{LL}(\pi^0)$ show notable differences when gluons are polarized [14].
- Spin transversity measurements using spin transfer: Correlations between the transversely polarized beam axis to the plane of two produced π^0 s, may yield some information on quark transversity structure functions [15].

¹It should be noted that in the case of transverse spin asymmetry, A_{NN} , the contribution from the Compton process vanishes and only the annihilation process contributes to the photon production asymmetry, which relates to the transversity of the quark polarization, $h_1(x)$ structure function. An A_{NN} signal from $q\bar{q}$ annihilation is diluted by a factor of 10 by the Compton process.

- Higher order QCD tests: the single transverse spin asymmetry, A_N , could well be related to twist-3 effects. Recent data from FNAL-E704 showed a large A_N , of more than 10%, at large p_T ($\sim 3\text{GeV}$) in $p \uparrow p \rightarrow \pi^0 + X$ reactions at $\sqrt{s} = 20\text{ GeV}$ [16]. It would be quite interesting to repeat this type of measurement at RHIC at high Q^2 .
- Parity violation in hadron interactions at high energy: The interference between strong and weak interactions may be large enough to see ($10^{-4} - 10^{-2}$) at RHIC energies. However, a high degree of control over the systematics is required for such a measurement.

Full details on detection of reconstructed π^0 in PHENIX in the range of $p_T \leq 25\text{ GeV}/c$ are given in R5[2].

7 Drell Yan Dilepton Production

Drell-Yan pair production is a probe of the sea quark structure function. Some information on the gluon structure function may also be obtained using high p_T di-leptons. The dominant sub-process for the total cross-section (integrated over p_T) is $q\bar{q} \rightarrow \gamma^* \rightarrow l^+l^-$. At large values of p_T , the contribution of the subprocess $gq \rightarrow \gamma^*q$ ($\gamma^* \rightarrow l^+l^-$) becomes dominant.

The sensitivity of the Drell Yan process to the parton spin structure functions is enhanced if the participant partons were at relatively large x_{bj} ($x_{bj} > 0.1$) since it is generally believed that at $x_{bj} = 0$, $\Delta q/q$ and $\Delta \bar{q}/\bar{q}$ are zero. The x_{bj} correlations for the PHENIX di-muon detector, which is centered at $y_{\mu^+\mu^-} \sim 1.8$ are given by simple kinematics:

$$x_1 = \sqrt{\tau}e^y \quad x_2 = \sqrt{\tau}e^{-y} \quad x_F = x_1 - x_2 = 2\sqrt{\tau} \sinh y \quad (11)$$

where $\sqrt{\tau} = m_{\mu^+\mu^-}/\sqrt{s}$. The PHENIX endcap di-muon detector covers the full azimuth over the rapidity range $1.1 \leq y_{\mu^+\mu^-} \leq 2.5$. The estimated event rates[7, 17] are given in the Table below for 4×10^6 sec running time at $\sqrt{s}=200$ and 500 GeV. The approximate values of x_1 and x_2 are given for 500 GeV. The Drell-Yan measurement has sensitivity at small $x_{bj} \leq 0.005$, while the parity violating W^\pm asymmetry has excellent sensitivity at $x_{bj}=0.16$.

$m_{\mu^+\mu^-}$ GeV	Events at 200 GeV	Events at 500 GeV	x_1	x_2
5 to 9	23,000	79,000	0.06	0.0017
9 to 12	4,000	19,000	0.11	0.0030
12 to 15	1,300	8,500	0.15	0.004

Table 2: Di-Muon rates for PHENIX Endcap and Barrel.

With transversely polarized beams the new field of transverse spin effects can be explored in the muon-pair channel by measuring the correlation of the plane of the muon-pair to the spin axis. This provides another approach to quark transversity, h_1 . Precision comparisons of A_{LL} and A_{NN} might reveal differences between the transverse and longitudinal spin structure functions. The single transverse spin asymmetry, A_N , should also be measured for di-muons as a complement to the more traditional channels. A recent calculation[18] predicts $A_N \simeq 0.2$ for di-muons with $x_F \leq 0.1$.

Measurement of the gluon structure function using high p_T di-muons, even with the large acceptance, is not competitive to direct photons, since at a given p_T , the di-muon rate is down by a factor[19] of $2\alpha/(3\pi) \times \ln(m_{max}/m_{min})$, roughly 1000, while the acceptance is higher by only a factor of 4. However, it may be possible to use low-mass dimuons to measure the gluon structure function at low $p_T \leq 5$ GeV/c, where background rather than rate is the problem, as a complement to direct photon measurements.

Full details on detection of di-muons in PHENIX/SPIN are given in R5[2], and other more recent information in PN84, *The PHENIX Muon Detector Review, June 1993*.

8 J/ψ and χ_2 production

Although so many years have passed after the first discovery of J/ψ and many charmonium experiments have been performed, the mechanism of charmonium production in hadronic interaction remains somewhat unresolved. For example, it is surprising that there is no experimental agreement on what fraction of J/ψ is via χ . The study of charmonium production with polarized beams could provide further information on this subject, and could serve as another channel to measure the gluon polarization [20]. New results have been obtained this past year by a Fermilab fixed target experiment[21] with a sample of 250 detected $\chi \rightarrow J/\psi + \gamma$ events, which indicate that the fraction of J/ψ production from radiative χ decays is 0.30 ± 0.04 in pp collisions.

A detailed discussion of J/ψ and χ detection in PHENIX has been given in R5[2]. Also, a new calculation of χ production in PHENIX was performed this year, in conjunction with a funding proposal for the High Resolution Photon Detector[22], which gives ~ 1200 detected $\chi \rightarrow J/\psi + \gamma$ events in PHENIX, if 30% of J/ψ production is from χ radiative decay. The p_T distribution of χ production is taken into account in this new calculation, leading to roughly twice as many detected events as estimated in R5[2]. The invariant mass resolution for $e^+e^- + \gamma$ is $\Delta m \simeq 20$ MeV, compared to the 46 MeV separation of the χ_1 and χ_2 states[22].

9 Triggering

The main trigger for PHENIX/SPIN will be the EM cluster or "Local Sum" measured in the EM Calorimeter as described in the CDR[1]. A threshold of 10 GeV for this sum provides perfect triggers for W^\pm , direct γ , and π^0 at high p_T . The trigger should count at the π^0 rate of ~ 15 nb in the PHENIX acceptance[2] or 3Hz. The RICH counter eliminates all charged hadrons below 4 GeV/c, which provides an excellent single e^\pm or $e^+ + e^-$ trigger, possibly even at LVL-1. The di-muon trigger rate is $\sim 10^{-5}$ of the interaction rate or 120 Hz. The di-muon rate could be improved another factor of 10 by a 2 GeV mass requirement at LVL-2. These rates are low and present no problem for the PHENIX On-line system.

10 Schedule and Request

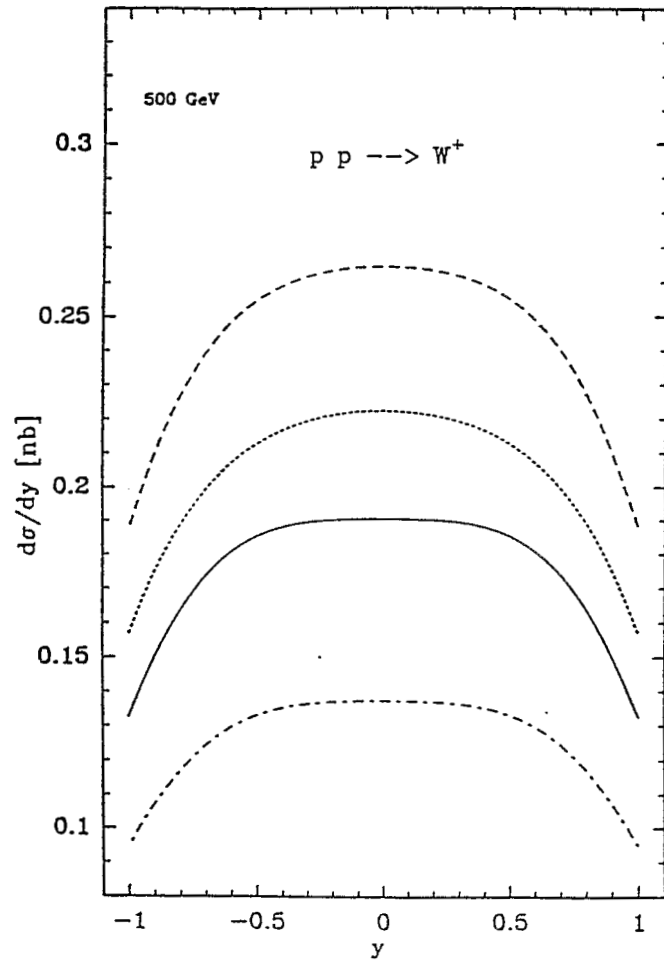
The scope of this proposal is based on the the PHENIX Baseline detector. We envisage no major additions or changes in either the detector setup or trigger system. The muon arm is

not in the Baseline detector but efforts are underway to secure additional funding so as to complete the muon arm at the same time as the Baseline detector for the turn-on of RHIC. We assume that the heavy ion run will precede the first run with polarized protons, thus the detector will have been tried and tested. Running at $\sqrt{s} = 200$ GeV could be a part of the normal heavy ion running schedule with protons. The $\sqrt{s} = 500$ GeV run will be separate.

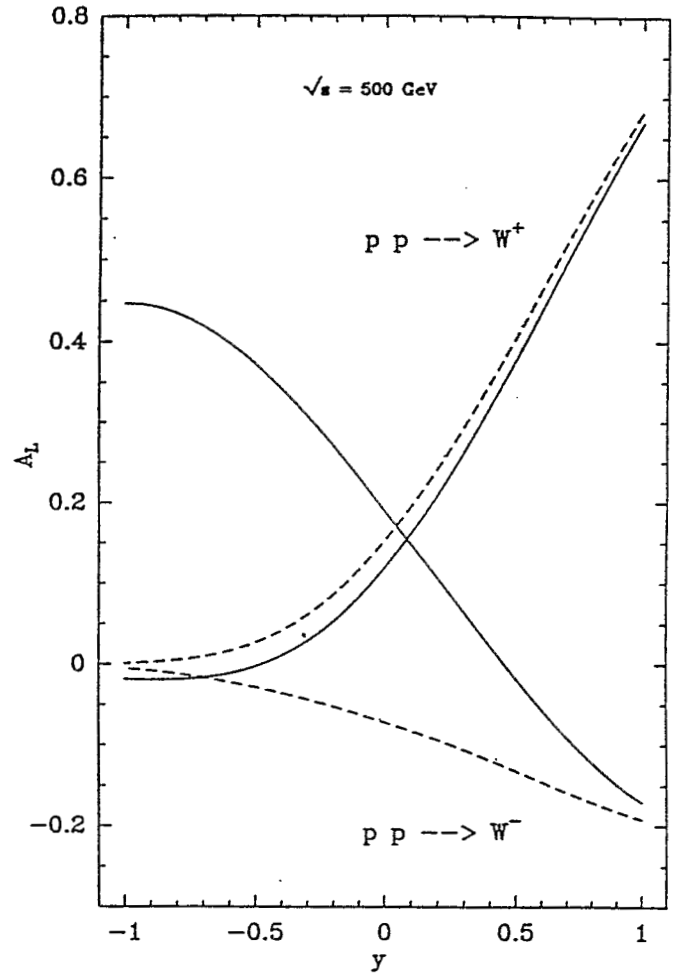
References

- [1] PHENIX, Conceptual Design Report, An Experiment to be Performed at the Brookhaven National Laboratory Relativistic Heavy Ion Collider, 29 January 1993.
- [2] Proposal on Spin Physics Using the RHIC Polarized Collider (R5) , 14 August 1992, section B, Experiments with the PHENIX detector.
- [3] See, however, T. Goldman and D. Preston, Phys. Lett. **168B**, 415 (1986), and references therein.
- [4] G. Altarelli and L. DiLella, *Proton-Antiproton Collider Physics*, World Scientific, Singapore, 1989.
- [5] M. J. Tannenbaum, *Polarized Protons at RHIC*, Proceedings of the Polarized Collider Workshop, University Park, PA (1990), eds J. Collins, S. Heppelmann and R. W. Robnett, AIP conf. proc. No. 223, AIP, New York (1991).
- [6] G. Bunce, et al., *W, Z⁰ Production at a PP collider*, Proceedings of the 1982 DPF Summer Study on Elementary Particle Physics and Future Facilities, June 28-July 16, 1982, Snowmass, CO, eds. R. Donaldson, R. Gustafson and F. Paige, pp 489-499.
- [7] A. A. Derevschikov and V. L. Rykov, *Notes on the Drell-Yan Pairs, Z⁰ and W[±] in STAR and PHENIX at RHIC*, RSC-BNL/IHEP-4, August 1992 (unpublished).
- [8] Claude Bourrely and Jacques Soffer, *Parton Distributions and Parity-Violating Asymmetries in W[±] and Z Production at RHIC*, CPT-93/P.2865, CNRS Luminy (France), January 1993, to appear in Phys. Lett. B.
- [9] R. D. Field and R. P. Feynman, Phys. Rev. **D15**, 2590 (1977).
- [10] New Muon Collaboration, P. Amaudruz, et al., Phys. Rev. Lett. **66**, 2712 (1991).
- [11] P. L. McGaughey, et al., Phys. Rev. Letters **69**, 1726 (1992)
- [12] Estia J. Eichten, Ian Hinchliffe and Chris Quigg, Phys. Rev. **D47**, R747 (1993).
- [13] M. A. Doncheski, F. Halzen, C. S. Kim and M. L. Stong, *Hadronic W production and the Gottfried Sum Rule*, Preprint MAD/PH/744, June 1993.
- [14] G. Ramsey and D. Sivers, ANL-HEP-PR-90-76. D. L. Adams et al. Phys. Lett. **261B**, 197 (1991).

- [15] J. Collins, private communication.
- [16] A. Yokosawa, in Proceedings of Polarized Collider Workshop, 1990.
- [17] Vladimir Rykov, S. Heppelmann, internal report to RSC, July 14, 1992.
- [18] C. Boros, Liang Zuo-tang, and Meng Ta-chung, Phys. Rev. Letters **70**, 1751 (1993).
- [19] UA1 Collaboration, C. Albajar, et al., Phys. Lett. **B209**, 397 (1988).
- [20] R. Robinett, Phys. Rev. **D43**, 113 (1991); M. A. Doncheski and R. W. Robinett, Phys. Lett. **B248**, 188 (1990).
- [21] E705 Collaboration, L. Antoniazzi, et al., Phys. Rev. Letters **70**, 383 (1993).
- [22] A High Resolution Photon Detector for PHENIX at RHIC, PHENIX Note 79, April 30, 1993.



(a)



(b)

Figure 2: a) $d\sigma/dy$ versus y for W^+ production at $\sqrt{s} = 500 \text{ GeV}$ for different choices of the anti-quark distributions [8]. b) The single-spin parity violating asymmetry A_L versus y for W^+ and W^- production. The solid lines correspond to a reasonable choice for the sea-quark polarization [8] and the dashed lines correspond to $\Delta\bar{u} = \Delta\bar{d} = 0$.

PART C

STAR - RSC (RHIC Spin Collaboration) UPDATE

02 September 1993

Abstract

The importance of the STAR detector with a large acceptance for spin measurements is emphasized. This will allow a determination of the nucleon spin-dependent structure functions over a large range in x and a collection of sufficient W and Z events to investigate extremely interesting spin-related phenomena. The results of detailed Monte Carlo calculations on these measurements are presented. Supplements to the STAR detector that are required and a cost estimate are described.

Contents

	<u>Page</u>
Introduction	4
Recent Theoretical Background	4
Reminding Note	5
1. Measurements with Barrel EMC and Shower Maximum Detector... 6	6
1.1. Single-Jet Production	7
1.2. Di-jet Production.....	7
1.3. Direct-Gamma Production	8
1.4. Direct-Gamma + Jet	9
1.5. A_N Measurements	10
1.5.1. A_N Measurements in Direct-Gamma and π^0 Production at Large p_T	10
1.5.2. A_N Measurements in π^0 , π^+ , π^- Production at Large x_F	10
1.5.3. A_N Measurements in High Mass e^+e^- Pair Production at $x_F = 0$...	11
1.6. W's and Z Production at 500 GeV	11
1.6.1. Parity-Violating Asymmetry	11
1.6.2. Parity-Conserving Asymmetry	15
1.6.3. Measurements of $h_1(x)$ in Z Production	16
2. Measurements with Barrel, One Endcap, and Shower Maximum Detector	17
2.1. Detecting the Direct- γ and the "Away-Side" Jet	17
2.2. Measurements of the Sea-Quark Helicity Distribution in the Drell-Yan Process	17

Contents (continued)

2.3.	Measurements of $h_1(x)$ in the Drell-Yan Process and Z Production	20
2.4	W's and Z Production at 500 GeV	20
3.	Cost Estimate and Schedule	20
	References	23
	Figure Captions	25
	Appendix I (Author List)	34

Introduction

This document is to update the original proposal R5 (Section C), and includes the results of simulation calculations on direct-gamma, W, and Z measurements showing expected signal to noise ratios.

For completeness, some parts of the original proposal are reintroduced.

Recent Theoretical Background

In the original proposal, a number of different reactions sensitive to gluon or sea-quark polarization in a longitudinally-polarized proton were described. These parton spin distributions are fundamental. The following additions including W and Z physics to the original proposal, R5, are introduced here.

A recent paper calculating K factors for direct-gamma production by A. P. Contogouris et al.¹ gives higher order QCD corrections to large- p_T direct-photon production and adds significant support to the suggestion that $\bar{p}p \rightarrow \gamma + x$ is a good probe of the polarized gluon distribution. In another recent paper,² higher QCD corrections to large p_T direct-photon production have again been obtained and the results been applied for longitudinal polarization for the incoming hadrons. Hadronic colliders have been discussed as tools to study proton-spin structure, with specific calculations at energies used at RHIC.³

Over the last several months, several theoretical papers have been written emphasizing important issues related to the potential spin program at RHIC. The question of the flavor asymmetry of the sea quarks (i.e. $\bar{u}(x) \neq \bar{d}(x)$) has emerged from the experimental evidence of violating the Gottfried sum rule.^{4,5} This can be studied further in the production of W^\pm and Z bosons in a proton-proton collider, because it is dominated by quark-antiquark annihilation, and therefore sensitive to the sea distributions. It was shown^{6,7} that in the central region the predicted unpolarized cross sections can vary by a large factor depending on whether or not one assumes a flavor symmetric sea. It has also been suggested to measure charge asymmetries in the W^+ and W^- production cross sections.⁷ Several observables should be considered concerning the helicity asymmetries. Predictions of the double-helicity parity-conserving asymmetry A_{LL} which is directly proportional to the polarization of the antiquarks (see Section 2.2.) have been made. Parity violating asymmetries with either one beam polarized A_L or with two beams polarized A_{LL}^{PV} (see section 1.6.2.) were predicted.⁶ Values for A_L and A_{LL}^{PV} turn out to be very different. The W^\pm asymmetries are sensitive to the polarization of the u

quarks (or antiquarks) or to the d quarks (or antiquarks), so they will allow a systematic check of many polarized parton distributions.

Single-and double-helicity asymmetries^{8,9} in the dilepton Drell-Yan processes have also been investigated, and sizable effects are expected for large values of p_T and dilepton mass.

Single particle production such as π production has been studied. The transverse spin asymmetry (or analyzing power) A_N can be described in terms of orbiting valence quark effects in quark-antiquark annihilation processes.¹⁰ This process is adequate only for the large x_F region where valence quarks (not sea quarks) dominate and this model description allows a satisfactory explanation of the FNAL data^{11,12} with polarized protons and polarized antiprotons (see Section 1.5.2.).

Reminding Note

The double helicity asymmetry, A_{LL} , is given by

$$A_{LL} = (1/P^2) \frac{N^{++} + N^{--} - N^{+-} - N^{-+}}{N^{++} + N^{--} + N^{+-} + N^{-+}},$$

where $+(-)$ refers to the spin state parallel (antiparallel) to the L direction (beam direction), and P is beam polarization.

The single transverse spin asymmetry, A_N is given by $A_N = (1/P) (N^{\uparrow} - N^{\downarrow}) / (N^{\uparrow} + N^{\downarrow})$. The double transverse spin asymmetry, A_{NN} is given by

$$A_{NN} = (1/P^2) (N^{\uparrow\uparrow} - N^{\uparrow\downarrow}) / (N^{\uparrow\uparrow} + N^{\uparrow\downarrow}),$$

where $N^{\uparrow\uparrow}$ and $N^{\uparrow\downarrow}$ have parallel and antiparallel spin directions, respectively.

For the following discussion of rates and sensitivities, the integrated luminosity will be taken as:

At 500 GeV, $\mathcal{L} = 2 \times 10^{32} \text{ cm}^{-2} \text{ sec}^{-1}$ for 4×10^6 seconds (100 days, 50% efficiency) or

$$\int \mathcal{L} dt = 8 \times 10^{38} \text{ cm}^{-2} = 800 \text{ pb}^{-1},$$

At 200 GeV, $\mathcal{L} = 8 \times 10^{31} \text{ cm}^{-2} \text{ sec}^{-1}$ for 4×10^6 seconds or $\int \mathcal{L} dt = 3.2 \times 10^{38} \text{ cm}^{-2} = 320 \text{ pb}^{-1}$. Most of the proposed measurements are at 200 GeV, with the exception of W and Z production. The polarization of both beams is taken as $P = 0.7$.

The statistical errors on the asymmetry are given as

$$\delta A_{LL} \text{ or } \delta A_{NN} = \frac{1}{P^2} \frac{1}{\sqrt{N}}, \text{ for the two-spin asymmetry, and}$$

$$\delta A = \frac{1}{P} \frac{1}{\sqrt{N}}, \text{ for the one-spin asymmetry.}$$

1. Measurements with Barrel EMC and Shower Maximum Detector

The proposed barrel EM calorimeter (see Fig. 1) is a lead-scintillator sampling calorimeter. It is located inside the aluminum coil of the STAR solenoid and covers $|\eta| \leq 1.0$ and 2π in azimuth, thus matching the acceptance for full TPC tracking. At $\eta \sim 0$, the amount of material in front of the EMC is ~ 0.5 radiation lengths (X_0). The inner radius is 2.20 meters, and the overall length is 6.20 meters.

A detector with fine spatial resolution will be placed at a depth of approximately $5 X_0$, near the location of the maximum number of shower electrons for photons of 3-5 GeV, to allow for the detection of direct photons. It will reject background photons emanating from decaying π^0 mesons having $p_T \leq 20 \text{ GeV}/c$ by examining the transverse shower profile at this depth. The radial space allotted for this device is 25 mm.

(Reference - EMC CDR)

TABLE 1
Barrel Electromagnetic Calorimeter Parameters

Barrel Calorimeter type	18 X_0 lead-scintillator 'EM' section
Mechanical segmentation:	60 azimuthal sectors, $\Delta\phi = 0.105 (6^\circ)$ 40 projective towers in $ \eta < 1.0$ $\Delta\eta = 0.05$
Inner radius:	2.20 m
Length:	6.20 m
Weight:	172.7 tons
Readout:	Waveshifting fiber (2/tile) to PMT
Towers:	1,200
Shower Max detector:	Scintillator strips parallel or wires/pads parallel and perpendicular to η

1.1 Single-Jet Production

We can study gluon-gluon scattering up to $p_T = 20$ GeV/c and then gluon-quark scattering above ~ 20 GeV/c. By measuring the asymmetry in A_{LL} in single-jet production in the region $10 < p_T < 20$ GeV/c, we can determine the gluon polarization $\Delta G/G$, where $\Delta G(x) = G^+(x) - G^-(x)$ is the helicity distribution of the gluon, as

$$A_{LL} = (\Delta G(x_1)/G(x_1)) \cdot (\Delta G(x_2)/G(x_2)) \cdot \hat{a}_{LL}(gg \rightarrow gg),$$

where $\hat{a}_{LL} = 0.8$ at $y = 0$.

In STAR, the electromagnetic component of jets can be detected with the EM calorimeter, and the charged particles using the TPC. Monte Carlo studies of the rates, acceptance, and resolution were made using the ISAJET program with EHLQ1 structure functions¹³ and GEANT.

The TPC operation for high-luminosity pp events is discussed in the original proposal (R5). Minimum bias events generated by the LUND program¹⁴ were used to evaluate the effects of pp interactions preceding and following the triggering event. As a result of the long TPC readout time (50 μ sec), there are thousands of tracks present in a TPC trigger. The track finding is efficient particularly for the outer pad rows. (Reference - EMC CDR)

Inclusive jet production cross sections are an order of magnitude larger at the same p_T than other channels described later. For the barrel EM calorimeter, the maximum jet rapidity would be $|\eta| < 0.3$, corresponding to $0.05 < x < 0.3$ at $p_T = 10$ GeV/c and $\sqrt{s} = 200$ GeV, and to large x at higher p_T . Sizable rates for jets occur for p_T up to 50 GeV/c.

1.2 Di-Jet Production

The advantage of di-jet production over the single-jet production is the kinematic constraint on the momentum fractions, x_i , of the two partons although the di-jet production cross section for both jets within the η acceptance is much smaller. The number of di-jet events, N_{pair} is given in the table below for $p_T \geq 10$ and 20 GeV/c and $|\eta| \leq 0.3$.

Jet + Jet Events		
PT	$ \eta $	N_{pair}
≥ 10	≤ 0.3	$1 \cdot 10^8$
≥ 20	≤ 0.3	$3 \cdot 10^6$

1.3. Direct-Gamma Production

Direct γ 's are produced through the $q\bar{q}$ annihilation subprocess and the q-g Compton subprocess, $qg \rightarrow \gamma q$. The Compton subprocess is the dominant one in pp interactions, since there are no valence antiquarks in the proton. The asymmetry A_{LL} in direct- γ production becomes directly proportional to $\Delta G(x)$ as:

$$A_{LL}(x) = (\Delta u(x)/u(x)) \cdot (\Delta G(x)/G(x)) \cdot \hat{a}_{LL}(qg \rightarrow \gamma q),$$

where $\Delta u(x)/u(x) = (u^+(x) - u^-(x))/(u^+(x) + u^-(x))$ with $\Delta u(x)$ being the helicity distribution of the quark. The values of $\Delta u(x)/u(x)$ are obtained from results of the EMC-SMC and SLAC experiments and $\hat{a}_{LL} = 0.6$ at $y = 0$. Direct- γ events, without looking at the away-side jet, provide information about the integrals of $\Delta G(x)$ in certain ranges of x (range of x from 0.05 to 0.2 at $\sqrt{s} = 200$ GeV).

Assuming a shower maximum detector with 1-cm strips, the estimated δA_{LL} at $\sqrt{s} = 500$ GeV is

$$\delta A_{LL} \sim \pm 0.0012 \sqrt{8 \times 10^{38} \text{ cm}^{-2} / \int L dt}.$$

At $\sqrt{s} = 200$ GeV, the uncertainty will be

$$\delta A_{LL} \sim \pm 0.006 \sqrt{3.2 \times 10^{38} \text{ cm}^{-2} / \int L dt}.$$

The error increases by a factor of 1.2 for 1.5-cm strips, and is reduced by a factor of 1.3 for 0.5-cm strips. For direct- γ , at $p_T \sim 20$ GeV/c, we note $R\Delta\theta_{\min} = 3.5$ cm, suggesting that the 1-cm width may be near optimum when cost vs. π^0 resolution is considered.

Monte Carlo simulations for this reaction are described in Ref. 15, and detection of direct photon production at RHIC was discussed by M. Werlen.¹⁶

We describe here the results of investigation²⁹ using PYTHIA 5.6 and JETSET 7.3. The hard processes $q + q \rightarrow q + q$, $g + q \rightarrow g + q$, and $g + g \rightarrow g + g$ are considered as a background to the direct gamma production.

At $\sqrt{s} = 200$ GeV, production cross section of direct gamma with $p_T > 10$ GeV/c into the acceptance of the STAR is (2.40 ± 0.05) nb, and there is a background of 24,000 events. And then there are 53 events with transverse momentum deposition > 10 GeV/c in one tower. The following three cuts were applied:

- | | | |
|----|--|-------------------------------|
| 1. | Isolation cut | Killed 24 events (out of 258) |
| | (In tower matrix 3×3 towers with a center in which direct gamma appears should not be energy deposited more than 0.5 GeV from gamma-quanta and electrons) | |
| 2. | No charged track in the tower | 5 events (out of the rest) |
| 3. | E (hadrons)/E (max. tower) | 7 events (out of the rest) |

Seventeen out of 53 events have survived, that corresponding to (3.15 ± 0.78) nb. Special calculations were made for scintillator/fiber shower max detector with 12 mm scintillator strip. By using electromagnetic shower shape (radius of a shower), it was found that at 90% efficiency of direct gamma detection, a background is suppressed in 10 times at $p_T = 30$ GeV/c. Taking into account factor 10 from shower max detector, we can come up with a signal-to-noise ratio $= 7.6 \pm 2.5$.

At $\sqrt{s} = 500$ GeV, the production cross section is (2.40 ± 0.05) mb, and there are 40,000 background events. There are 258 events with $p_T > 10$ GeV/c in one tower. After the three cuts, and the use of the shower max detector, we obtain a signal-to-noise ratio $= 3.9 \pm 0.7$.

1.4. Direct-Gamma + Jet

The measurement of " γ + jet" events allows the kinematics of the primary quark-gluon scattering to be determined. The kinematics of the primary partons (x_1 and x_2) can be reconstructed by determining the kinematics of the gamma and jet. For the p_T acceptance of 10 to 20 GeV/c, x_1 and x_2 vary from 0.1 to 0.2 at $\sqrt{s} = 200$ GeV. The cross section for inclusive direct- γ + jet production with $-0.3 < \eta_{jet} < 0.3$

and $-1.0 < \eta_\gamma < 1.0$ in the p_T interval 15-20 GeV/c is equal to 28 pb. For 320 pb⁻¹, the expected number of events is 9,000, which corresponds to

$$\delta A_{LL} \sim \pm 0.034 \sqrt{3.2 \times 10^{38} \text{ cm}^{-2} / \int \mathcal{L} dt}.$$

1.5. A_N Measurements

1.5.1. A_N Measurements in Direct-Gamma and π^0 Production at Large p_T

Single transverse spin asymmetries, A_N , in hard processes are expected to vanish in perturbative QCD. The asymmetries vanish at the leading-twist (twist-2) level, however this is no longer true if one considers higher-twist contributions. These higher-twist techniques were applied to the simple case of $pp \rightarrow \gamma X$, in which the twist-3 contribution, leading to a potentially larger asymmetry, increases with x_F .^{17,18} The twist-3 parton distribution involves the correlation between quark fields and the gluon field strength. Clearly the normalization, sign, and x -dependence of this new partonic distribution will remain unknown until it is measured.

A measurement of higher-twist effects not only provides a valuable test on perturbative QCD, it also yields information on the hadron structure. The higher-twist distributions represent correlations between quarks and gluons inside a hadron. These correlations have specific structures in QCD. If extracted from experimental data, they provide useful constraints on nucleon models, in particular, the non-valence degrees of freedom that include sea quarks and gluons.

The statistical error, δA_N , will be similar to the one described in Section 1.3.

1.5.2. A_N Measurements in π^0 , π^+ , π^- Production at Large x_F

Single-spin asymmetries were measured in π^\pm production at 200 GeV/c.¹⁹ The asymmetry values (A_N) in the $p^\uparrow p$ reaction are shown in Fig. 2 as a function of x_F for π^+ and π^- data over a p_\perp range of 0.2 - 2.0 GeV/c. Further study of these data shows a threshold effect in which A_N increases dramatically above $p_\perp = 0.7$ GeV/c. The A_N values in the $\bar{p}^\uparrow p$ reaction¹² are shown in Fig. 3 for the π^+ and π^- data. We observe a similar behavior on A_N magnitude with respect to x_F but the sign of A_N is positive for the π^- data and negative for the π^+ data.

These results were explained using two methods that have been published to date. The first one²⁰ is a pion-exchange model that relates $pp \rightarrow \pi^\pm X$ scattering to the πp backward scattering. The antiprocesses of $\pi^+ p \rightarrow p \pi^+$ and $\pi^- p \rightarrow p \pi^-$ are $\pi \bar{p}$

$\rightarrow \bar{p}\pi$ and $\pi^+ \bar{p} \rightarrow \bar{p}\pi^+$ respectively. Thus we have opposite signs of A_N for p^\uparrow and \bar{p}^\uparrow beams. The second one¹⁰ claims that these experimental results provide crucial tests for the existence of orbiting valence quarks. Large asymmetries are expected to exist when annihilation of orbiting valence quarks takes place. The effective orbital motion is counterclockwise to the polarization axis. For π^+ , an orbiting u quark picks up a \bar{d} quark and for π^- , an orbiting d quark picks up a \bar{u} quark. In this model, the valence quark contributes to the proton spin and therefore there is no "proton spin crisis".

From this mirror-symmetry effect in π^+ and π^- , one may speculate that $A_N = 0$ for π^0 production. By applying isospin relations for single-particle distributions,²¹ $\sigma^+ A_N^+ + \sigma^- A_N^- = 2\sigma^0 A_N^0$, where σ^+ and A_N^+ are for the cross section and analyzing power in $p^\uparrow p \rightarrow \pi^+ X$ respectively, σ^- and A_N^- in $p^\uparrow p \rightarrow \pi^- X$, and σ^0 and A_N^0 in $p^\uparrow p \rightarrow \pi^0 X$, we can conclude the following: experimental data show $\sigma^+ > \sigma^-$ and $A_N^+ \sim -A_N^-$ therefore we expect $A_N^0 > 0$. Asymmetry measurements, A_N , in $p^\uparrow p \rightarrow \pi^0 X$ and $\bar{p}^\uparrow p \rightarrow \pi^0 X$,²² on the x_F dependence at 200 GeV/c covering p_\perp up to 2 GeV/c were carried out. A_N values are consistent with zero up to $x_F = 0.3$ and 0.4, and then linearly increase to +20% near $x_F = 1.0$. Since π^0 has $u\bar{u}$ and $d\bar{d}$ terms, we indeed observed similar behavior in $p^\uparrow p \rightarrow \pi^0 X$ and $\bar{p}^\uparrow p \rightarrow \pi^0 X$.

We propose to investigate these effects at RHIC energies and at high p_T . We expect sizable rates for these reactions.

1.5.3. A_N Measurements in High-Mass e^+e^- Pair Production at $x_F = 0$

While pion production at large x_F is regarded as direct quark-antiquark fusion producing a large asymmetry, high-mass lepton-pairs produced at $x_F = 0$ are solely due to quark-antiquark annihilation. The prediction by the orbiting quark model¹⁰ is $A_N = +35\%$ in the lepton-pair mass region of 4 to 7 GeV.

1.6 W's and Z Production at 500 GeV

1.6.1. Parity-Violating Asymmetry

The observable A_L is defined as,

$$A_L = (N^- - N^+) / (N^- + N^+),$$

where $-(+)$ are minus (plus) helicity, respectively. A_L^{FV} is expected to vanish unless some partonic subprocess involves the parity-violating interaction.

When the helicities of both beams are the same, we define another parity-violating asymmetry, namely,

$$A_{LL}^{PV} = (N^{--} - N^{++}) / (N^{--} + N^{++}).$$

W bosons are predicted to be produced by a parity-violating mechanism, using Standard Model couplings. The PVA can be measured in the hadroproduction of $W \rightarrow e + \nu, \mu + \nu$.

In the Standard Model the W is a purely left handed current and the asymmetries in W^+ production are:⁶

$$A_L(y) = \frac{\Delta u(x_1) \bar{d}(x_2) - (u \leftrightarrow \bar{d})}{u(x_1) \bar{d}(x_2) + \bar{d}(x_1) u(x_2)} \text{ and}$$

$$A_{LL}^{PV}(y) = \frac{[\Delta u(x_1) \bar{d}(x_2) - \Delta \bar{d}(x_2) u(x_1)] - (u \leftrightarrow \bar{d})}{[u(x_1) \bar{d}(x_2) - \Delta u(x_1) \Delta \bar{d}(x_2)] + (u \leftrightarrow \bar{d})}$$

If one makes the reasonable assumption that $\Delta u \Delta \bar{d} \ll u \bar{d}$ for all x ,

$$A_{LL}^{PV} = A_L(y) + A_L(-y).$$

The results of predictions⁶ for W^\pm production are shown in Fig. 4 with polarized sea quarks²³ and $\Delta \bar{u} = \Delta \bar{d} = 0$. In the case of W^- production, one observes a drastic difference between the cases $\Delta \bar{u} \neq 0$ and $\Delta \bar{u} = 0$.

Production cross sections are estimated using PYTHIA V5.3/V5.6 for W and Z in pp interactions at $\sqrt{s} = 500$ GeV as

$$\begin{aligned} \sigma_B(pp \rightarrow W^+ + X \rightarrow e^+ + \nu + X) &= 120 \text{ pb} \\ \sigma_B(pp \rightarrow W^- + X \rightarrow e^+ + \bar{\nu} + X) &= 43 \text{ pb} \\ \sigma_B(pp \rightarrow Z^0 + X \rightarrow e^+e^- + X) &= 10 \text{ pb} \end{aligned}$$

The STAR detector with electromagnetic calorimeters is especially suitable for experiments measuring W and Z bosons due to its large acceptance for electrons produced by high-mass particle decays.

The estimates for the event rate at $\sqrt{s} = 500$ GeV for an integrated luminosity of 800 pb^{-1} and with a triggering cut applied to transverse momenta of detected electrons $p_T^e > p_T^{e*} = 20 \text{ GeV}/c$ are: (In the right column the geometrical acceptance $|\eta| < 1.05$ is decreased to the fiducial one $|\eta| < 0.95$ excluding the edge counters.)

Boson	$ \eta < 1.05$	$ \eta < 0.95$
W^+	68,000	62,400
W^-	15,000	13,700
Z^0	3,840	3,100

We start with studying the background for hard electron/positron from W decays, with contributions from Z decay, π^0 Dalitz decay, and misidentified high- p_T charged hadrons as electrons. All results were obtained³⁰ by Monte Carlo simulations with the Lund set of routines PYTHIA V5.6/JETSET V7.3.

The background from $Z \rightarrow e^+e^-$ decay with a missing one electron is unrejectable in principle. For the integrated luminosity of 800 pb^{-1} , the expected number of events with missing e^- , but detected e^+ in a fiducial acceptance is expected to be about 1,700, and the same number of events with missing e^+ , but detected e^- . Thus, the background from Z decays to W^+ will be about 2.7%, but for W^- about 12.4%.

In the following table, the upper limit for the background from π^0 Dalitz decay ($\pi^0 \rightarrow \gamma + e^+/e^-$) is presented. We assume the event contributes to the background if at least one Dalitz decay electron has $p_T^e > p_T^{e*}$. No other cuts were applied. All event rates are normalized to the event rate for W^+ with $p_T^{e*} = 10 \text{ GeV}/c$ in the fiducial EMC acceptance level $|\eta| < 0.95$.

$p_T^{e*}, \text{ GeV}/c$	W^+	e^+ from Dalitz	W^-	e^- from Dalitz
10	1.00	0.59	0.22	0.59
15	0.98	0.11	0.22	0.11
20	0.93	0.02	0.20	0.02
25	0.82	0.005	0.18	0.005

We observe that at $p_T^{e*} = 20\text{-}25 \text{ GeV}/c$, the background from Dalitz decays is at the same level or even lower than the Z boson while the efficiency for W detecting drops only by 7-18% comparing to $p_T^{e*} = 10 \text{ GeV}/c$. Taking into account, that applying

other criteria to the W^+ events selection (isolation cut, rejecting pairs of close unlike sign electrons distinguishable in the tracking system and with the Maximum Shower Detector (SMD, etc.), the background from π^0 Dalitz decays can be considered as negligible.

The contamination of the W sample by high- p_T charged hadrons misidentified as electrons is expected to be the most serious source of background. One can see from the table below (see Fig. 5 also) that the number of the positively charged hadrons with p_T higher than 20-25 GeV is 25-80 times more than of e^+ from W^+ decay (for W^- the situation is even worse: 100-380 times). The ability to extract W^\pm signals depends on the detector capability to reject hadrons from electrons. The results of the first-stage simulations for STAR shown in the table below represent the estimate for the rejection power for two criteria.

- Matching the momentum measured in the STAR tracking system to the energy deposited in the EMC. We assumed the EMC energy resolution for e^\pm is equal to

$$\sigma_E / E = 20\% / \sqrt{E}, \text{ where } E \text{ is in GeV,}$$

and the STAR tracking system (TPC and SVT) momentum resolution is expected to be the following (extrapolation to higher momenta of the Fig. 4C-12, Page 4C-31 in the CDR for STAR, PUB-5347, June 15, 1992):

$$\sigma_p / p = 0.3\% p, \text{ where } p \text{ is in GeV/c.}$$

The probability for the hadron to deposit a certain part of its energy in the EMC had been estimated with the use of the beam test results with the EMC prototype performed at the 70 GeV proton accelerator in IHEP, Protvino (to be published). We assumed that a charged hadron is rejected if it generates a signal in EMC below $2\sigma_E$ of its energy measured with the tracking system.

- Isolation cut. Effectiveness of the isolation cut is illustrated in Fig. 6. The electron candidate was considered as being produced from W decay if the sum of energies $E_{EMC} + E_{charged}$ detected in the cone $R = \sqrt{(\Delta\eta)^2 + (\Delta\phi)^2} < 0.4$ centered around the candidate e^\pm is less than $0.1 E_e$. Here E_{EMC} is the energy deposited by all particles except the candidate electron in the EMC, $E_{charged}$ - the sum of energies of all charged particles (excluding e^\pm candidate) measured in tracking system; E_e - the energy of the candidate e^\pm . Otherwise

an event was considered as background and rejected. In the table below, as before, all event rates are normalized to the event rate of W^+ within the fiducial acceptance before applying any cuts.

P_{T^*}, GeV	No Cuts			With Cuts		
	W^+	W^-	All Charged Background	W^+	W^-	All Charged Background
10	1.00	0.22	3,600	0.96	0.21	5.92
15	0.98	0.22	500	0.95	0.21	1.16
20	0.93	0.20	75	0.89	0.20	0.32
25	0.82	0.18	20	0.80	0.18	0.16
30	0.66	0.15	6	0.64	0.14	0.09
35	0.45	0.10	2.2	0.43	0.09	0.05

We did not take into account an additional rejection power of the shower max detector. The rejection power could be as high as 20 - 25 times.³² However, due to correlations of the SMD responses to the fraction of energy deposited by hadron in the whole calorimeter already used in the estimates presented here, the resulting rejection power will be less than simple multiplication of two factors. A more certain conclusion needs additional study, and has not been completed yet.

We are investigating a number of other background sources, for example, from overlapping in EMC/SMD high p_T gamma quanta with charged hadrons, electrons from charm and beauty, etc.

1.6.2. Parity-Conserving Asymmetry

In W^\pm and Z production with two beams longitudinally polarized, we can consider the parity conserving asymmetry A_{LL} defined on Page 5. For W^+

$$A_{LL} = \frac{\Delta u(x_1) \Delta \bar{d}(x_2)}{u(x_1) \bar{d}(x_2)}$$

and similarly for W^- with $u \leftrightarrow d$. This observable is sensitive to the polarization of the antiquarks and, for example, if $\Delta \bar{q} = 0$, we get $A_{LL} = 0$. Predictions²⁴ for A_{LL} at $\sqrt{s} = 500$ GeV are shown in Fig. 7.

1.6.3. Measurements of $h_1(x)$ in Z Production

The state of quarks in the nucleus is usually specified by two leading-twist structure functions: $f_1(x)$ (or $q(x)$), the spin averaged over quark distribution measured in unpolarized deep inelastic scattering, and $g_1(x)$ (or $\Delta q(x)$), the helicity distribution obtained in deep inelastic scattering with a longitudinally polarized lepton beam on a longitudinally polarized nucleon. However, there is a third fundamental function²⁵ $h_1(x)$ which is also leading-twist and which measures the transversity distribution of quarks in a transversely polarized nucleon. Nothing is known about this function, and since it measures the correlation between left-handed and right-handed quarks, it decouples from deep inelastic scattering. It is only accessible in certain hadronic processes with two initial beams transversely polarized and requires quark-antiquark annihilation. For lepton pair production (e^+e^- , $\mu^+\mu^-$, ...), the corresponding asymmetry A_{TT} is given in terms of $h_1(x)$ as,²⁶

$$A_{TT} = \hat{a}_{TT} \frac{\sum_a e_a^2 h_1^a(x_1) h_1^{\bar{a}}(x_2)}{\sum_a e_a^2 f_1^a(x_1) f_1^{\bar{a}}(x_2)},$$

where \hat{a}_{TT} is the asymmetry at the partonic level, which has a simple expression in terms of the polar and azimuthal angles of one of the outgoing leptons. For W production, this asymmetry is zero because the W is a pure left-handed object and it is not possible to produce a left-right interference.²⁴ However, this is not the case for Z production and if one assumes, at a first approximation $h_1 = g_1$ (which could turn out to be false) one obtains

$$A_{TT}/\hat{a}_{TT} \sim -A_{LL},$$

where A_{LL} is the parity-conserving double helicity asymmetry previously considered and shown in Fig. 7. Given the fact that Z production will be rather copious and its decay in e^+e^- is a very clean signal, it will be possible to make this measurement to a respectable level of accuracy.

2. Measurements with Barrel, One Endcap, and Shower Maximum Detector

An endcap calorimeter is to be placed inside the iron pole pieces as shown in Fig. 1. The endcap increases solid angle and acceptance and allows better measurements of the following reactions.

2.1. Detecting the Direct- γ and the "Away-Side" Jet

In order to measure $\Delta G(x)$, the gluon spin structure function, both the direct- γ and the "away-side" jet must be detected in coincidence so that the kinematics of the incoming partons can be calculated.

The Compton and annihilation subprocesses both involve $2 \rightarrow 2$ scatterings. The incoming partons are assumed to have fractions x_1 and x_2 of the beam momentum and collide collinearly. Then x_1 and x_2 are given in terms of pseudorapidity as:

$$x_1 = (2p_T/\sqrt{s})(e^{\eta_1} + e^{\eta_2})/2, \quad x_2 = (2p_T/\sqrt{s})(e^{-\eta_1} + e^{-\eta_2})/2.$$

Figure 8 shows the x coverage for $x_T = 0.1$ as functions of the direct- γ and jet pseudorapidities.

Error on Asymmetry, δA_{LL} , for Incoming Partons with x_1 and x_2
at $\sqrt{s} = 200$ GeV

min (x_1, x_2)	2 (x_1, x_2)			
	≤ 0.2	0.2 - 0.3	0.3 - 0.4	> 0.4
0.00 - 0.05		0.014	0.011	0.008
0.05-0.10	0.007	0.007	0.012	0.014
0.10-0.15	0.008	0.012	0.024	0.036
0.15-0.20	0.025	0.022	0.045	0.072
> 0.20		0.042	0.059	0.088

2.2. Measurements of the Sea-Quark Helicity Distribution in the Drell-Yan Process

A measurement of the Drell-Yan process is one way to determine the polarization of sea quarks. The $q\bar{q}$ annihilation into a vector boson gives a large asymmetry at the partonic level, and selects sea antiquarks with valence quarks.

The asymmetry A_{LL} for Drell-Yan in pp collisions is related to the sea-quark helicity distribution:

$$A_{LL} = \hat{a}_{LL} \frac{\sum_i e_i^2 [\Delta q_i(x_1) \Delta \bar{q}_i(x_2) + \Delta q_i(x_2) \Delta \bar{q}_i(x_1)]}{\sum_i e_i^2 [q_i(x_1) \bar{q}_i(x_2) + q_i(x_2) \bar{q}_i(x_1)]},$$

where $x_1 - x_2 = x_F$, $x_1 \cdot x_2 = M^2/s$, and $\hat{a}_{LL} = -1$.

Larger values of A_{LL} are expected at higher x_F as shown in Fig. 9.

The Drell-Yan pair production was studied by Monte-Carlo simulations using PYTHIA V 5.3 of the LUND set of routines.¹⁴ The EHLQ1 set of parton structure functions²⁷ was used. Estimates of the event rate for e^+e^- Drell-Yan pairs in STAR at $\sqrt{s} = 200$ GeV are shown below using a triggering cut of electron $p_T > 4$ GeV/c.²⁸

M_{ee} GeV/c ²	5-9	9-12	12-15	15-20
	21,000	14,000	6,000	4,000

Competing backgrounds to $q\bar{q} \rightarrow \gamma^* \rightarrow e^+e^-$ are $q\bar{q} \rightarrow g + \gamma \rightarrow e^+e^-$, $gq \rightarrow q + \gamma \rightarrow e^+e^-$, and $g\bar{q} \rightarrow q + \gamma \rightarrow e^+e^-$. These are t-channel contributions to the cross sections of Drell-Yan, with a k-factor = 2.5 (the increase in the measured cross section of Drell-Yan as compared to the calculated one if one takes into account only process $q\bar{q} \rightarrow e^+e^-$).

Results of the background study are shown as:³¹

a. Ratio $R = t\text{-channel DY}/\text{Standard DY}$

Here standard DY stands for the conventional s-channel production mechanism $q + \bar{q} \rightarrow e^+ + e^-$. t-channel DY - higher order QCD corrections, $2 \rightarrow 3$ processes as $q\bar{q} \rightarrow g + \gamma \rightarrow e^+e^-$, $gq \rightarrow q + \gamma \rightarrow e^+e^-$, and $g\bar{q} \rightarrow q + \gamma \rightarrow e^+e^-$.

Table 1
10 < mass (e^+e^-) < 14 GeV/c²

p_T GeV/c	2.5	5.0	7.5	10.0
Standard DY mb/GeV/c	$4 \cdot 10^{-9}$	$5 \cdot 10^{-10}$	10^{-10}	$2 \cdot 10^{-11}$
t-channel DY mb/GeV/c	$4.5 \cdot 10^{-9}$	$1.2 \cdot 10^{-9}$	$3 \cdot 10^{-10}$	10^{-10}
R	1.1	2.4	3	5

b. Signal to Noise Ratio

Table 2
Drell-Yan Pair Production at $y(e^+e^-) = 0$
 $2 < p_T < 10 \text{ GeV/c}$

Mass (e^+e^-), GeV/c ²	10	12	14
DY = sum of standard DY + t-channel DY, mb/GeV/c	$2.4 \cdot 10^{-9}$	$1.4 \cdot 10^{-9}$	$6.5 \cdot 10^{-10}$
Noise (background) from π^0 -Dalitz and charm from twojet events	$2 \cdot 10^{-10}$	$8 \cdot 10^{-11}$	$4.5 \cdot 10^{-11}$
R = DY/twojet background or signal to noise ratio	12	17.5	14.5
R/k, where k is explained below	6	9	7

Here $k = k_1 \cdot k_2 \cdot k_3$, where $k_1 = 1.25$ takes into account the η (549) contribution to Dalitz pairs, $k_2 = 1.5$ takes into account the missed contribution from multi-jet events. According to ISAJET we have $\sigma(\text{inelastic})/\sigma(\text{twojet}) = 62 \text{ mb}/27 \text{ mb} = 2.3$, hence from $1 < k_2 < 2$ we take $k_2 = 1.5$ as a reasonable value. k_3 takes into account the unresolved π^0 's which being combined with a charged track simulate electrons (positrons). These π^0 's are assumed to be unresolved if the distance between two γ 's from π^0 is less than 3 cm as is required by the "shower max" properties. This k_3 coefficient has not yet been estimated. So in the last line of Table 2 we use $k_3 = 1$ instead of $k_3 > 1$.

Table 3
Drell-Yan Pair Produced at All $y(e^+e^-)$
 $2 < p_T < 10 \text{ GeV/c}$

Mass (e^+e^-), GeV/c ²	10	12	14
DY = sum of standard DY + t-channel DY, mb/GeV/c	$4.2 \cdot 10^{-9}$	$2.2 \cdot 10^{-9}$	$1.3 \cdot 10^{-9}$
Noise (background) from π^0 -Dalitz and charm from twojet events	$1 \cdot 10^{-9}$	$5 \cdot 10^{-10}$	$2.5 \cdot 10^{-10}$
R = DY/twojet background or signal to noise ratio	4.2	4.4	5.2
R/k	2.2	2.3	2.7

Drell-Yan measurements seem to be preferable at $y(e^+e^-) = 0$, where one can hope to reach a signal to noise ratio slightly less than 6-7. This is for $10 < \text{mass}(e^+e^-) < 14 \text{ GeV}/c^2$ and $2 p_T < 10 \text{ GeV}/c$.

2.3. Measurements of $h_1(x)$ in the Drell-Yan Process and "Z Production"

In the Drell-Yan process, we will accumulate 21,000 events in a mass region of 5 to 9 GeV, which allows the measurement of the new structure function $h_1(x)$ to a reasonable accuracy.

This new structure function is also accessible in Z_0 production by measuring A_{TT} , as we discussed in Section 2.3.5, and here the statistical accuracy is greatly improved. (See Section 2.4.)

2.4. W's and Z Production at 500 GeV

W^+ 74,000 events

W^- 22,000 events

For W's the detected electron (or positron) has $p_T > 20 \text{ GeV}/c$

Z 5,300 events

For Z at least one of the detected electrons has $p_T > 20 \text{ GeV}/c$

3. Cost Estimate and Schedule

The modular nature of the calorimeter design makes it possible to stage the construction of this detector in a number of ways. Depending upon which staging plan is adopted, the physics capabilities of the EMC also vary. The present report addresses two possible options, both of which extend the reach of the STAR physics program significantly.

The first option is to construct the 120 modules necessary to complete the full EMC barrel. Each module constructed would contain the hardware for the shower maximum detector, to avoid the difficult problem of retrofitting this detector at a later date. However, the shower maximum detector would not be instrumented with electronics until further funding became available. Construction of the endcap calorimeter would also be deferred. In addition, to reduce the initial cost, fiber bundles from towers adjacent within $\Delta\eta \sim 0.2$ would be coupled to the same photomultiplier. As a consequence, the total number of photomultipliers and electronics channels would be ~ 600 . The cost of this option is \$7.5 M in FY93 dollars when cost savings from universities, foreign collaborators, etc. are taken into account.

nels would be ~ 600 . The cost of this option is \$7.5 M in FY93 dollars when cost savings from universities, foreign collaborators, etc. are taken into account.

Several areas have been identified in which contributions from participating institutions could result in significant savings. These include machining of mechanical components, labor for module assembly, and fabrication of the shower maximum detector. The estimated total cost of components and labor that could be contributed is $\sim \$1.5$ M in FY93 dollars.

The amount of physics that can be accomplished by this implementation of the calorimeter is significant. The improved resolution provided by the EMC will afford a more detailed understanding of the transfer of energy from projectile rapidity to mid-rapidity. As the EMC barrel is large compared to a jet radius $\sqrt{(\Delta\eta)^2 + (\Delta\phi)^2} \lesssim 0.7$, it will also be possible to measure inclusive jets and high- p_T π^0 's from parton scatters within $|\eta| \lesssim 0.3$ to 0.5 . This will allow STAR to study the energy loss of hard-scattered partons using inclusive jets as well as γ -jets and jet-jet coincidences as penetrating probes of the early stages of the collision.

The assembly scenario for this implementation of the EMC leads naturally to a descope configuration in the event of reduced funding. As the mechanical supports for the TPC capture the modules within $\Delta\phi \sim 12^\circ$ at two locations which are back-to-back, the modules located in these regions of the barrel would be built up from two sections that are 180° apart. It would be possible to complete two back-to-back sections comprising half of the EMC barrel for $\sim \$4.5$ M before contributions. This would allow STAR some capability for all of the physics discussed above, with some reduction in resolution, sensitivity, and acceptance.

The second option considered is to construct the full EMC barrel and one of the endcap calorimeters. The EMC barrel would be instrumented with 1,200 channels of tower electronics. The number of electronics channels for the endcap would be 600. The shower maximum hardware would be completed for installation in both the barrel and endcap calorimeters, but would only be instrumented with electronics in the endcap. The estimated cost for this option before contributions is \$13M in FY93 dollars.

Much of the engineering required to interface the barrel and endcap calorimeters to the STAR detector has already been carried out. In addition, considerable engineering directed at the choice of technology has been accomplished. As a consequence, it is possible, given an appropriate funding profile for all of the EMC construction, to be completed for the start of RHIC operations. Specifically, it is envisioned that given the choice of technology in summer of 1993, a full-scale pro-

totype would be constructed and tested within a year. Upon completion of this phase, construction of modules would commence. Schedule estimates based upon the construction of similar modules for ZEUS suggest that modules could be completed at the rate of ~ 30 per year. Consequently, based upon feasibility alone, the full barrel calorimeter would be available for assembly at RHIC in mid-1998.

Assuming a level funding profile of ~ \$1M per year, the construction of all the modules for the full EMC barrel, including front-end electronics, trigger electronics, and data acquisition, would require approximately six years. In this instance, most of the EMC barrel modules would be installed before the start of RHIC in mid-1999, with the remaining modules being installed during the first scheduled RHIC shutdown.

The cost summary is:

Full barrel and shower max detector	\$10.5M
End cap	\$4.4M

References

- 1) A. P. Contogouris *et al.*, Phys. Lett. B304, 329 (1993), to appear in Phys. Rev. D.
- 2) L. E. Gordon and W. Vogelsang, to appear in Phys. Rev. D.
- 3) P. Chiappeta *et al.*, to appear in Z. Phys. C.
- 4) K. Gottfried, Phys. Rev. Lett. 18, 1174 (1967).
- 5) P. Amaudruz *et al.* (New Muon Collaboration) Phys. Rev. Lett. 66, 2712 (1991); D. Allasia *et al.* Phys. Lett. B249, 366 (1992).
- 6) C. Bourrely and J. Soffer, CPT-93/P.2865, Phys. Lett. B to appear.
- 7) M. A. Doncheski, F. Halzen, C. S. Kim, and M. L. Stong, MAD/PH/744, submitted for publication.
- 8) E. Leader and K. Sridhar, Phys. Lett. B311, 324 (1993).
- 9) Hai-Yang Cheng, Melin Huang, and C. F. Wai, ITP-SB-93-07, submitted for publication.
- 10) C. Boros, Liang Zuo-tang and Meng Ta-chung, Phys. Rev. Lett. 70, 1751 (1993).
- 11) D. L. Adams *et al.*, Phys. Lett. B261, 201 (1991); Zeit. Phys. C56, 181 (1992); A. Yokosawa, Proc. XXI Int. Symp. on Multiparticle Dynamics, Wuhan, China, p. 545, September, 1991.
- 12) E-704 preliminary data.
- 13) E. Eichten, I. Hinchliffe, K. Lane, and C. Quigg, Rev. Mod. Phys. 56, 579 (1984); 58, 1065 (E) (1986).
- 14) H. U. Bengtsson and T. Sjostrand, A Manual to PYTHIA V5.3 in "The LUND Monte Carlo Programs Long Writeup," Pool programs W5035/W5046/W5047/W5048, CERN, 1 November 1989.
- 15) M. E. Beddo, H. Spinka, and D. G. Underwood, ANL-HEP-TR-92-59, STAR Note # 77.
- 16) M. Werlen, MW/RSC 92/8 (1992) and private communication.
- 17) J. Qiu and G. Sterman, Phys. Rev. Lett. 67, 2264 (1991).
- 18) X. Ji, Phys. Lett. B289, 137 (1992).
- 19) D. L. Adams *et al.*, Phys. Lett. B264, 462 (1991).
- 20) J. Soffer and N. A. Tornqvist, Phys. Rev. Lett. 68, 907 (1992).
- 21) J. Soffer and D. Wray, Wis-72/31-ph, unpublished.
- 22) D. L. Adams *et al.*, Phys. Lett. B261, 201 (1991).

- 23) A. D. Martin, W. J. Sterling, and R. G. Roberts, Preprint RAL-92-021 (1992).
- 24) J. Soffer, to be published.
- 25) J. Ralston and D. E. Soper, Nucl. Phys. B152 (1979) 109; J. Odrtes, B. Pire, and J. Ralston, Z. of Phys. (Sept. 1992); R. Jaffee and X. Ji, Phys. Rev. Lett. 67 (1991) 552.27 E. Eichten, I. Hinchliffe, K. Lane, and C. Quigg, Rev. Mod. Phys. 56, 579 (1984); 58, 1065 (E) (1986).
- 26) X. Ji, Phys. Lett. B284, 137 (1992).
- 27) E. Eichten, I. Hinchliffe, K. Lane, and C. Quigg, Rev. Mod. Phys. 56, 579 (1984); 58, 1065 (E) (1986).
- 28) A. A. Derevschikov and V. L. Rykov, Internal RSC Report RSC-BNL/IHEP-4, Brookhaven, August 1992.
- 29) A. Pavlinov et al.
- 30) V. Rykov and K. Shestermanov
- 31) Y. Arestov et al.
- 32) B. V. Chujko et al., IHEP 92-104, Protvino, (1992).

Figure Captions

- Figure 1 A cross-sectional view of one-half of the STAR detector. The barrel EMC covers $|\eta| \leq 1.0$. The endcap calorimeter subtends $1.05 \leq |\eta| \leq 2.0$. The barrel EMC is supported by aluminum rings located between the coils of the conventional magnet. Fibers from the towers of the barrel pass through spaces between the aluminum rings and the coils and are subsequently routed between the iron flux return bars to the exterior of the magnet.
- Figure 2 A_N for p^+ and π^- production versus x_F integrated over p_T .
- Figure 3 A_N for π^+ (squares) and π^- (circles) in the $\bar{p}^{\uparrow}p$ reaction.
- Figure 4 The parity violating asymmetry A_{LL}^{FV} vs. y for W^+ and W^- production at $\sqrt{s} = 500$ GeV. Solid lines correspond to non-zero sea quark polarizations where as dashed lines correspond to $\Delta\bar{u} = \Delta\bar{d} = 0$.
- Figure 5 Positive hadrons background vs. p_T before and after applying rejection criteria (isolation and EMC-tracking matching) along with e^+ from W^+ decay.
- Figure 6a Tracks in an average event with high- p_T particle production at $\sqrt{s} = 500$ GeV.
- Figure 6b Tracks in W production at $\sqrt{s} = 500$ GeV.
- Figure 7 A_{LL} for parity-conserving W production.
- Figure 8 Plots of x_1 and x_2 as a function of the direct- γ and jet pseudorapidities. The solid lines represent contours for x_1 and the dashed lines are contours for x_2 .
- Figure 9 A_{LL} vs. x_F in the Drell-Yan process.

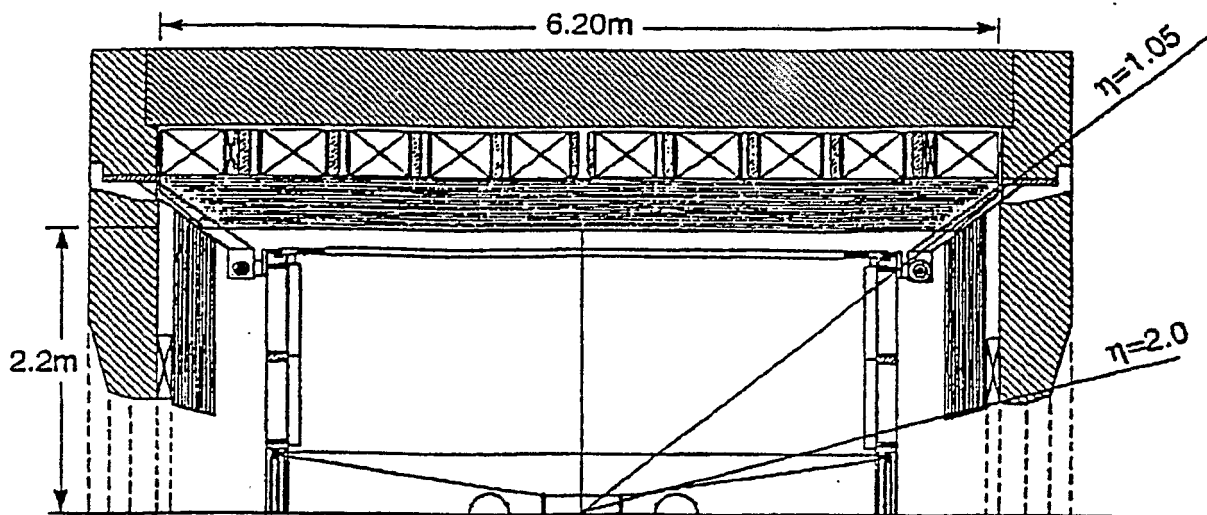


Figure 1

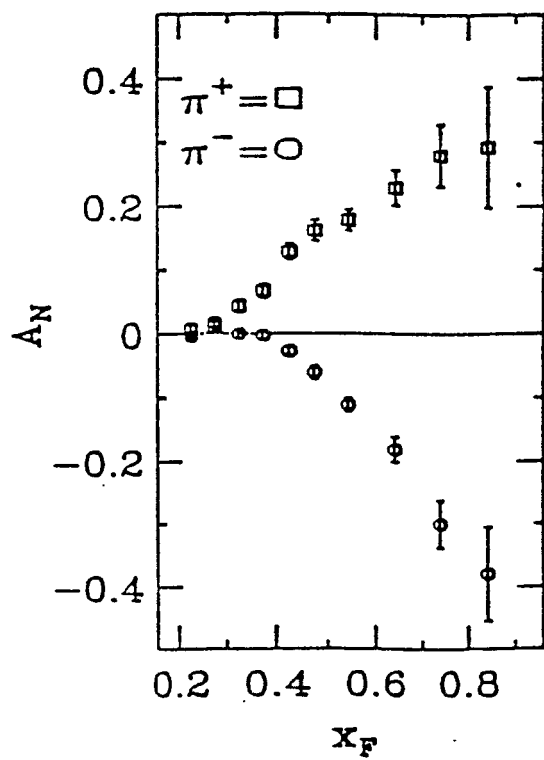


Figure 2

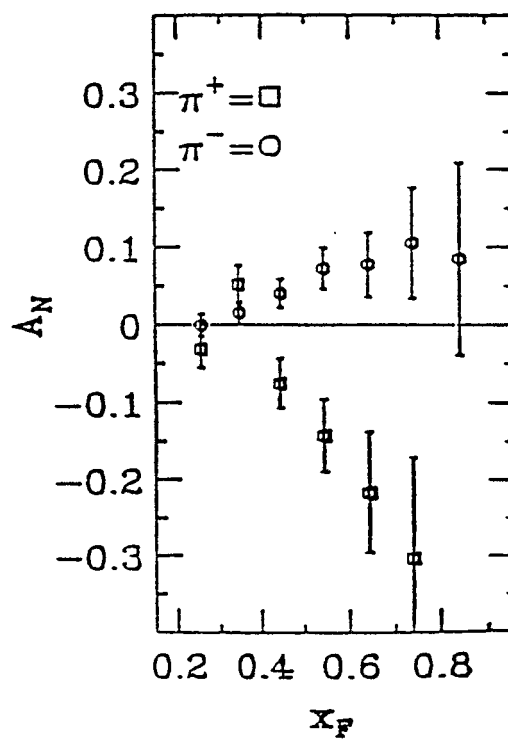


Figure 3

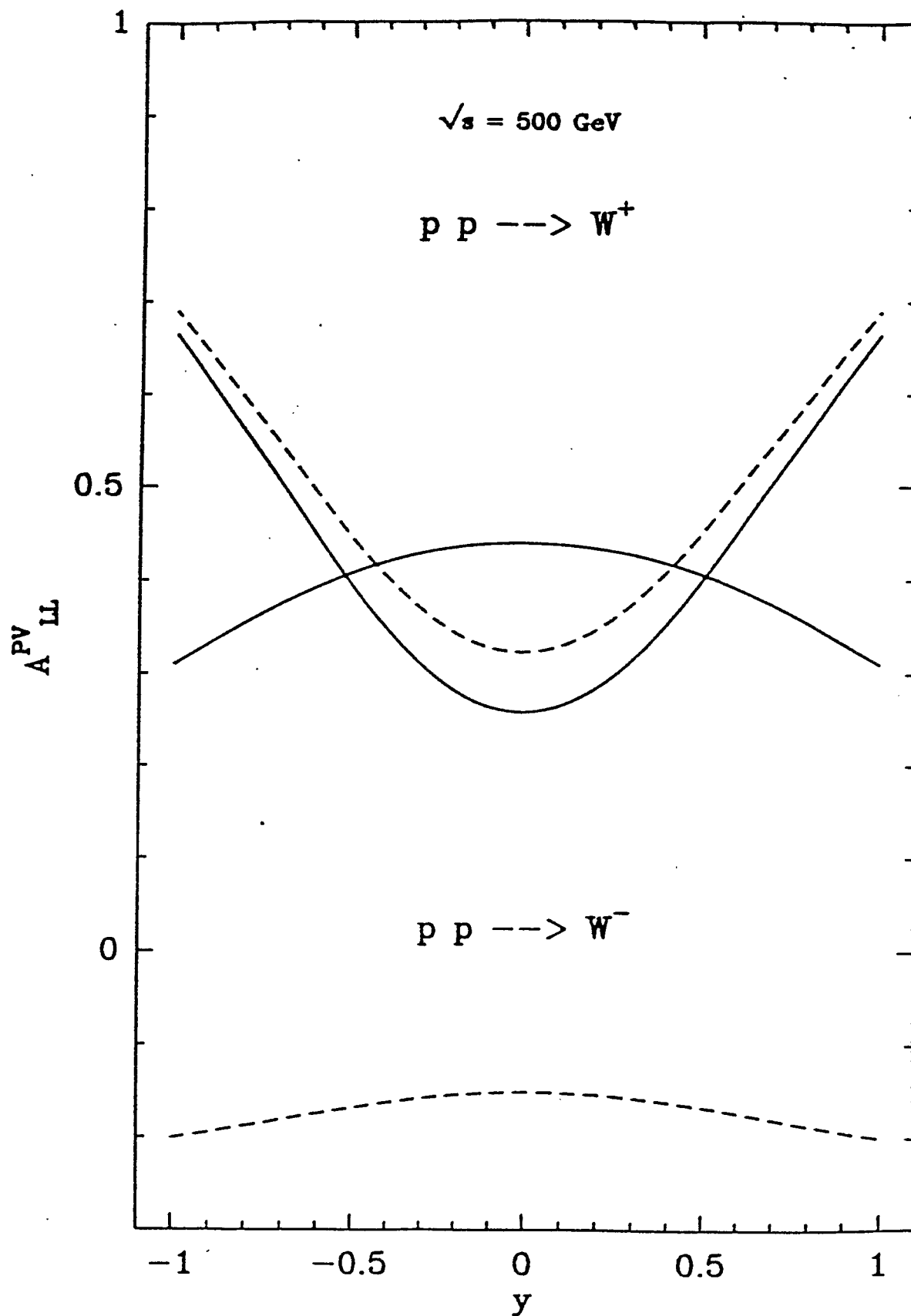


Figure 4

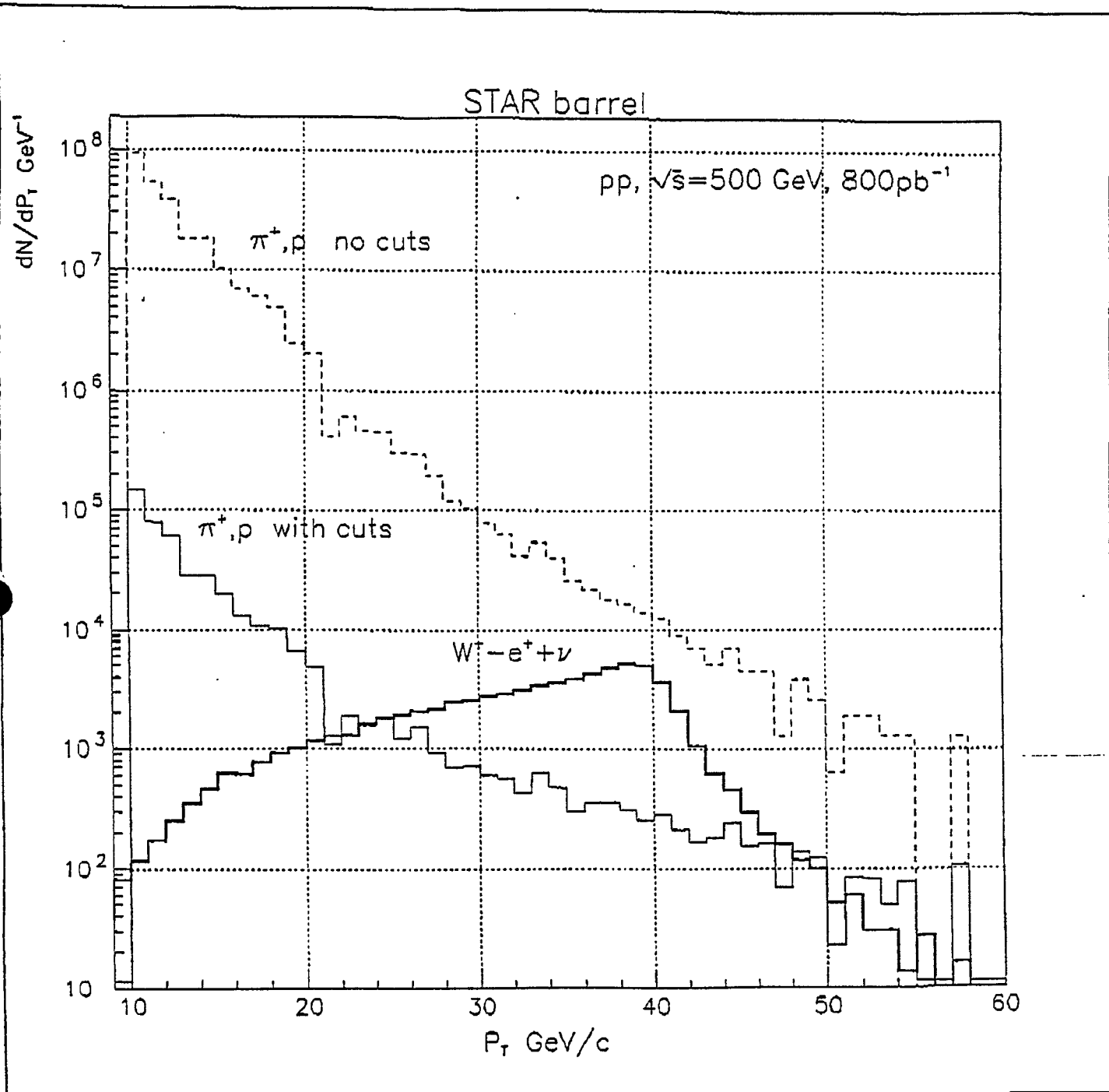


Figure 5

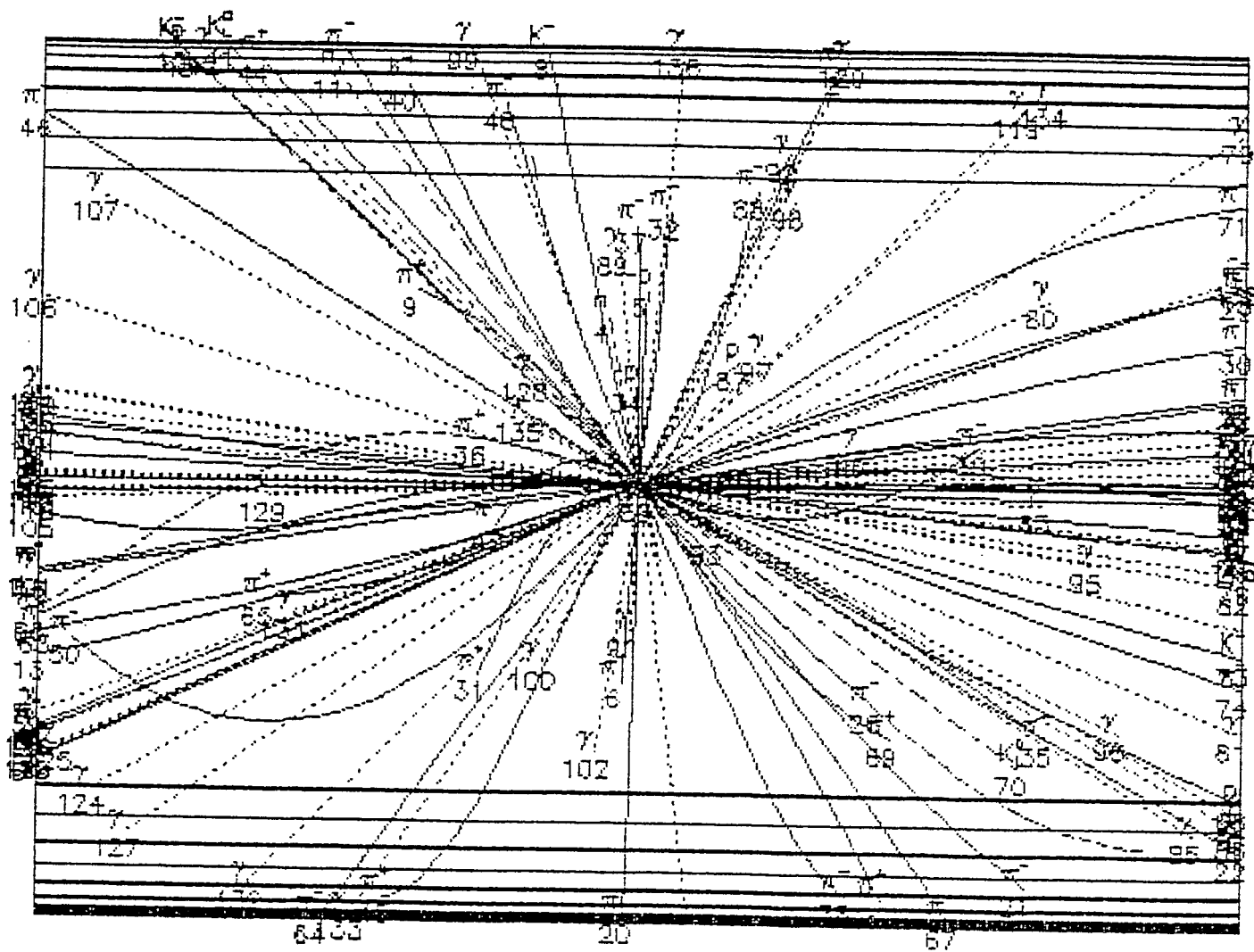


Figure 6a

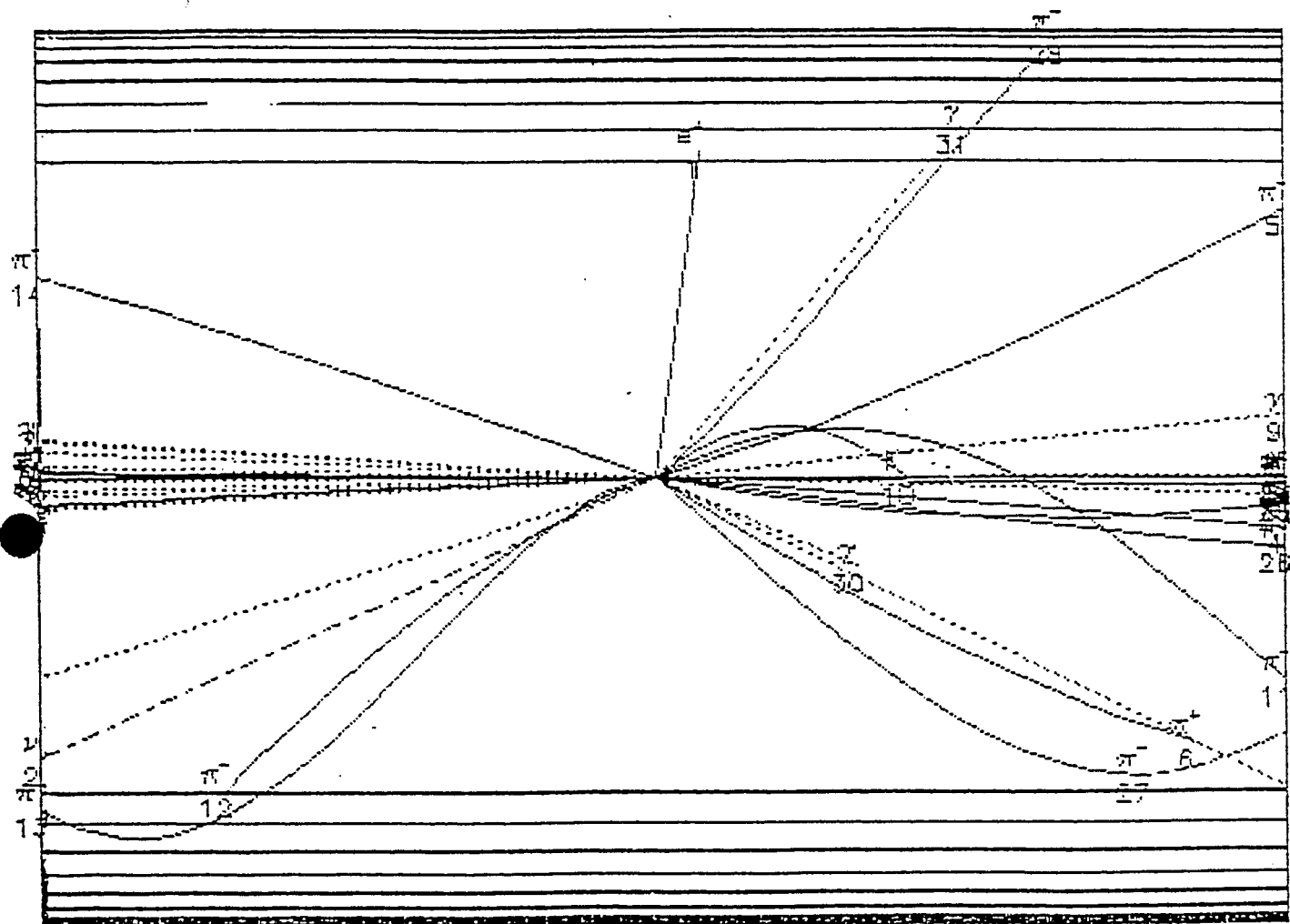


Figure 6b

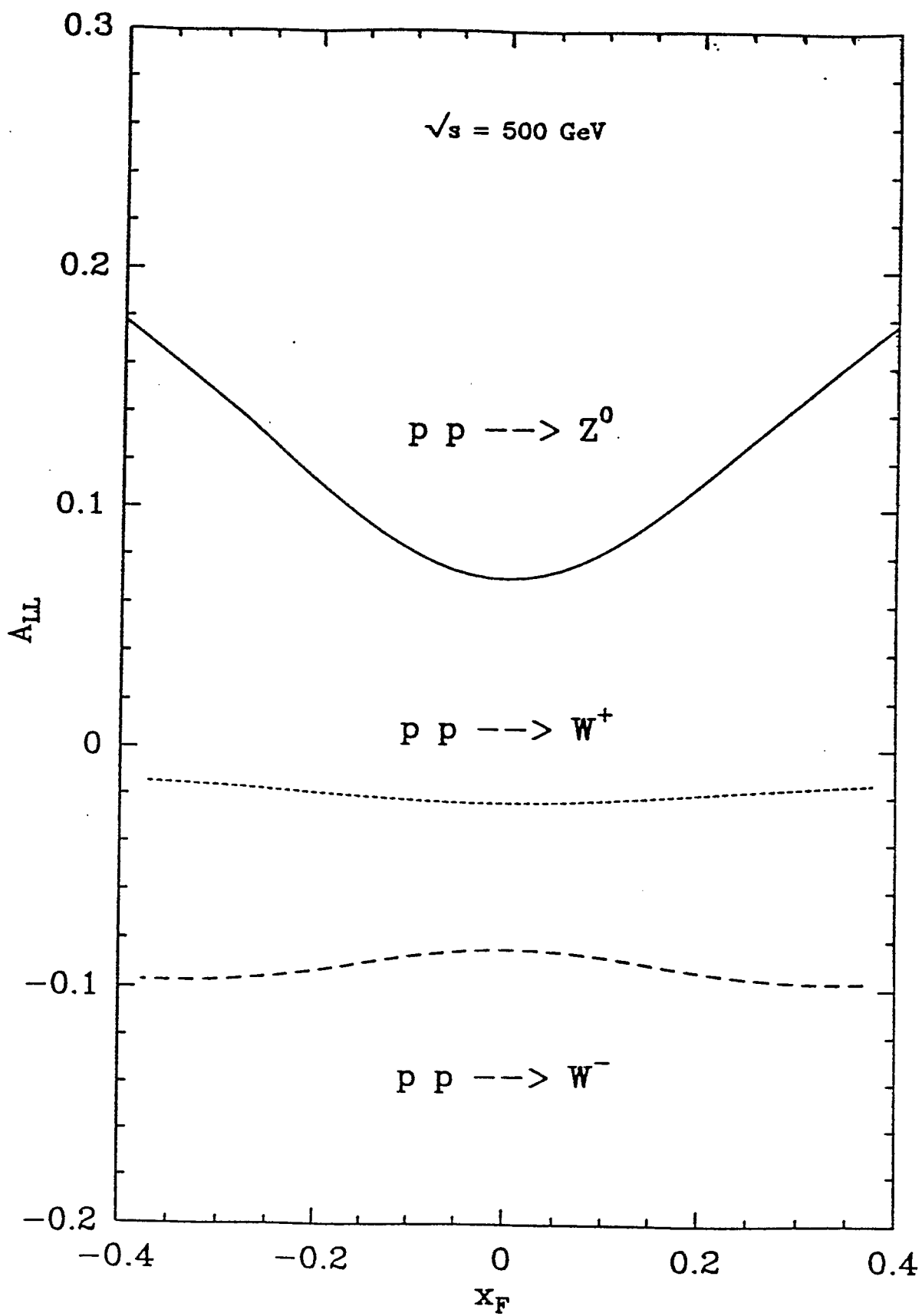


Figure 7

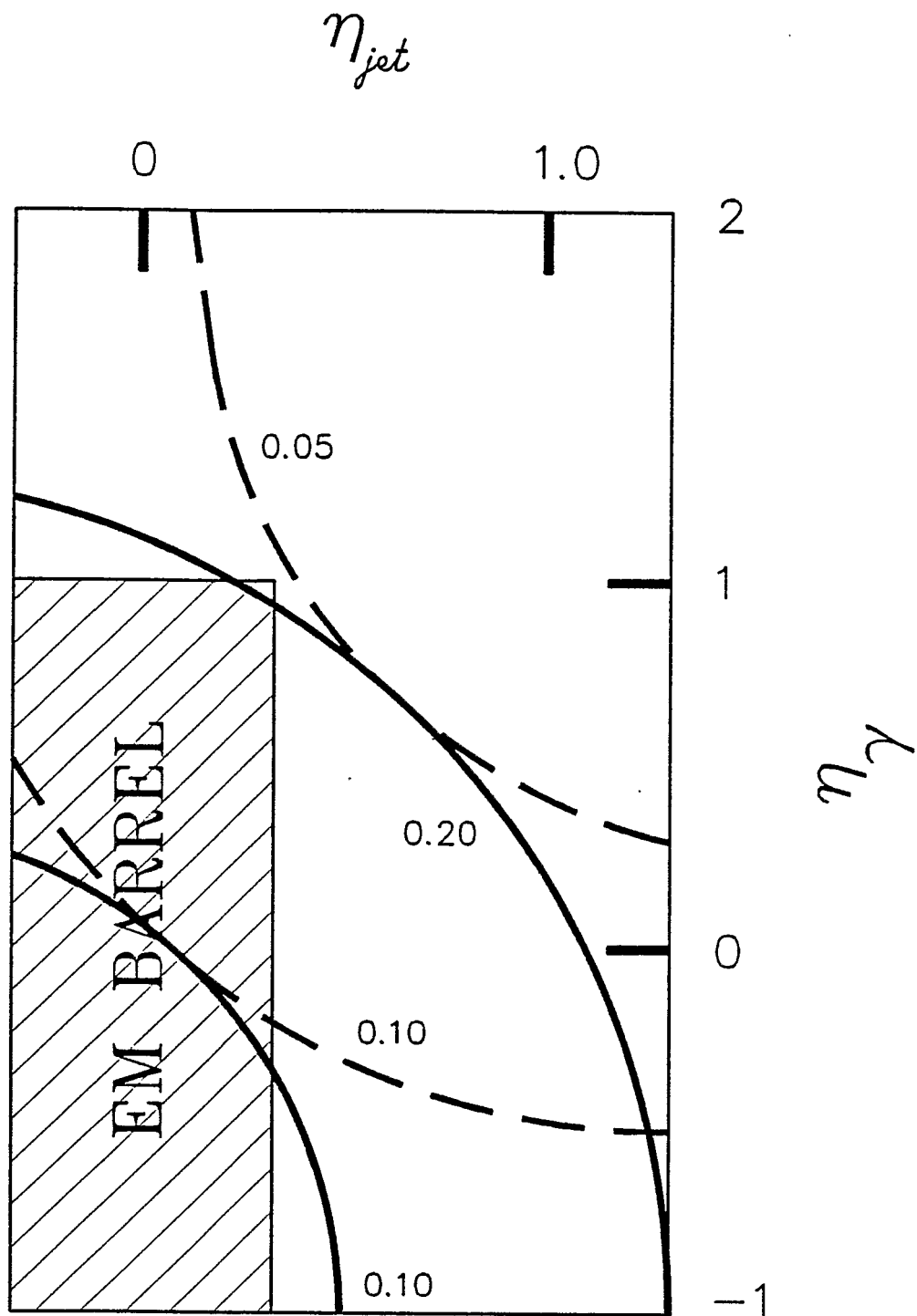


Figure 8

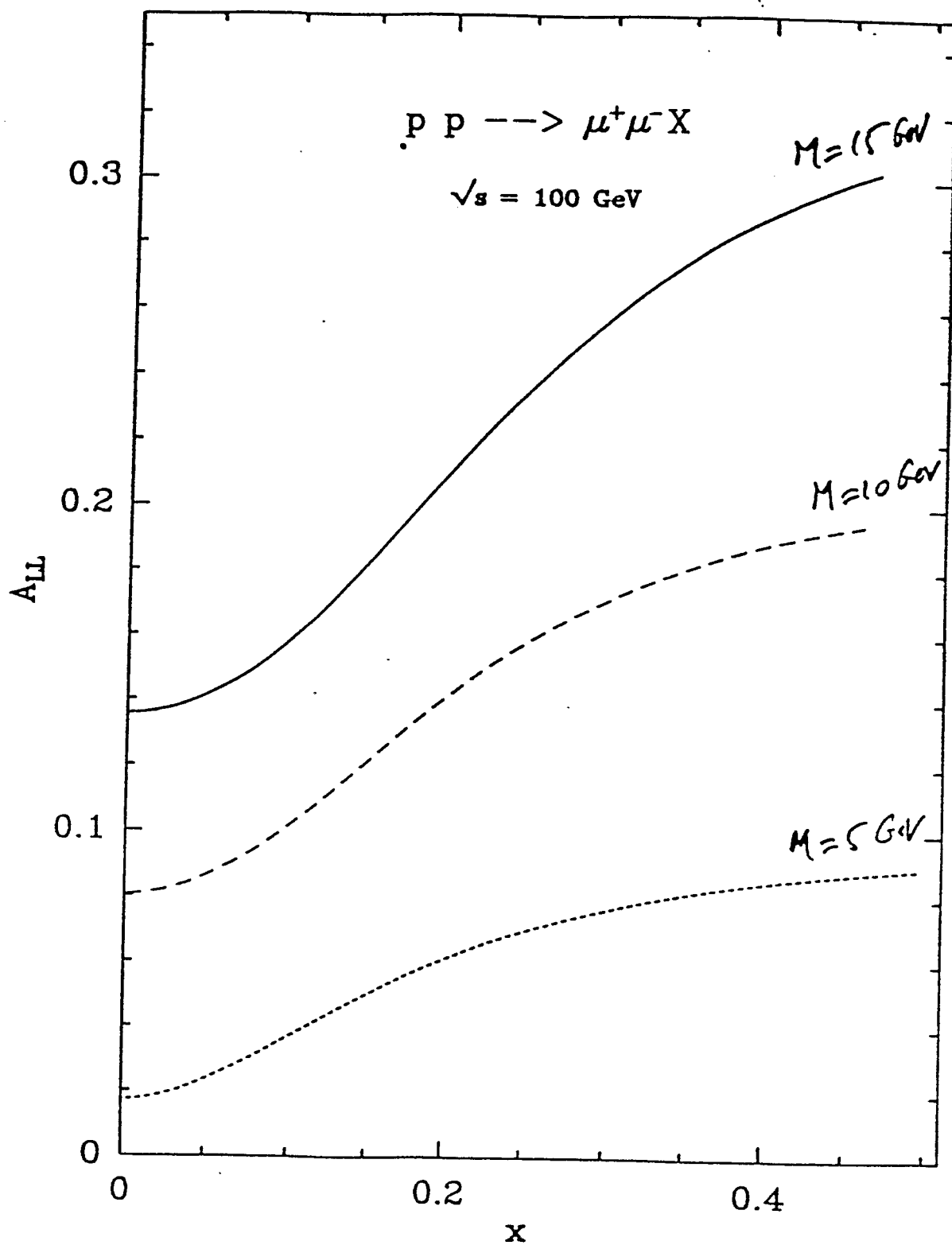


Figure 9

APPENDIX I

Author List

M. Beddo, D. Grosnick, D. Hill, D. Lopiano, H. Spinka, D. Underwood, A. Yokosawa
High Energy Physics Division, Argonne National Laboratory, Argonne, Illinois 60439, USA

P. Buncic, D. Ferenc, K. Kadija, G. Paic, and D. Vranic
Rudjer Boskovic Institute, 41001 Zagreb, Croatia

G. Danby, S.E. Eiseman, A. Etkin, K.J. Foley, R.W. Hackenburg, M.J. LeVine, R.S. Longacre, W.A. Love, E.D. Platner, P. Rehak, A.C. Saulys, and J.H. Van Dijk
Brookhaven National Laboratory, Upton, New York, 11973, USA

H.J. Crawford, J.M. Engelage, and L. Greiner
University of California, Berkeley, California 94720, USA

F.P. Brady, J.E. Draper, and J.L. Romero
University of California, Davis, California 95616, USA

J.B. Carroll, V. Ghazikhanian, E. Gulmez, T. Hallman, G.J. Igo, S. Trentalange, and C. Whitten, Jr.
University of California, Los Angeles, California 90024, USA

M. Kaplan, P.J. Karol, Z. Miolosevich, and E. Vardaci
Carnegie Mellon University, Pittsburgh, Pennsylvania 15213, USA

M. Cherney, T.S. McShane, and J. Seger
Creighton University, Omaha, Nebraska 68178, USA

M. Gazdzicki, R.E. Renfordt, D. Röhrich, R. Stock, H. Ströbele, and S. Wenig
University of Frankfurt, D-6000, Frankfurt am Main 90, Germany

L. Madansky and R. Welsh
The Johns Hopkins University, Baltimore, Maryland 21218, USA

B. Anderson, M. L. Justice, D. Keane, Y. Shao, and J. Watson
Kent State University, Kent, Ohio 44242, USA

A. S. Akimenko, Yu. I. Arestov, N. I. Belikov, B. V. Chujko, A. M. Davidenko, A. A. Derevschikov, S. V. Erin, O. A. Grachov, A. S. Konstantinov, I. V. Kotov, Yu. A. Matulenko, A. P. Meschanin, A. I. Mysnick, S. B. Nurushev, A. I. Pavlinov, A. Yu. Polyarush, A. I. Ronzhin, V. L. Rykov, V. A. Sergeev, K. E. Shestermanov, L. F. Soloviev, O. D. Tsay, A. G. Ufimtsev, A. N. Vasiliev
IHEP, Institute for High Energy Physics, Protvino, Russia

F. Bieser, M.A. Bloomer, D. Cebarta, S.I. Chase, W. Christie, W.R. Edwards, M. Green, D. Greiner,
J.W. Harris, H. Huang, P. Jacobs, P. Jones, S. Kleinfelder, P. Lindstrom, S. Margetis, J. Marx,
H.S. Matis, C. McParland, J. Mitchell, T. Moore, R. Morse, C. Naudet, T. Noggle, G. Odyniec,
D. Olson, A.M. Poskanzer, G. Rai, J. Rasson, H.-G. Ritter, I. Sakrejda, J. Schambach, L.S. Schroeder,
D. Shuman, R. Stone, T.J.M. Symons, H. Wieman, and W.K. Wilson
Lawrence Berkeley Laboratory, Berkeley, California 94720, USA

W. Llope, A. Vandermolen, G. Westfall
Michigan State University, East Lansing, Michigan 48824, USA

C. S. Chan, M.A. Kramer, S.J. Lindenbaum, K.H. Zhao, and Y. Zhu
City College of New York, New York, New York 10031, USA

A. Aprahamian, N.N. Biswas, U. Garg, V.P. Kenney, and J. Piekarz
University of Notre Dame, Notre Dame, Indiana 46556, USA

T. Humanic
University of Pittsburgh, Pittsburgh, Pennsylvania 15213, USA

D.D. Carmony, Y. Choi, A. Hirsch, E. Hjort, N. Porile, R.P. Scharenberg, B. Srivastava, and M. L.
Tincknell
Purdue University, West Lafayette, Indiana 47907, USA

D.L. Adams, S. Ahmad, B.E. Bonner, J.A. Buchanan, C.N. Chiou, J.M. Clement, M.D. Corcoran,
T. Empl, H.E. Miettinen, G.S. Mutchler, J.B. Roberts, J. Skeens, and I. Stancu
Rice University, Houston, Texas 77251, USA

A.D. Chacon, R.K. Choudhury, and K.L. Wolf
Texas A&M University, College Station, Texas 77843, USA

W. Dominik
Warsaw University, Warsaw, Poland

T. Pawlak, W. Peryt, and J. Pluta
Warsaw University of Technology, Warsaw, Poland

R. Bellwied, S. Bennett, J. Bielecki, T.M. Cormier, F. Gang, J. Hall, Q. Li, A. Lukaszew, R. Matheus,
C. Pruneau, and G. Roger
Wayne State University, Detroit, Michigan 48201, USA

W. J. Braithwaite, J.G. Cramer, D. Prindle, T.A. Trainor, and X.-Z. Zhu
University of Washington, Seattle, Washington 98195, USA

Z. Fraenkel and I. Tserruya
Weizmann Institute of Science, Rehovot 76100, Israel